DATE ISSUED NOV 22 1982

820309

ORNL/TM-8284

ornl

OAK
RIDGE
NATIONAL
LABORATORY

UNION
CARBIDE

ORNL
MASTER COPY

Sorption/Desorption Behavior of Iodine on Graphite

R. A. Lorenz 3
F. F. Dyer 1
R. L. Towns 3

OPERATED BY
UNION CARBIDE CORPORATION
FOR THE UNITED STATES
DEPARTMENT OF ENERGY

Printed in the United States of America. Available from
National Technical Information Service
U.S. Department of Commerce
5285 Port Royal Road, Springfield, Virginia 22161
NTIS price codes—Printed Copy: A05; Microfiche A01

This report was prepared as an account of work sponsored by an agency of the United States Government. Neither the United States Government nor any agency thereof, nor any of their employees, makes any warranty, express or implied, or assumes any legal liability or responsibility for the accuracy, completeness, or usefulness of any information, apparatus, product, or process disclosed, or represents that its use would not infringe privately owned rights. Reference herein to any specific commercial product, process, or service by trade name, trademark, manufacturer, or otherwise, does not necessarily constitute or imply its endorsement, recommendation, or favoring by the United States Government or any agency thereof. The views and opinions of authors expressed herein do not necessarily state or reflect those of the United States Government or any agency thereof.

ORNL/TM-8284
Dist. Category UC-77

Contract No. W-7405-eng-26

CHEMICAL TECHNOLOGY DIVISION

HTGR BASE TECHNOLOGY PROGRAM
HTGR Chemistry Studies (189a 01329)

SORPTION/DESORPTION BEHAVIOR OF IODINE ON GRAPHITE

R. A. Lorenz
F. F. Dyer*
R. L. Towns

*Analytical Chemistry Division.

Date Published - November 1982

OAK RIDGE NATIONAL LABORATORY
Oak Ridge, Tennessee 37830
operated by
UNION CARBIDE CORPORATION
for the
DEPARTMENT OF ENERGY

CONTENTS

	Page
ABSTRACT	1
1. INTRODUCTION	1
2. APPARATUS	2
3. GRAPHITE SAMPLES	4
4. EXPERIMENTAL PROCEDURE	4
4.1 Run 3	6
4.2 Run 4	7
4.3 Run 5	7
4.4 Run 6	8
4.5 Run 7	8
4.6 Run 8	9
4.7 Run 9	10
5. RESULTS AND DISCUSSION	12
5.1 Equilibrium Loadings	12
5.2 Adsorption Rate	13
5.3 Desorption	13
5.4 Iodine Deposition on Quartz and Other Materials	14
6. CONCLUSIONS	15
7. REFERENCES	16
8. TABLES AND FIGURES	17

SORPTION/DESORPTION BEHAVIOR OF IODINE ON GRAPHITE

R. A. Lorenz
F. F. Dyer
R. L. Towns

ABSTRACT

An experimental program was undertaken to extend the data on the sorption and desorption of iodine on graphite to more realistic high-temperature gas-cooled reactor (HTGR) operating conditions. This was accomplished by heating compacts of H-451 or S-2020 graphite at 250 to 1000°C in continuously flowing helium (at atmospheric pressure) that contained iodine at pressures of 10^{-6} to 10^{-1} Pa (10^{-11} to 10^{-6} bar).

Equilibrium adsorption data were generally well-behaved and reproducible with the H-451 graphite. Type S-2020 graphite sorbed more iodine, especially in the temperature range 700 to 800°C. Although desorption appeared to initiate as reversible sorption, the rate of loss of iodine decreased with time. During desorption from the S-2020 graphite at 700 and 800°C, a temporary plateau was reached that was sensitive to helium flow and pressure.

1. INTRODUCTION

Although only a small fraction of fission product iodine is expected to escape from fuel kernels during normal operation of a high-temperature gas-cooled reactor (HTGR), knowledge of its location in the reactor circuit is important in assessing hazards associated with iodine as a result of abnormal or accident conditions. The two principal locations of iodine in the reactor circuit are believed to be the metal pipe and heat exchanger surfaces,[1] and the graphite surfaces.[2,3] A previous analysis, based on data available at the time, determined that more of the iodine in the reactor circuit would be associated with graphite than with metal surfaces.[4]

With the exception of one series of tests,[3] previous experiments for iodine sorption on graphite were conducted at iodine pressures of

10^{-3} Pa (10^{-8} bar) or higher.[4-7] It has been estimated that the iodine pressure in an operating HTGR should be of the order of 10^{-7} to 10^{-4} Pa (10^{-12} to 10^{-9} bar).[2] Our experimental program was designed to extend the sorption data to the more realistic HTGR operating conditions — bulk graphite in helium at iodine pressures of 10^{-6} to 10^{-1} Pa (10^{-11} to 10^{-6} bar). Most of the previous studies used powdered graphite in vaccum.

2. APPARATUS

The apparatus used in runs 3 and 4 is shown in Fig. 1. In operation, helium flows continuously at atmospheric pressure through flowmeter FE-2 and the U-tube containing refrigerated I_2 (the saturator) and also through flowmeter FE-1 to provide dilution of the iodine-containing stream. The temperature of the refrigerated iodine and the ratio of dilution and saturator flows control the concentration or partial pressure of I_2 entering the furnace which contains the cup-shaped graphite test piece (Fig. 2). The graphite specimen is placed in the furnace so that the helium-iodine flow stream enters the opening of the cup and is forced to flow through the open pores of the graphite. Pressure drop measurements taken during the runs showed that the seal between the leading edge of the graphite cups and a mating surface in the quartz furnace tube was effective except for run 9.

Minor changes were made in the apparatus throughout the series of runs. For run 4, a NaI crystal was installed to monitor the ^{131}I collected on the charcoal filters at the furnace exit. Instrument connections were completed that permitted automatic typing and paper-tape punching of data: date, time of day, counting time, counts on the two NaI crystals, and total flow through FE-1 and FE-2 for the counting period. A computer program was written to correct the counting data for radioactive decay and to calculate the mass of iodine on the graphite and backup charcoal filters, the helium flow, and the iodine concentration in the helium. The program also included plotting of the processed data. Heating tape was added to the furnace inlet and outlet lines to reduce sorption of iodine on the quartz tubing.

The greatest change in the apparatus was made for tests beginning with run 5, as shown in Fig. 3. Scattered and possibly some direct radiation from iodine collected on the backup filter or deposited on the quartz tubing in the inlet and outlet regions of the furnace resulted in an increase in the background of the NaI crystal that monitored the graphite specimen. A multichannel analyzer had been used periodically to measure the background for the 364-keV peak of ^{131}I, but this was time-consuming and not entirely satisfactory; therefore, the following changes were made to minimize background radiation:

1. The collimation between the NaI crystal and graphite specimen was changed to focus on the graphite specimen, provide better shielding from radioactivity located near the graphite, and to reduce the natural background.
2. The backup charcoal filter was moved to the side so that scattered radiation reaching the crystal would be minimized.
3. The quartz tubing carrying iodine to the graphite sample was reduced in diameter to decrease the deposition of iodine on these quartz surfaces.

For run 5 the iodine saturator was changed from a tube filled with glass beads to a simple 1-mm-ID U-tube. It was felt that this reduction in surface area might speed up attainment of equilibrium following refrigerator temperature changes. The valve to the bypass charcoal was attached to the iodine supply line so that dilution flow would keep the furnace and graphite free of iodine during bypass operation.

For run 6 the NaI crystal monitoring iodine in the backup charcoal filter was moved slightly to permit counting of iodine deposited in the outlet region of the furnace. Strips of shielding material were used to provide nearly uniform counting efficiency for iodine deposited at any location in the furnace outlet region.

Following run 6, the iodine saturator U-tube was increased to 2-mm inner diameter to help alleviate a problem of flow stoppage apparently caused by water freezing in the refrigerated saturator tube. The flow blockage during run 6 was cleared by temporarily warming the saturator tube. An analysis of the accumulated water-like material in the tube showed that the liquid contained no carbon, so we deduced from this and

its freezing behavior that the material was indeed water. Table 1 shows the changes and operating conditions for the helium cleanup system used during the test series. All helium supply tanks were analyzed before use. Table 2 lists the analyses for tanks used during runs 8 and 9. During run 8 the titanium sponge trap was operated unheated for three different time periods; no effect on iodine sorption or desorption was observed.

3. GRAPHITE SAMPLES

The H-451 graphite was made by Great Lakes Carbon Co. as a preproduction run and was supplied to Oak Ridge National Laboratory (ORNL) by General Atomic Co. as Lot No. 408.[8] The crucibles for the iodine adsorption tests were cut from billet No. 5651-91B, slab No. 1, block L3 (ORNL designations). This location is close to the center of a cylindrical extrusion so that the crucibles should have characteristics similar to "low-density" H-451 specimens tested in other programs at ORNL.[8] Sample identifications and masses are given in Table 3. The measured densities and BET surface area of H-451 and typical impurities in samples from lot No. 408 are given in Tables 4 and 5. H-451 graphite was used in runs 3-8.

The S-2020 graphite was made by Stackpole Carbon Co. and came from lot No. 297D. The density, surface area, and impurity levels are given in Tables 4 and 5. This graphite was used in run 9.

The H-451 graphite has fewer impurities and a larger grain size than the S-2020. The open porosity of the H-451 graphite is much greater as shown by flow resistance listed in Table 6. After machining, each sample was cleaned with ethyl alcohol in an ultrasonic cleaner. The H-451 samples were then dried at 800°C in argon; the S-2020 sample was dried in argon at 700°C.[9]

4. EXPERIMENTAL PROCEDURE

The ^{131}I tracer was purchased either from the ORNL Isotopes Sales or from New England Nuclear Corp. as NaI in aqueous solution. Usually 10 mCi was ordered and allowed to decay to 5 mCi before preparing the iodine source. The source preparation procedure has been described previously.[1]

Following preparation, the iodine source in a breakseal tube and two aliquots of the diluted NaI solution were counted to determine the specific activity of the iodine.

After the source tube was fused to the system, the adsorption apparatus was then evacuated to ~1.3 to 2.7 Pa (~10 to 20 μm Hg); then the graphite was heated to 250°C. The flow of purified helium was established at ~30 cm^3/min, and the furnace temperature was raised to 1000°C for overnight bakeout with purging.

The radioactive iodine was transferred from the sealed source tube to the refrigerated saturator tube by the following procedure. The refrigerator was set at -50°C (-83°C in runs 3 and 4), the valve at the outlet of the furnace was closed, and the valve to the bypass charcoal cartridge was opened. Helium flow through the saturator tube was set at ~10 cm^3/min and the dilution flow at ~20 cm^3/min. The apparatus arrangement of Fig. 3 enabled the helium dilution flow to prevent diffusion of iodine into the furnace tube. The seal on the source tube was then broken, and the radioactivities of the saturator tube and bypass charcoal were monitored with portable instruments. The source tube and tubing connecting it to the saturator inlet flow line were heated to improve the rate of transfer of iodine vapor. Several hours were usually required because of the length of small tubing and the small opening in the breakseal. The transfer process both loaded the saturator tube and purged out volatile forms of iodine such as CH_3I that might have existed in the original iodine source. When essentially all of the iodine was transferred, the source tube was sealed off and removed.

The refrigerator temperature was then adjusted to the temperature expected to give the desired pressure of iodine. A fresh charcoal cartridge was placed in the bypass system for measurement of the rate of transport of iodine and calculation of the iodine pressure. This charcoal cartridge was replaced after ~2 h of flow for an overnight measurement. Usually three charcoal cartridges were used during this iodine pressure determination period.

The refrigerator temperature required to obtain a desired iodine pressure was usually within 2°C of that used in the following equation:

$$P = e^{\left(\frac{8088.5}{T} - 2.013 \ln T + 30.795\right)},$$

where

T = temperature (K),

P = pressure of iodine (bar).

When the helium-iodine mixture enters the heated furnace, the I_2 decomposes to form I; the amount of decomposition is greater at higher temperatures and lower pressures of iodine.[2,3,10] In this report the iodine concentration or partial pressure is that for $(I + I_2)$. In other reports,[1-3] the $(I + I_2)$ is used to determine the iodine partial pressure and is called the iodine burden. These values are the same as the iodine concentrations (atom fraction) shown in Tables 7-13 since our tests were performed at atmospheric pressure.

The flow was then changed to the furnace tube by closing the bypass valve and opening the furnace outlet valve. The flow rates of helium through the dilution and saturator lines were adjusted to obtain the desired iodine pressure. This was normally designated as time zero for each test. In run 8 the opening of the breakseal on the iodine source tube was designated as time zero.

During most desorption tests, a small helium flow of $\approx$10 cm^3/min was taken from the helium dilution line through a capillary flow restriction tube and charcoal cartridge attached to the bypass valve. This procedure was included to ensure that iodine would not diffuse into the furnace during the desorption test. Theoretically, the "wet-test meter outflow" of Tables 4 through 13 should be ~10 cm^3/min lower than the "total input" during the desorption tests.

4.1 Run 3

This was the first run made for data collection. (Runs 1 and 2 were devoted to apparatus checkout.) Run 3 was performed at a constant temperature, ~428°C; the iodine pressure was increased in several stages during the run. Operating conditions are summarized in Table 7 and in Figs. 4 and 5. Measurements made with the multichannel analyzer (Figs. 4 and 5) were assumed to be correct. Single-channel counts were biased high

because of scatered radiation. Type H-541 graphite was used in this experiment.

4.2 Run 4

Graphite type H-451 was used in run 4 at a constant temperature of 600°C. Three different iodine pressures were used followed by desorption with pure helium, as shown in Table 8 and Fig. 6. Counting periods during the desorption were too long to obtain details of the initial rapid desorption.

4.3 Run 5

Run 5 used type H-451 graphite with the equipment modified to the arrangement shown in Fig. 3. Operating conditions are shown in Table 9, and the graphite loading measurements are summarized in Fig. 7. In this test the iodine pressure was maintained essentially constant except for periods of desorption. The graphite temperature was changed at intervals in the range 1000°C down to 250°C. Figures 8 through 11 present more details of the graphite loading. Figure 12 shows the cumulative mass of iodine transported from the saturator tube; it is the sum of the masses of iodine detected by the two NaI crystals illustrated in Fig. 3.

Within the accuracy of our measurements, equilibrium iodine loadings were reproduced at 600, 400, and 250°C following temperature changes and desorptions. This indicates essentially reversible adsorption and desorption.

The initial adsorption of iodine was often observed to be essentially quantitative when the graphite temperature was lowered to 400 or 250°C. Similar behavior was noticed in later experiments when the iodine pressure was increased while the graphite remained at either 400 or 250°C. Forced flow of the iodine-helium mixture through the pores of the cup-shaped graphite specimens made this possible. Figure 13 demonstrates this behavior for the first 4 h following a temperature reduction at 27.8×10^5 s from the start of the run.

A plant-wide power failure which allowed the furnace to cool to ~27°C occurred on a Friday evening at 6.1×10^5 s. All helium flow was

stopped, and heaters were turned off until Monday morning. Power to the refrigerator for the iodine saturator tube and gamma-counting system was resumed after ~2 h. As shown in Figs. 7 and 8, the pickup of iodine by the graphite during this "no-flow" period must have come from iodine previously deposited in the quartz tubing.

4.4 Run 6

This run was similar to run 5 except that the iodine concentration (pressure) in the helium was lower by a factor of approximately 100. Data summaries appear in Table 10 and Fig. 14. Details of the temperature reduction at 10.43×10^5 s appear in Fig. 15, where essentially quantitative sorption of iodine occurred for ~4 h.

The temperature increase to 800°C at 20.787×10^5 s (Fig. 16) resulted in a reduction to an iodine loading on graphite of 3×10^{-3} μg/g (2×10^{-2} μg iodine, total) compared with a previous equilibrium loading of 3×10^{-4} μg/g (2×10^{-3} μg iodine, total). The decrease in graphite temperature to 600°C at 21.736×10^5 s resulted in a loss of iodine to approximately the previous equilibrium loading at 600°C. This behavior, seen in Fig. 14, is more detailed in Fig. 17. The incomplete or very slow desorption that occurred at 800°C is not understood. Further discussion of similar events appears with run 9.

Details of the desorption behavior at 400°C are shown in Fig. 18. The total amount of iodine leaving the saturator is displayed in Fig. 19.

4.5 Run 7

Data in run 7 were obtained at still lower iodine pressures followed by testing at high iodine pressures. Summaries of operating conditions and data are given in Table 11 and Fig. 20. Figure 21 presents details of sorption behavior as temperatures were decreased to 400 and 250°C.

Two stepwise ramp desorption tests were performed during run 7. After near-equilibrium loadings at 250°C, the iodine input was stopped; pure helium was then purged through the graphite. The graphite temperature was raised 50 or 100°C every 50 min. Data from these tests are shown in Figs. 22 and 23. The first test was initiated at an iodine

loading of 0.021 μg/g and the second at 0.47 μg/g. There was no observable effect of initial iodine loading on the fractional release (desorption) of iodine.

Details of iodine loading on the graphite and iodine transported to the backup filter are shown in Fig. 24 for a portion of the operating period. Total iodine transported from the saturator tube is shown in Fig. 25.

4.6 Run 8

The purpose of run 8 was to obtain additional adsorption data at the low and high pressure extremes of previous data. Operating conditions and data are summarized in Table 12 and Figs. 26-28. A seemingly permanent iodine loading of 2.3×10^{-4} μg per gram of graphite, which occurred at the beginning of the run, obscured the additional small loading changes expected at low iodine pressures and high graphite temperatures.

This permanent loading of iodine occurred while the entire loading tube—saturator tube—furnace system was evacuated to 6.565 to 26.66 Pa (50 to 200 μm Hg) pressure with the graphite temperature at ~200°C, and the iodine loading-tube seal was broken. The evacuation was performed to assist in cracking a very stubborn breakseal. The iodine source tube was cooled with liquid nitrogen and the saturator tube to -83°C at the time the loading-tube seal was broken. Approximately 3 μg of iodine that was released from the loading tube passed through the graphite specimen and was collected on the backup charcoal filter. The furnace outlet valve was closed so that no iodine escaped. The first 1000-s count following seal breakage indicated 0.5 μg of iodine on the graphite (0.076 μg/g). This quickly decreased to 0.002 μg of iodine (3×10^{-4} μg/g) as the furnace was heated to 1000°C with no helium flow through the furnace. As shown in Fig. 26, no significant change in iodine loading on the graphite was observed at 1000°C in spite of periods of desorption (starting at 1.739×10^5 s and 5.315×10^5 s) and adsorption (starting at 4.21×10^5 s). No detectable increase in iodine loading was observed until the graphite temperature was reduced to 400°C. A count taken with a tungsten plate shield placed between the furnace and main counting tube verified that

the measured radioactivity was coming from the graphite specimen and furnace tube above the NaI crystal.

When the heater for the titanium-sponge gas-cleanup trap failed at 11.2×10^5 s (Fig. 26), it appeared that the desorption of iodine might have accelerated. However, when the cleanup trap heater was deliberately turned off at 16.5×10^5 s and 26.8×10^5 s for longer periods of time, no effect on iodine sorption or desorption was observed. A commercially available dryer (Drierite) remained in service preceding the cleanup trap during the entire run as indicated in Table 1.

Near the end of the run at $\sim 40 \times 10^5$ s, the iodine saturator tube became depleted and could not maintain the desired concentration (pressure) in the flowing helium. A desorption cycle beginning at 41.3×10^5 s did not result in much additional iodine removal. The iodine loading that remained at the end of the run (Fig. 28) is suspect because of the low count rate at this time, ~0.1 count/s compared with a background of 0.6 count/s. Measurements made during disassembly of the apparatus suggest that most of the counts above background may have come from the large amount of iodine on the backup filter.

During run 8, two ramp desorption tests were made by raising the graphite temperature at the rate of ~3°C/min. Results are shown in Figs. 29-31. Total iodine from the saturator is shown in Fig. 32.

4.7 Run 9

Run 9 was the only test made with type S-2020 graphite; all others used type H-451. Nominal iodine pressures of 10^{-4} and 10^{-2} Pa (10^{-9} and 10^{-7} bar) were used. Table 13 and Figs. 33-35 summarize the operating conditions and results.

Of special interest in this run is the observation that S-2020 graphite loses iodine when the temperature is lowered from 800 or 700°C to 600°C, as seen in Figs. 33 and 34 at 9.50×10^5 s and 27.71×10^5 s. We speculate that most of the iodine sorbed at 700 to 800°C is chemisorbed as a result of impurities in the S-2020 graphite. This behavior will be discussed later.

A temperature ramp desorption test was initiated at 22.439×10^5 s by raising the graphite temperature ~3°C/min while purging with pure helium. The results are plotted in Figs. 36 and 37. The loss of iodine during this test was not significantly different from the losses recorded for similar tests with H-451 graphite.

Details of adsorption at 250°C, desorption at 250°C, and adsorption when the temperature was increased to 700°C are shown in Fig. 38. The dip in iodine loading at 34.5×10^5 s seen in both Figs. 35 and 38 is believed to result from a rapid loss of physically adsorbed iodine followed by a slower pickup of "chemisorbed" iodine.

A second interesting phenomenon occurred with S-2020 graphite; desorption at 700°C was very sensitive to helium flow rate and its associated pressure drop through the graphite. Desorption at 700°C, which started at 38.879×10^5 s, appeared to be slower than expected (Fig. 39). When the helium purge rate was reduced at 39.012×10^5 s (to conserve helium overnight), a rapid unloading of iodine occurred. At 39.757×10^5 s the flow was reduced further with only a marginal additional reduction in iodine loading on the graphite.

To verify this behavior, iodine was again loaded to near equilibrium at 700°C and desorption was begun at 41.338×10^5 s (Figs. 35 and 40). As before, the desorption was slow; however, when the helium flow was reduced at 42.181×10^5 s, the iodine again "desorbed" rapidly. The helium flow stream was cycled between 65 and 180 cm^3/min at 42.346×10^5 s, resulting in an additional iodine unloading.

Desorption from a near equilibrium loading at 400°C was initiated at 45.029×10^5 s, as shown in Fig. 41. At 45.668×10^5 s the helium purge flow was reduced from 177 to 61 cm^3/min with no change in iodine loading. Several high-to-low flow cycles did not produce any significant change in iodine loading or desorption rate. Our tentative (but incomplete) explanation of the above behavior is that the "chemisorbed" iodine at 700°C is sensitive to flow and pressure conditions during desorption, but the iodine "physically" adsorbed at 400°C is not. The pressure at the inlet end of the graphite was 4.23 kPa (17 in. H_2O) above ambient at the high flow rate and 1.49 kPa (6 in. H_2O) above ambient at the low flow rate.

Figures 42 and 43 show the total transport of iodine from the saturator tube during the test.

5. RESULTS AND DISCUSSION

5.1 Equilibrium Loadings

The design of the apparatus facilitated rapid attainment of equilibrium iodine loadings on graphite by forcing the iodine-bearing helium to flow through the open pores of the graphite. The results for H-451 graphite obtained from runs 3 through 8 are shown in Fig. 44 and in Tables 7-12. The error bars shown in Fig. 44 are estimates of precision with large errors resulting from poor counting statistics, lack of attainment of a constant equilibrium loading, or disagreement in iodine pressures as determined by the available methods of measurement. The lines shown for each temperature (and the band for 1000°C) converge toward a single point and are intended to be guides for data evaluation. They were not determined by any mathematical best-fit method. The consistency is very good, in our opinion, especially considering the large range of iodine pressures and loadings. The greatest scatter occurs at 250 and 1000°C; poor counting statistics for the low iodine loadings at 1000°C may caused most of that scatter. Sorption isotherms for S-2020 graphite are shown in Fig. 45.

Direct comparison of our results with those of others[2-6] is difficult because of different test parameters: graphite type, graphite form (compact or powder), iodine pressure range, temperature range, and the use of a carrier gas (helium in our case, vacuum in most other tests). Since sorption measurements at 400°C were common to all investigations, equilibrium iodine loadings were compared at that temperature (Fig. 46). The iodine loadings are presented as μg per m^2 of BET surface area in an attempt to compensate for the effect of the large surface areas of the powdered graphites. Loadings of the H-451 and S-2020 compacts were lower than for the other graphites.

A comparison of iodine loadings (μg per gram of graphite) as a function of temperature at a constant iodine pressure is given in Fig. 47. The peak in iodine loading at ~750°C on the S-2020 graphite is believed

to be associated with the higher impurity level in S-2020 than in H-451. Iwamoto and Oishi[6] observed a similar peak with natural graphite powder using higher iodine pressures. The natural graphite is believed to contain relatively high levels of impurities.

5.2 Adsorption Rate

When iodine was first added following desorption or when the graphite temperature was lowered, the initial adsorption was essentially quantitative at least for graphite temperatures of 400 and 250°C. At these temperatures the approach to equilibrium loading typically required 2 and occasionally 3 d. Much of this delay resulted from the slow transport of iodine from the saturator compared with the total mass required for the equilibrium loading. At higher temperatures where the required total mass of iodine was much less (and diffusion rates were higher), the time to reach equilibrium was more like 1 d.

We gave some thought to modeling this behavior, but the approach to equilibrium was often irregular and seemingly not reproducible. Very roughly speaking, one-third of the iodine was usually adsorbed without apparent restriction; the remaining two-thirds was slowed by diffusion into restricted pores or by removal of receptive sorption sites. A further complication in devising a simple sorption rate model is that all portions of the graphite specimens did not receive iodine at the same rate because the bottom was thicker than the walls. The outside bottom corners would receive an even slower supply of iodine.

5.3 Desorption

Three types of desorption tests were performed. The first, or isothermal desorption, test was performed by attaining a near-equilibrium loading and then interrupting the addition of iodine to the helium flow. The helium flow rate was usually increased to ~100 cm^3/min in order to minimize the restriction to desorption presented by readsorption from the flowing gas. The fractional release rate or loss rate observed in this type of desorption test decreased with time, suggesting delayed release of

iodine from pores with restricted access. A constant fractional desorption rate (fraction of remaining iodine lost per unit time) would appear as a straight line for data on a semilogarithmic plot such as Fig. 41. Isothermal desorption data could usually be correlated when the log of the fraction of iodine remaining (or the mass of iodine remaining) was plotted against the square root of time, as in Fig. 48. The 400°C isothermal desorption data for S-2020 graphite shown in Fig. 41 were very similar to those for H-451, run 6, at 400°C when plotted as in Fig. 48. Not all isothermal desorption data behaved in this manner. As discussed previously, the desorptions at 700°C from S-2020 graphite were sensitive to pressure and flow changes.

In the second type of desorption test, the graphite temperature was raised following attainment of an equilibrium loading while the iodine pressure was maintained constant.

The third type of desorption test was a temperature ramp from an equilibrium loading at 250°C at a ramp rate of ~3°C/min. Pure helium was used during the heatup; the ramp was performed in small steps, usually 5°C every 100 s or 10°C every 200 s. A longer desorption time at 250°C was taken during a run 8 test before starting the temperature ramp. During run 7, two tests were performed in which the temperature was raised 50 or 100°C every 50 min.

The ramp tests were performed in the hope of obtaining information regarding the strength of the iodine-graphite bond. Analysis of the data indicated that the rate-limiting steps for desorption in our tests were probably controlled by diffusion and transport in the helium and by diffusion from restricted pores rather than by the strength of the sorption bond. Calculations showed that the concentration (pressure) of iodine in the helium exiting from the graphite shortly after desorption began was approximately equal to that required to reach the equilibrium adsorption loading. There was a greater difference when high helium flow rates were used for desorption.

5.4 Iodine Deposition on Quartz and Other Materials

Iodine deposited in small amounts on the heated surfaces of quartz and other materials even at ~200°C. This was especially true in the

region following the graphite specimen; a higher proportion of the iodine leaving the furnace plated out shortly after the run started. For example, at 8.431×10^5 s in run 5 during the cooldown following the power failure, the backup charcoal filters that were removed contained only 2.8 μg of iodine, compared with 22 μg that was counted by the NaI crystal located at the furnace outlet. Similar behavior was verified in run 5 and later runs by occasionally placing a tungsten sheet absorber between the first charcoal filter and the crystal. At the beginning of each run, most of the iodine plated out on quartz surfaces near the outlet of the furnace, both inside and outside the furnace housing. Some iodine collected on the Teflon plug which was used to stopper the main furnace tube and divert flow to the side stream containing the charcoal filters. It was not determined whether this plateout at >200°C was caused by sorption of iodine on the various surfaces or by the formation of a form of iodine from impurities in the graphite that could condense at ~200°C. Table 14 shows the amounts of iodine distributed throughout the apparatus at the end of several of the runs. Very little iodine was found to be deposited on quartz at the inlet to the furnace; this tubing was made with smaller diameter beginning with run 5. The iodine material balance was good in most runs, but the deviation was more than 10% in runs 6 and 8.

6. CONCLUSIONS

Equilibrium adsorption data were generally well-behaved and reproducible with the six samples of H-451 graphite taken from the same block. Type S-2020 graphite sorbed more iodine, especially in the temperature range 700 to 800°C. The amounts of iodine adsorbed on both types of graphite were less than the sorptions previously reported by others for different graphites; however, most earlier measurements were made under different conditions, usually with powdered graphite and in vacuum. Although desorption appeared to initiate as reversible sorption, the rate of loss of iodine decreased with time. During desorption from S-2020 graphite at 700 to 800°C, a temporary plateau was reached that was sensitive to helium flow and pressure.

7. REFERENCES

1. M. F. Osborne, R. B. Briggs, and R. P. Wichner, *Iodine Sorption on Low-Chromium Alloy Steel*, ORNL/TM-7755 (January 1982)

2. E. L. Compere, M. F. Osborne, and H. J. de Nordwall, *Iodine Behavior in an HTGR*, ORNL/TM-4744 (February 1975).

3. M. F. Osborne, E. L. Compere, and H. J. de Nordwall, *Studies of Iodine Adsorption and Desorption on HTGR Coolant Circuit Materials*, ORNL/TM-5094 (April 1976).

4. Public Service Company of Colorado 330-MW(E) High-Temperature Gas-Cooled Reactor Research and Development Program, *Quarterly Progress Report for the Period Ending September 30, 1967*, GA-8270, pp. 162-64 (October 1967).

5. P. Connor, J. B. Lewis, and W. J. Thomas, "The Adsorption of Iodine by Graphite," pp. 120-24 in *Proceedings Of The Fifth Conference on Carbon*, Vol. 1, S. Mrozowski, M. L. Studebaker, P. L. Walker, Jr., eds., Pergamon Press, New York, 1962.

6. K. Iwamoto and J. Oishi, "The Behavior of Iodine in Adsorption and Desorption by Graphite," *J. Nucl. Sci. Technol.* 5(9), 437-46 (1968).

7. F. J. Salzano, "The Behavior of Iodine in Graphite," *Carbon* 2, 73-84 (1964).

8. W. J. Eatherly, Metals and Ceramics Division, ORNL, personal communication to R. A. Lorenz, 1981.

9. C. R. Kennedy, Metals and Ceramics Division, ORNL, personal communication to R. A. Lorenz, 1981.

10. E. Hoinkis, *A Review of the Adsorption of Iodine on Metal and Its Behavior in Loops*, ORNL/TM-2916 (1970).

8. TABLES AND FIGURES

Table 1. Helium cleanup system

Run	Cleanup material[a]	Temperature (°C)
3	Zirconium chips	487-520
4	Zirconium chips	649-672
5	Zirconium chips	600-670
6	Zirconium chips	616-774[b]
7	Zirconium chips[c]	638-668
8	Titanium sponge[d]	778-860[e]
9	Titanium sponge[d]	816-860

[a]Volume of container, ~100 cm^3.

[b]<752°C after 16.5×10^5 s.

[c]Liquid nitrogen—cooled trap followed zirconium chips.

[d]Drierite cartridge located before Titanium sponge; no liquid nitrogen—cooled trap.

[e]Temperature ~25°C from 11.250×10^5 to 11.390×10^5 s, 16.547×10^5 to 17.145×10^5 s, and 26.793×10^5 to 29.220×10^5 s.

Table 2. Analysis of helium tank gas (in vol %)

Component	Run 8	Run 8	Run 9	Run 9
Ar	<0.0001	<0.0001	<0.0001	<0.0001
O_2	0.0004	0.0002	<0.0001	0.0006
N_2 + CO	0.0026	0.0008	0.0005	0.0029
CO_2	<0.0001	<0.0001	<0.0001	<0.0001
H_2O	<0.0002	<0.0002	0.0002	0.0005
H_2	0.0001	<0.0001	<0.0001	<0.0001
He	99.995	99.997	99.998	99.994
Ne	0.0019	0.0020	0.0019	0.0020

Table 3. Graphite sample data

Run	Graphite type	Sample	Graphite mass (g)	
			Beginning of run	End of run
3	H-451	4	6.3976	
4	H-451	5	6.5826	6.5100
5	H-451	6	6.5334	6.4800
6	H-451	7	6.6119	6.5609
7	H-451	8	6.6280	6.5802
8	H-451	9	6.6334	
9	S-2020	1	6.4829	

Table 4. Properties of graphites

Property	Graphite type	
	H-451	S-2020[a]
Bulk density,[b] g/cm^3	1.72	1.76
Helium density, g/cm^3	2.05-2.06	2.03-2.05
Helium density (degassed),[c] g/cm^3	2.08-2.10	2.04-2.05
BET surface area, m^2/g	0.96	0.36

[a]Sample taken from same billet as our test specimens, but not necessarily from nearby location.

[b]Determined from crucible dimensions and weight.

[c]Same samples after degassing overnight at 350°C.

Table 5. Impurities in graphite as determined by neutron activation[a]

Element	Impurity concentration (μg/g)	
	H-451	S-2020
Ca	<2	280
Ti	1.5	65
Fe	5	35
Al	1	28
Mg	5	26
V	6	18
Ba	0.1	15
K	1	9
Cl	5	7
Zn	2	3
Na	1.5	3
Cr	2	2
Ce	<0.01	2
Nd	<0.05	1
La	0.005	1
Mo	0.9	0.5
Sc	<0.0001	0.4
Mn	0.02	0.1
W	0.03	0.1
I	0.025	<0.1
Br	0.015	0.06
Ag	0.04	<0.08
Ni	<14.0	<14.0

[a]Median of several analyses.

Table 6. Pressure drop across graphite crucibles for a helium flow rate of 70 cm^3/min (at 20°C)

Graphite	Temperature (°C)	Pressure drop	
		kPa	in. H_2O
H-451	22	0.42	1.7
	250	1.02	4.1
	800	1.73	7.0
S-2020	22	6.23	25.0
	250	1.05	4.2[a]
	800	1.99	8.0[a]

[a]Low pressure drop believed to result from poor seal between graphite cup and quartz furnace tube.

Table 7. Operating conditions for run 3

Time at start of period (10^5 s)	Graphite temperature (°C)	Iodine saturator temperature (°C)	Helium flow rate (cm^3/min at 20°C)			Iodine concentration (atom fraction)	$p(I + I_2)$ (bar)	Equilibrium iodine loading on graphite (μg/g)
			Saturator input	Dilution input	Total input			
0.0	425	-67.3	12.1	40.7	52.8	2.06×10^{-9}	2.06×10^{-9}	0.023 ± 0.005
5.406	425	-58.3	12.1	40.7	52.8	9.80×10^{-9}	9.70×10^{-9}	0.04 ± 0.01
6.742	427	-53.1	12.5	44.8	57.3	2.16×10^{-8}	2.13×10^{-8}	0.07 ± 0.005
17.286	428	-37.9	12.7	44.8	57.5	2.08×10^{-7}	1.89×10^{-7}	0.24 ± 0.005
19.080	428	-37.9	4.1	14.7	18.8	2.04×10^{-7}	1.86×10^{-7}	
20.850	428	-29.7	3.9	13.3	17.2	6.32×10^{-7}	5.40×10^{-7}	0.4 ± 0.1
22.122	428	-83.9	3.9	13.3	17.2	7.70×10^{-11}	7.70×10^{-11}	
24.096	429	-29.8	3.9	13.3	17.2	6.24×10^{-7}	5.30×10^{-7}	0.37 ± 0.05
26.667	429	-84.4	0.0	13.3	13.3			
32.865[a]								

[a]End of run.

Table 8. Operating conditions for run 4

Time at start of period (10^5 s)	Graphite temperature (°C)	Iodine saturator temperature (°C)	Helium flow rate (cm^3/min at 20°C)				Iodine concentration (atom fraction)				$p(I + I_2)$ (bar)	Equilibrium iodine loading on graphite (μg/g)
			Saturator input	Dilution input	Total input	Wet-test meter outflow	From input data	From backup filter	From bypass filter	Best estimate		
0.0	600	-63.7	6.26	66.1	72.4	76.3	1.47×10^{-9}	1.04×10^{-9}	1.98×10^{-9}	1.7×10^{-9}	1.7×10^{-9}	0.0008 ± 0.0001
6.045	600	-63.7	6.62	0.97	7.59	9.08	1.49×10^{-8}	1.91×10^{-8}		1.7×10^{-8}	1.7×10^{-8}	0.005 ± 0.001
22.642	600	-47.8	3.03	0.10	3.13	3.24	2.18×10^{-7}	2.08×10^{-7}	2.60×10^{-7}	2.2×10^{-7}	2.2×10^{-7}	0.045 ± 0.003
27.824	600	-84.0	0.0	65.4	65.4							
30.180[a]												

[a]End of run.

Table 9. Operating conditions for run 5

Time at start of period (10^5 s)	Graphite temperature (°C)	Iodine saturator temperature (°C)	Helium flow rate (cm^3/min at 20°C)				Iodine concentration (atom fraction)				$p(I + I_2)$ (bar)	Equilibrium iodine loading on graphite (μg/g)
			Saturator input	Dilution input	Total input	Wet-test meter outflow	From input data	From backup filter	From bypass filter	Best estimate		
0.0	1000	-49.7	2.70	0.09	2.79	2.69	1.63×10^{-7}	1.48×10^{-7}	1.36×10^{-7}	1.5×10^{-7}	1.5×10^{-7}	0.0002 ± 0.00002
3.278	800	-49.7	2.70	0.09	2.79	3.00	1.63×10^{-7}	1.58×10^{-7}		1.6×10^{-7}	1.6×10^{-7}	0.008 ± 0.001
6.117	27	[a]	0.0	0.0	0.0							
8.417	27	-49.7	0.0	64.9	64.9		0.0					
8.491	800	-49.7	0.0	61.6	61.6		0.0					
8.533	800	-49.7	2.73	0.15	2.88		1.60×10^{-7}			1.6×10^{-7}	1.6×10^{-7}	
9.520	600	-49.7	2.70	0.09	2.79	2.91	1.63×10^{-7}			1.6×10^{-7}	1.6×10^{-7}	0.033 ± 0.003
14.667	400	-49.3	2.70	0.09	2.79	2.82	1.73×10^{-7}			1.7×10^{-7}	1.5×10^{-7}	0.43 ± 0.01
18.089	250	-49.1	12.4	0.26	12.7	12.85	1.80×10^{-7}	1.76×10^{-7}		1.8×10^{-7}	9.1×10^{-8}	1.2 ± 0.1
21.419	250	-49.1	0.0	68.1	68.1		0.0					
24.009	600	-49.1	13.3	0.54	13.8		1.78×10^{-7}			1.8×10^{-7}	1.8×10^{-7}	
24.235	600	-49.1	2.91	0.37	3.28	3.60	1.64×10^{-7}	1.44×10^{-7}		1.5×10^{-7}	1.5×10^{-7}	0.019 ± 0.001
26.593	600	-49.1	0.0	47.1	47.1		0.0					
27.572	250	-49.1	3.66	0.49	4.2	4.20	1.63×10^{-7}	1.52×10^{-7}		1.6×10^{-7}	8.1×10^{-8}	1.0 ± 0.1
32.589	400	-48.9	3.00	0.35	3.4		1.70×10^{-7}			1.7×10^{-7}	1.4×10^{-7}	0.46 ± 0.04
33.455	600	-48.9	3.00	0.35	3.4		1.70×10^{-7}			1.7×10^{-7}	1.7×10^{-7}	0.018 ± 0.003
33.744[b]												

[a] The saturator temperature reached a maximum temperature of -30°C during a 1.5-h power failure at the start of this time period.

[b] End of run.

Table 10. Operating conditions for run 6

Time at start of period (10^5 s)	Graphite temperature (°C)	Iodine saturator temperature (°C)	Helium flow rate (cm^3/min at 20°C)				Iodine concentration (atom fraction)				$p(I + I_2)$ (bar)	Equilibrium iodine loading on graphite (μg/g)
			Saturator input	Dilution input	Total input	Wet-test meter outflow	From input data	From backup filter	From bypass filter	Best estimate		
0	1000	-68.9	10.6	30.0	40.6	40.0	1.75×10^{-9}	1.97×10^{-9}	2.06×10^{-9}	2.0×10^{-9}	2.0×10^{-9}	0.000065 ± 0.00003
2.720	800	-69.6	10.5	31.0	41.5	40.7	1.49×10^{-9}	2.00×10^{-9}		2.0×10^{-9}	2.0×10^{-9}	0.00033 ± 0.00005
6.134	600	-69.5	4.00	10.8	14.8	14.9	1.62×10^{-9}	1.80×10^{-9}		1.8×10^{-9}	1.8×10^{-9}	0.0007 ± 0.0001
10.430	400	-69.4	3.61	10.4	14.0	14.1	1.58×10^{-9}	1.42×10^{-9}		1.5×10^{-9}	1.5×10^{-9}	0.021 ± 0.001
16.599	250	-68.9	14.0	38.2	52.2	54.1	1.80×10^{-9}	1.78×10^{-9}	1.80×10^{-9}	1.8×10^{-9}	1.1×10^{-9}	0.09 ± 0.005
20.787	800	-68.9	14.0	38.3	52.3	50.4						
21.736	600	-68.9	13.1	36.7	49.8	48.7	1.77×10^{-9}	1.16×10^{-9}		1.3×10^{-9}	1.3×10^{-9}	0.0007 ± 0.0002
23.315	250	-68.9	13.4	38.4	51.8	50.4						
23.487	400	-68.9	13.1	38.2	51.3	50.0	1.72×10^{-9}	1.25×10^{-9}		1.3×10^{-9}	1.3×10^{-9}	0.019 ± 0.004
24.372	400	-68.9	0.0	62.1	62.1	61.6	0.00					
26.758	250	-68.9	12.8	36.9	49.7	48.8	1.73×10^{-9}	0.99×10^{-9}		1.2×10^{-9}	7.5×10^{-10}	0.083 ± 0.01
30.401	250	-84.1	0.0	66.4	66.4	65.2						
33.730[a]												

[a] End of run.

Table 11. Operating conditions for run 7

Time at start of period (10^5 s)	Graphite temperature (°C)	Iodine saturator temperature (°C)	Helium flow rate (cm^3/min at 20°C)				Iodine concentration (atom fraction)				$p(I + I_2)$ (bar)	Equilibrium iodine loading on graphite (μg/g)
			Saturator input	Dilution input	Total input	Wet-test meter outflow	From input data	From backup filter	From bypass filter	Best estimate		
0	1000	-83.0	7.9	61.6	69.5	71.1	4.68×10^{-11}	1.21×10^{-10}	1.21×10^{-10}	1.1×10^{-10}	1.1×10^{-10}	<0.00002
1.666	800	-83.0	8.9	67.6	76.5	74.6	4.78×10^{-11}	9.2×10^{-11}		9.2×10^{-11}	9.2×10^{-11}	0.000033 ± 0.00001
4.190	600	-83.0	9.6	67.7	77.3	78.2	5.12×10^{-11}	9.8×10^{-11}		9.8×10^{-11}	9.8×10^{-11}	0.00008 ± 0.00002
5.932	400	-82.0	10.0	69.7	79.7	80.9	6.38×10^{-11}	8.8×10^{-11}		8.8×10^{-11}	8.8×10^{-11}	0.0027 ± 0.0003
8.748	250	-80.3	9.5	66.5	76.0	76.1	9.08×10^{-11}	1.30×10^{-10}		1.3×10^{-10}	9.9×10^{-11}	0.025 ± 0.003
14.541	250	-84.0	0.0			58.7	0.0					
14.571	300	-84.0	0.0			60.7	0.0					
14.601	400	-84.0	0.0			49.5	0.0					
14.631	500	-84.0	0.0			45.6	0.0					
14.661	600	-84.0	0.0			51.8	0.0					
14.691	700	-84.0	0.0			53.6	0.0					
14.721	800	-84.0	0.0			57.4	0.0					
14.751	900	-84.0	0.0			55.9	0.0					
14.781	1000	-84.0	0.0			56.0	0.0					
14.813	1000	-69.2	0.0	0.0	0.0	0.0	0.0					
15.458	250	-61.8	12.6	62.5	75.1	74.5	3.98×10^{-9}	4.88×10^{-9}		4.6×10^{-9}	2.6×10^{-9}	0.6 ± 0.1
18.002	250	-84.0	0.0			58.5	0.0					
18.030	300	-84.0	0.0			58.7						
18.060	400	-84.0	0.0			57.7						
18.090	500	-84.0	0.0			56.8						
18.120	600	-84.0	0.0			58.3						
18.150	700	-84.0	0.0			59.2						
18.174	800	-84.0	0.0			61.5						
18.204	900	-84.0	0.0			59.2						
18.234	1000	-84.0	0.0			57.4						
18.264	800	-47.0	5.54	0.97	6.51	6.60	2.16×10^{-7}	2.74×10^{-7}		2.6×10^{-7}	2.6×10^{-7}	0.009 ± 0.002
20.643	800	-84.0	0.0	64.8	64.8	65.7	0.0					
20.831	1000	-60.7	5.00	1.05	6.1	6.26	2.36×10^{-8}		2.4×10^{-8}		2.4×10^{-8}	0.00012 ± 0.00010
22.521[a]												

[a] End of run.

Table 12. Operating conditions for run 8

Time at start of period (10^5 s)	Graphite temperature (°C)	Iodine saturator temperature (°C)	Helium flow rate (cm^3/min at 20°C)				Iodine concentration (atom fraction)				$p(I + I_2)$ (bar)	Equilibrium iodine loading on graphite (μg/g)
			Saturator input	Dilution input	Total input	Wet-test meter outflow	From input data	From backup filter	From bypass filter	Best estimate		
0	997	-50.9	0	0	0	0	[a]			0.0	0.0	
1.739	997	-82.3	0	107	100	100	0.0					
2.664	997	-84.0	0	0	0	0	[a]					
4.210	997	-84.0	4.8	124	129	168	1.2×10^{-11}		4.5×10^{-11}	3×10^{-11}	3×10^{-11}	
5.315	997	-84.0	0	158	158	175	0.0			0.0	0.0	
5.975	600	-84.0	0	158	158	170	0.0			0.0	0.0	
6.175	600	-84.0	6.5	152	159	165	1.4×10^{-11}			1.6×10^{-11}	1.6×10^{-11}	0.0002
7.005	400	-83.9	5.6	138	144	150	1.3×10^{-11}	1.1×10^{-11}	2.3×10^{-11}	1.5×10^{-11}	1.5×10^{-11}	0.0014 ± 0.0002
10.475	400	-83.7	0	187	187	200	0.0			0.0	0.0	
12.081	400	-83.7	0	0	0	0	[a]					
12.832	250	-84.1	6.0	142	148	159	1.3×10^{-11}	4.5×10^{-11}	1.93×10^{-11}	1.3×10^{-11}	1.2×10^{-11}	0.0025
17.214	250	-84.2	0	0	0	0						
18.130[b]	250	-84.2	0	135	135		0.0					
18.287	999	-63.3	0	135	135	140	0.0			0.0	0.0	
18.911	999	-63.3	0	0	0	0						
19.744	999	-63.3	5.75	11.37	17.12	19.2	6.1×10^{-9}		2.32×10^{-10}			<0.0002
20.724	800	-63.0	5.85	11.85	17.70	19.2	6.4×10^{-9}					<0.00025
22.348	600	-63.0	5.71	11.10	16.81	19.2	6.5×10^{-9}	8.3×10^{-11}				0.0002 ± 0.0001
24.077	400	-63.0	5.79	11.78	17.57	19.2	6.4×10^{-9}	8.3×10^{-11}				0.0014
28.386	400	-63.0	0	152	152	172	0.0			0.0	0.0	
29.220	250	-63.0	5.66	13.56	19.22	18.6	5.7×10^{-9}	8×10^{-11}	4.7×10^{-9}			0.0033
34.445	250	-63.2	0	0	0	0	[a]			[c]		
35.557	25	-63.2	0	0	0	0						
37.039[d]	250	-63.2	0	145	145	125	0.0			0.0	0.0	
38.121	998	-22.1	4.28	6.23	10.51	10.2	2.88×10^{-6}	2.62×10^{-6}	2.22×10^{-6}	2.6×10^{-6}	2.6×10^{-6}	0.012 ± 0.005
38.801	800	-22.0	4.26	6.34	10.60	10.0	2.91×10^{-6}	2.12×10^{-6}	2.19×10^{-6}	2.3×10^{-6}	2.3×10^{-6}	0.07 ± 0.02
41.343	800	-83.6	0	121	121	130	0.0				0.0	
42.393	997	-83.9	0	122	122	130	0.0				0.0	
43.076[e]												

[a] No flow through graphite. Flow went to bypass charcoals.

[b] At 18.140×10^5 s, graphite temperature was raised ~10°C every 200 s (3.06°C/min av); reached 1000°C at 18.287×10^5 s.

[c] Iodine in saturator was not supplying normal vapor pressure while refrigerator was at -63°C.

[d] Beginning at 37.164×10^5 s, graphite temperature was raised ~20°C every 400 s (3.04°C/min av); reached 1000°C at 37.312×10^5 s. Desorption continued at 998°C until 38.121×10^5 s.

[e] End of run.

Table 13. Operating conditions for run 9

Time at start of period (10^5 s)	Graphite temperature (°C)	Iodine saturator temperature (°C)	Helium flow rate (cm^3/min at 20°C)				Iodine concentration (atom fraction)				$p(I + I_2)$ (bar)	Equilibrium iodine loading on graphite (μg/g)
			Saturator input	Dilution input	Total input	Wet-test meter outflow	From input data	From backup filter	From bypass filter	Best estimate		
0	1000	-68.8	8.3	33.3	41.6	40.3	1.4×10^{-9}	1.3×10^{-9}	1.03×10^{-9}	1.3×10^{-9}	1.3×10^{-9}	0.0002 ± 0.00005
2.671	801	-68.9	10.3	33.6	43.9	43.7	1.6×10^{-9}	1.9×10^{-9}		1.6×10^{-9}	1.6×10^{-9}	0.005 ± 0.001
9.501	600	-68.9	8.8	35.6	44.4	45.4	1.3×10^{-9}	1.0×10^{-9}		1.2×10^{-9}	1.2×10^{-9}	0.0018 ± 0.0004
12.101	400	-68.9	9.4	35.6	45.0	46.2	1.4×10^{-9}	1.0×10^{-9}		1.2×10^{-9}	1.2×10^{-9}	0.023 ± 0.002
15.581	400	-68.9	0	<173		172.8	0			0		
17.301	250	-68.9	8.8	32.9	41.7	41.7	1.4×10^{-9}	1.2×10^{-9}		1.3×10^{-9}	8.0×10^{-10}	0.18 ± 0.02
22.439	250	-68.9	0	<158		~160	0			0		
22.467	400	-68.9	0			~150	0			0		
22.485	500	-68.9	0			~140	0			0		
22.505	600	-68.9	0			~130	0			0		
22.527	700	-68.9	0			~120	0			0		
22.547	800	-68.9	0			~110	0			0		
22.565	900	-68.9	0			~105	0			0		
22.585	1000	-68.9	0	<105		102	0			0		
23.206	1000	-49.9	0	0	0	0						
24.244	1000	-49.9	4.22	3.97	8.19	7.85	8.4×10^{-8}	7.6×10^{-8}	8.8×10^{-8}	8.4×10^{-8}	8.4×10^{-8}	0.0065
25.114	900	-49.8	4.11	3.53	7.64	7.62	8.9×10^{-8}			8.4×10^{-8}	8.4×10^{-8}	0.029 ± 0.005
25.972	800	-49.8	4.35	3.74	8.09	7.91	8.9×10^{-8}				8.4×10^{-8}	0.12 ± 0.01
26.849	700	-49.7	4.37	3.76	8.13	7.94	9.0×10^{-8}				8.4×10^{-8}	0.26 ± 0.01
27.715	600	-49.6	4.36	3.73	8.09	7.89	9.2×10^{-8}				8.4×10^{-8}	0.042 ± 0.004
28.355	550	-49.6	4.36	3.73	8.09	7.89	9.2×10^{-8}				8.4×10^{-8}	0.047 ± 0.005
28.575	500	-49.7	3.84	3.66	7.50	7.79	8.6×10^{-8}				8.4×10^{-8}	0.10
29.430	400	-49.7	4.45	3.72	8.17	5.0	9.2×10^{-8}				7.5×10^{-8}	0.30 ± 0.03
31.143	250	-49.7	5.68	5.21	10.89	10.6	8.8×10^{-8}	7.8×10^{-8}		8.3×10^{-8}	4.2×10^{-8}	0.78 ± 0.05
32.888	250	-49.7	0.0	<164		159	0			0		
34.408	700	-49.6	4.0	3.2	7.2	7.24	9.5×10^{-8}	8.4×10^{-8}		8.9×10^{-8}	8.9×10^{-8}	0.45 ± 0.05
38.879	700	-49.4	0.0			170	0			0		
39.012	700	-49.5	0.0	<57.0		54.0	0			0		
39.757	700	-49.4	0.0			17.8	0			0		
39.807	700	-49.4	4.4	3.4	7.8	7.78	9.9×10^{-8}	8.3×10^{-8}		9.1×10^{-8}	9.1×10^{-8}	0.49 ± 0.05
41.338	700	-49.4	0.0	<169		165	0			0		
42.181	700	-49.4	0.0	<45.0		52.0	0			0		
42.346	700	-49.4	0.0	cycled			0			0		
42.352	700	-49.4	0.0	cycled			0			0		
42.435	400	-49.4	7.03	1.00	8.03	7.69	1.5×10^{-7}	1.4×10^{-7}		1.4×10^{-7}	1.2×10^{-7}	1.2 ± 0.2
45.029	400	-49.4	0.0	<167		177	0			0		
45.668	400	-49.4	0.0	<64.0		61.2	0			0		
50.848	1000	-83.0	0.0	<60.0			0			0		
51.057[a]												

[a] End of run.

Table 14. Distribution of iodine (μg) at end of runs 4-9

Location	Run No. 4	5	6	7	8	9
Breakseal residue	1.2	72.5	30.6	60.9	95.8	180.4
Saturator tube	306.7	110.5	202.4	455.3	18.7	496.7
Furnace tube						
Inlet end	1.6	10.0	0.0	0.03	0.03	0.0
Outlet end	16.3		3.0	1.7	2.1	3.6
Graphite	0.03	0.18	0.29	0.034	0.009	0.011
Quartz retaining rod			0.3	1.27	0.10	3.3
Charcoal filters	45.5	182.4	7.57	42.9	543.2	103.3
Teflon plug		16.4	0.58	3.8	40.8	2.8
Bypass charcoal cartridges	11.2	26.8	49.5	10.4	206.2	12.5
Total at end of run	382.5	418.8	294.2	576.3	906.9	802.6
Original source	392.1	445.7	377.5	588.5	638.5	782.5
Specific activity of ^{131}I at start of run (μCi/μg I)		2.227	0.986	2.208	4.000	

ORNL-DWG 79-37R2

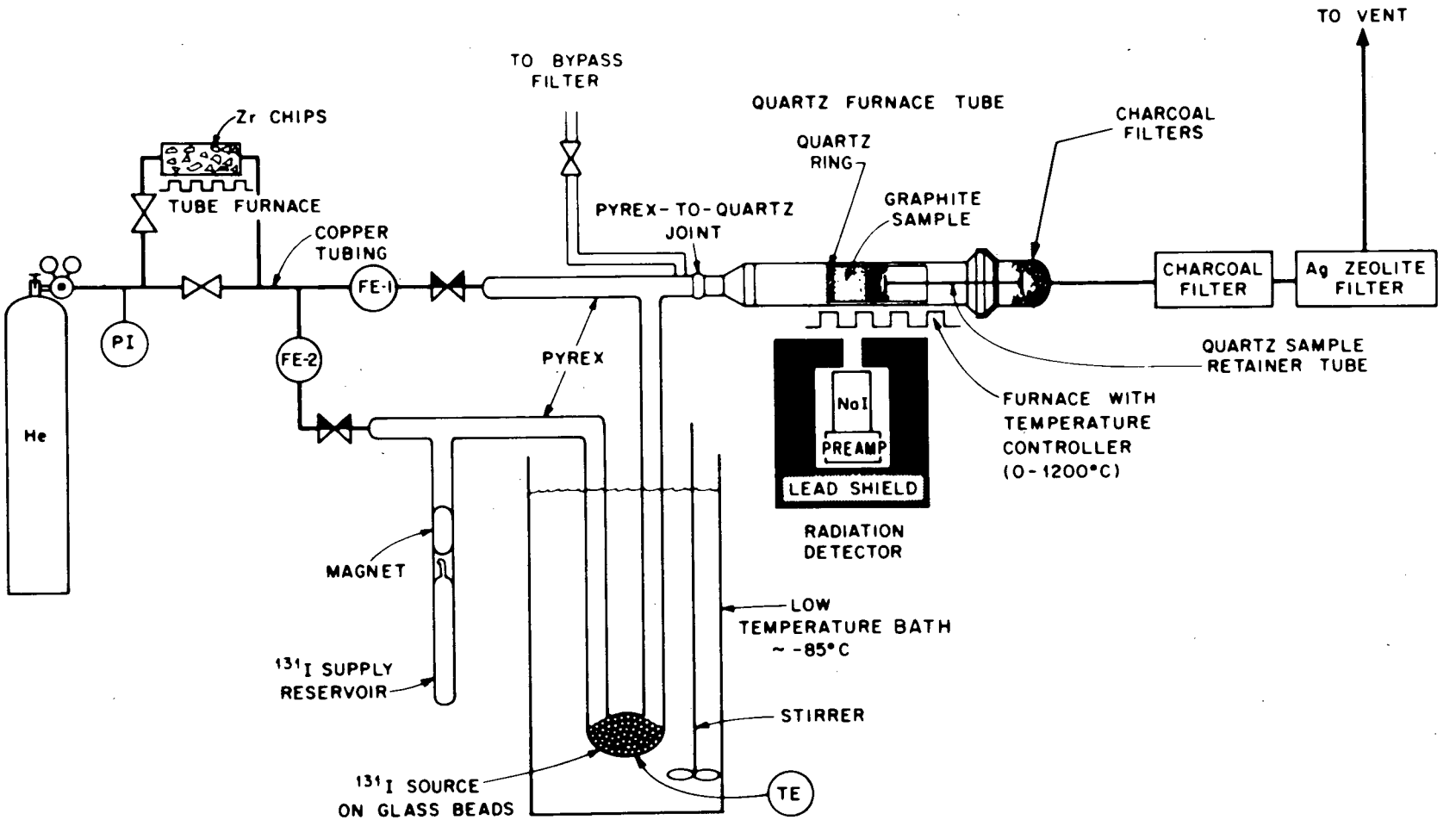

Fig. 1. Iodine sorption-desorption apparatus (runs 3 and 4), which operates at 1-bar pressure.

ORNL DWG 80-480

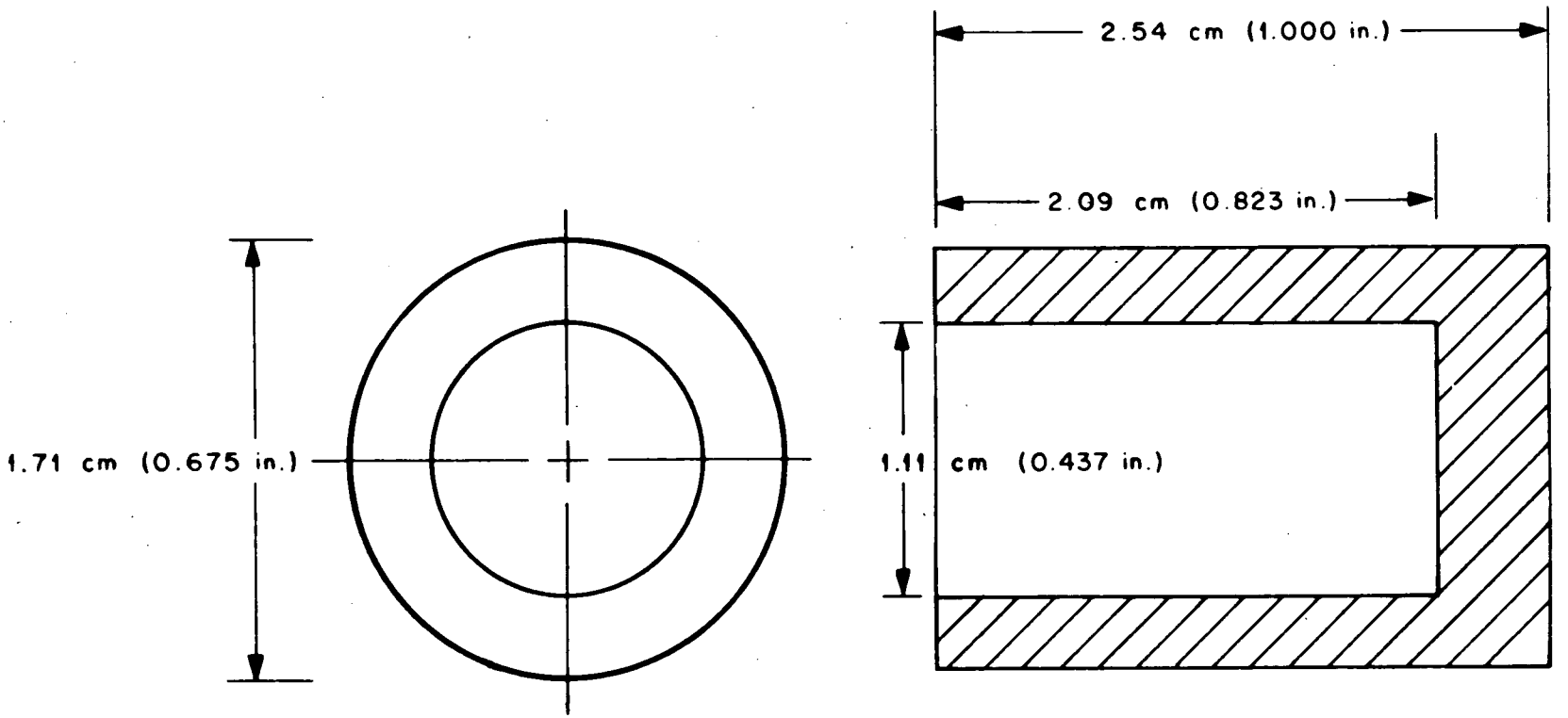

Fig. 2. Graphite test specimen.

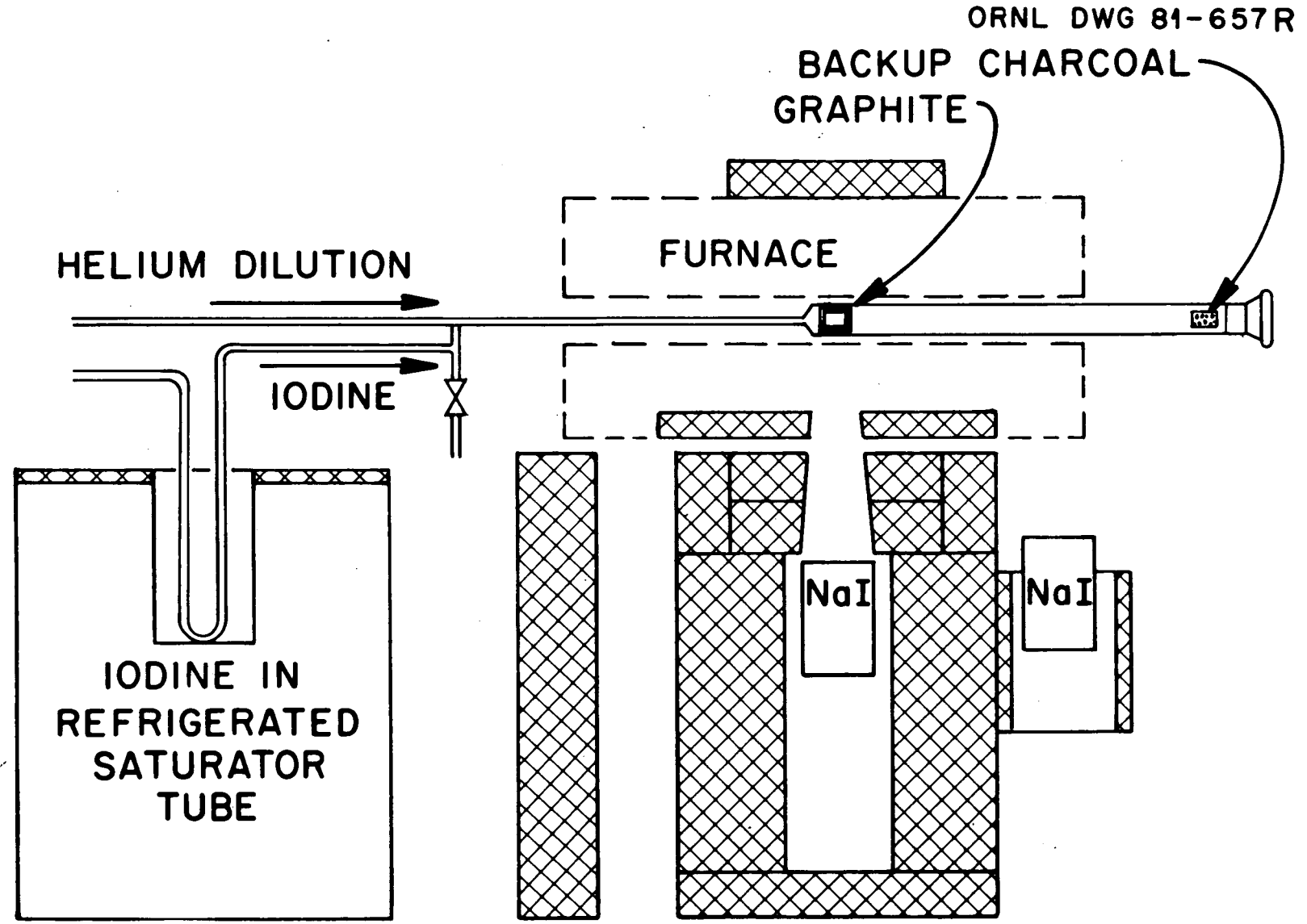

Fig. 3. Modified iodine sorption-desorption apparatus (runs 5-9).

ORNL DWG 82-962

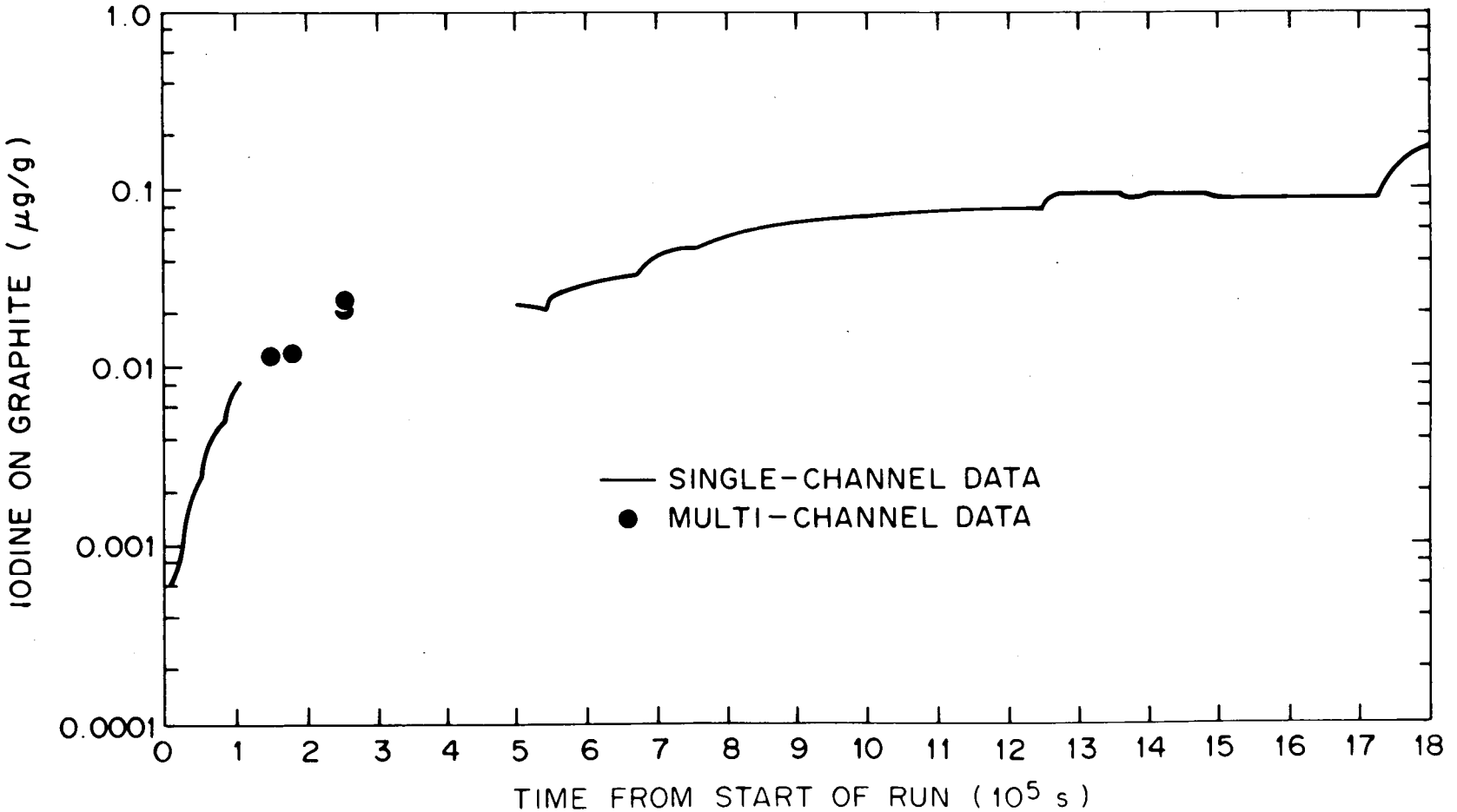

Fig. 4. Iodine loadings on graphite in run 3 (0–16.0 × 10^5 s).

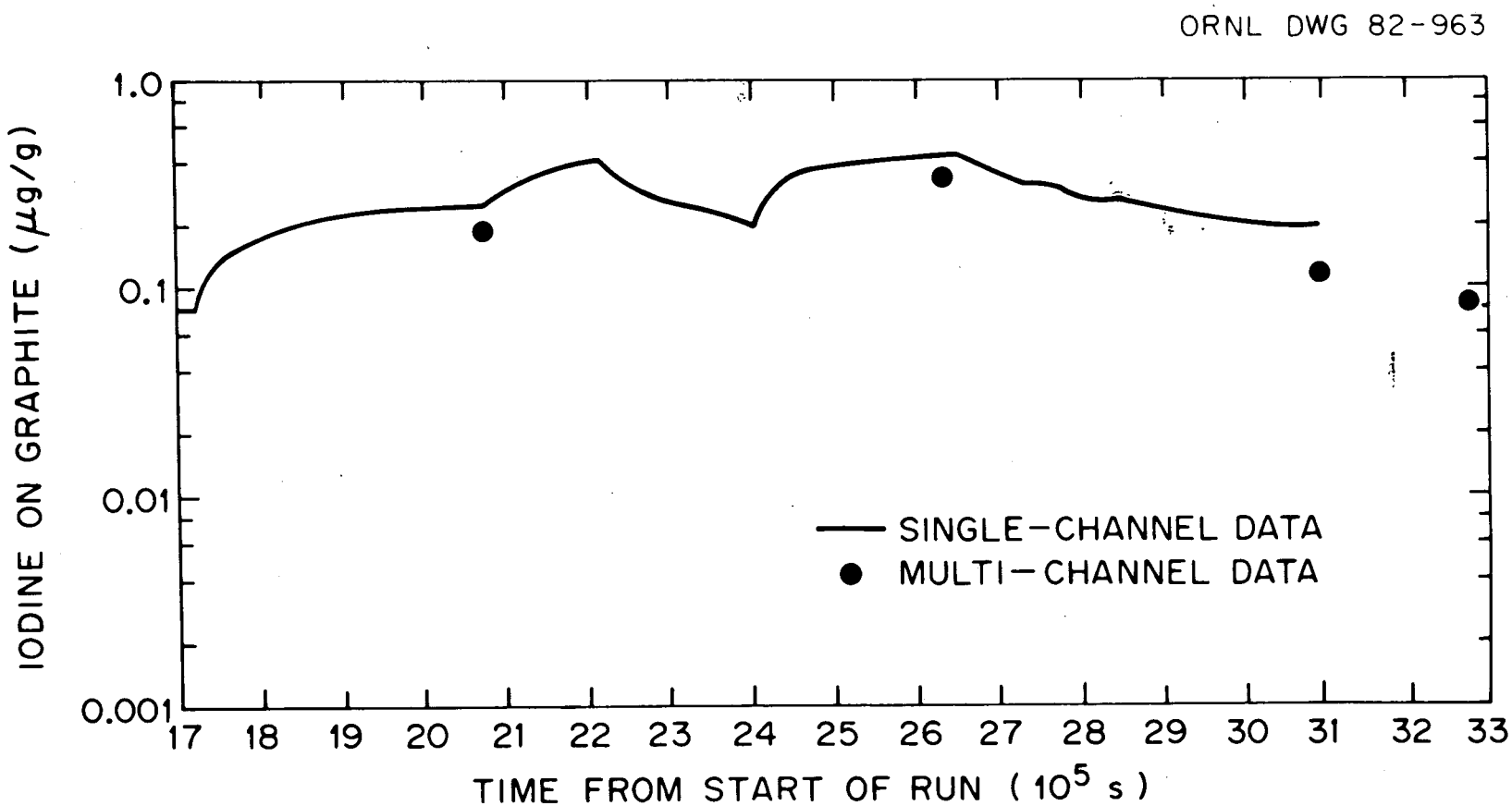

Fig. 5. Iodine loading on graphite in run 3 (17.0×10^5–34.5×10^5 s).

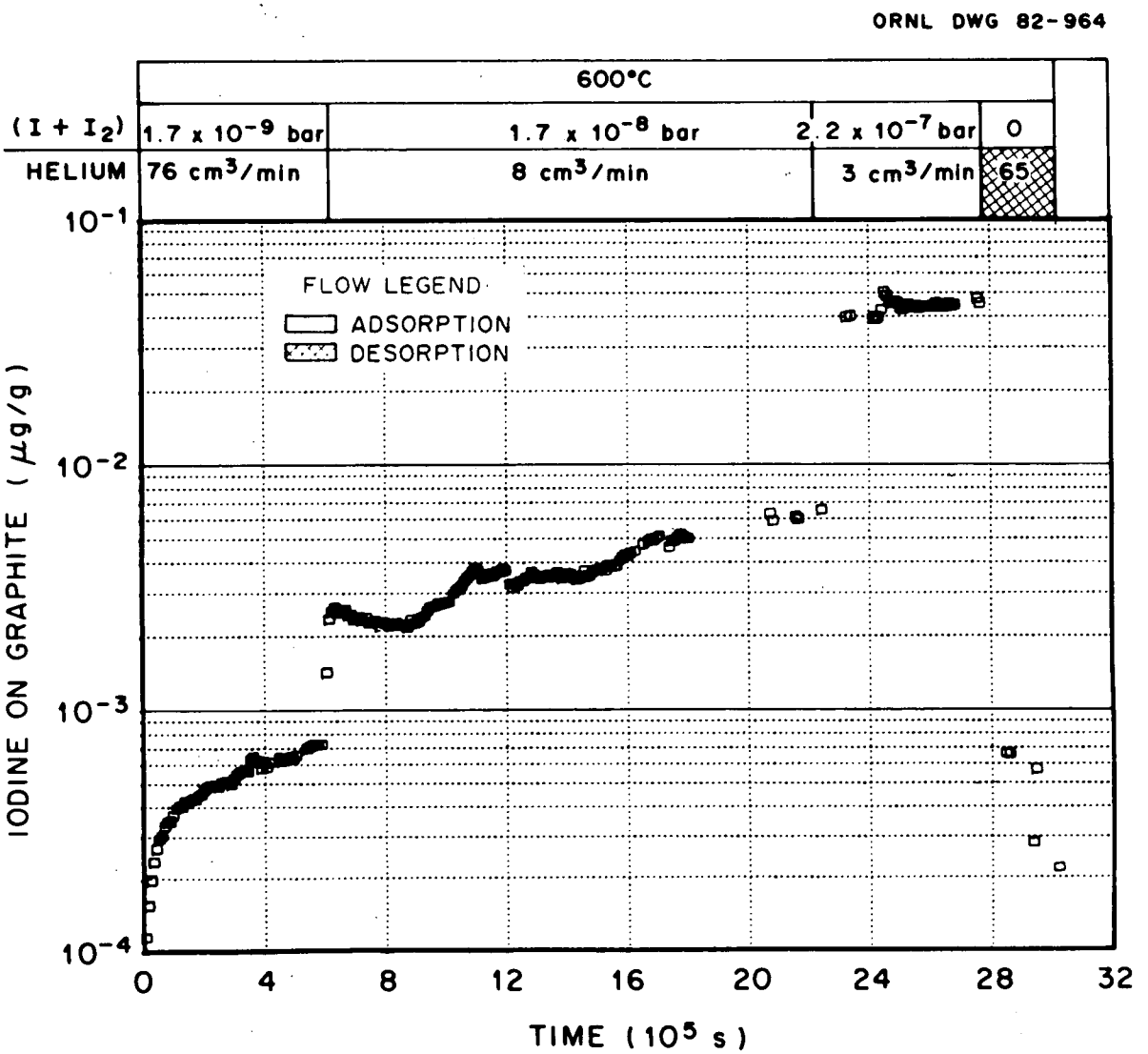

Fig. 6. Iodine loading on graphite, run 4.

ORNL DWG 82-965

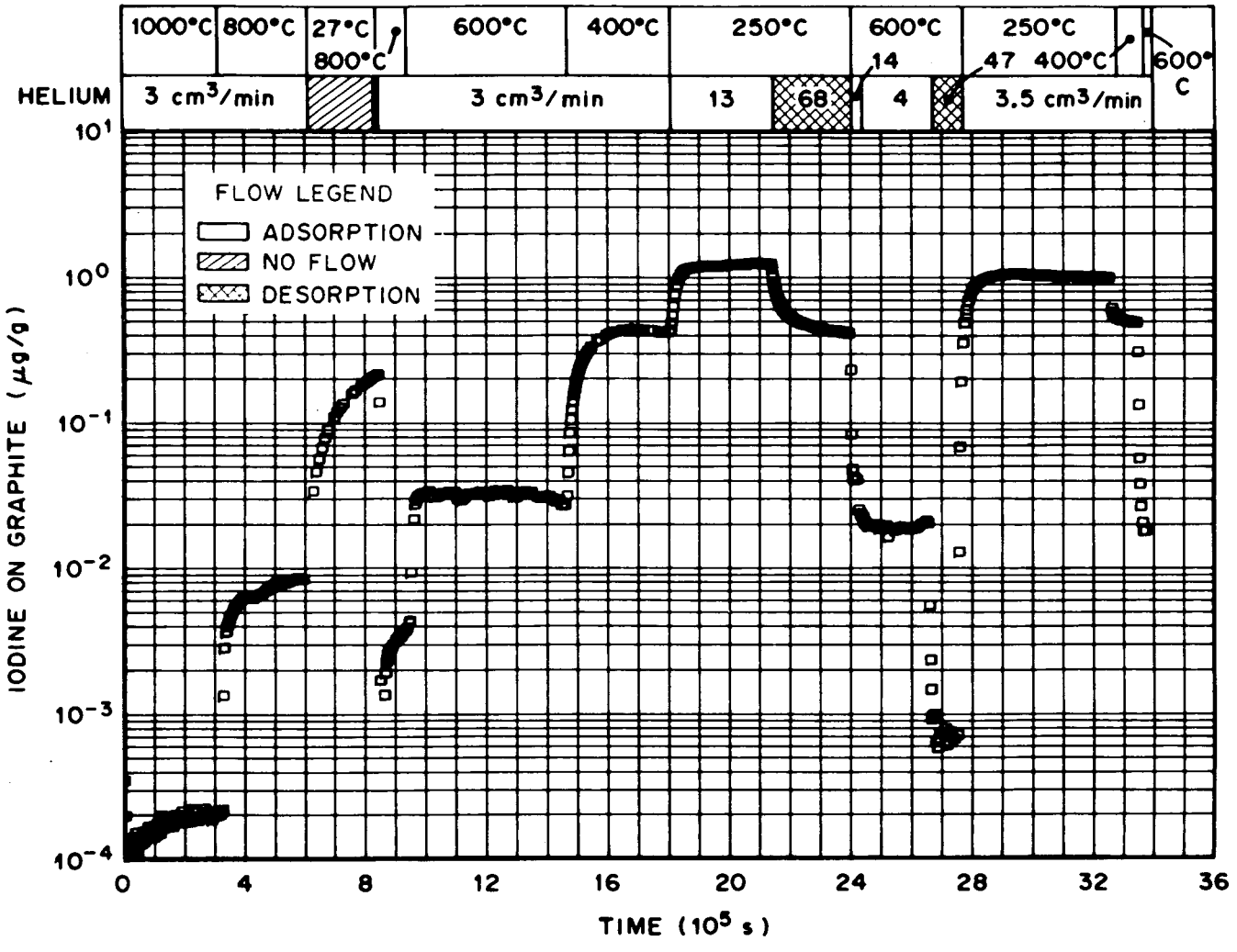

Fig. 7. Iodine loading on graphite, run 5.

ORNL DWG 82-966

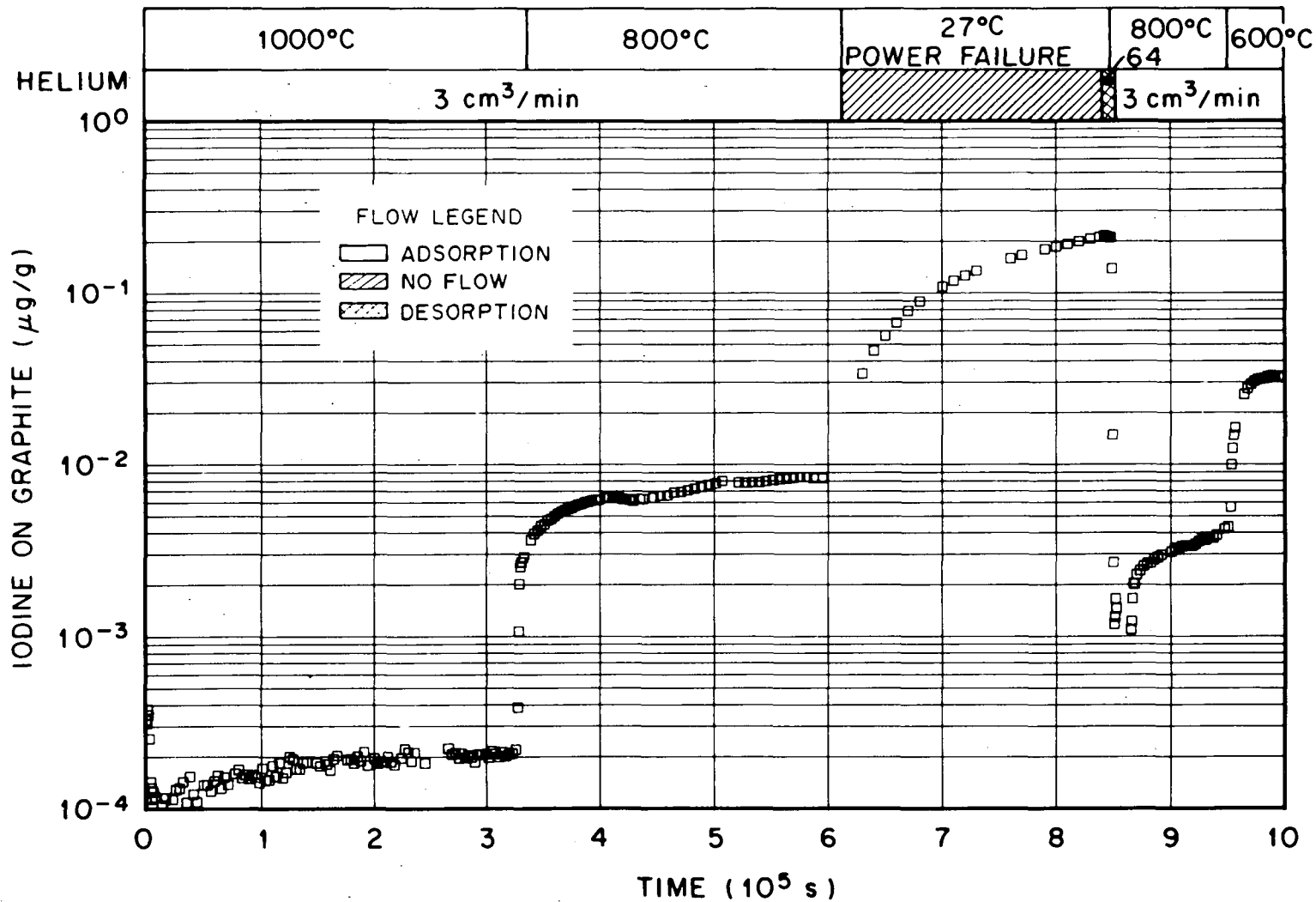

Fig. 8. Iodine loading on graphite in run 5 (0-1 × 10^6 s).

ORNL DWG 82-967

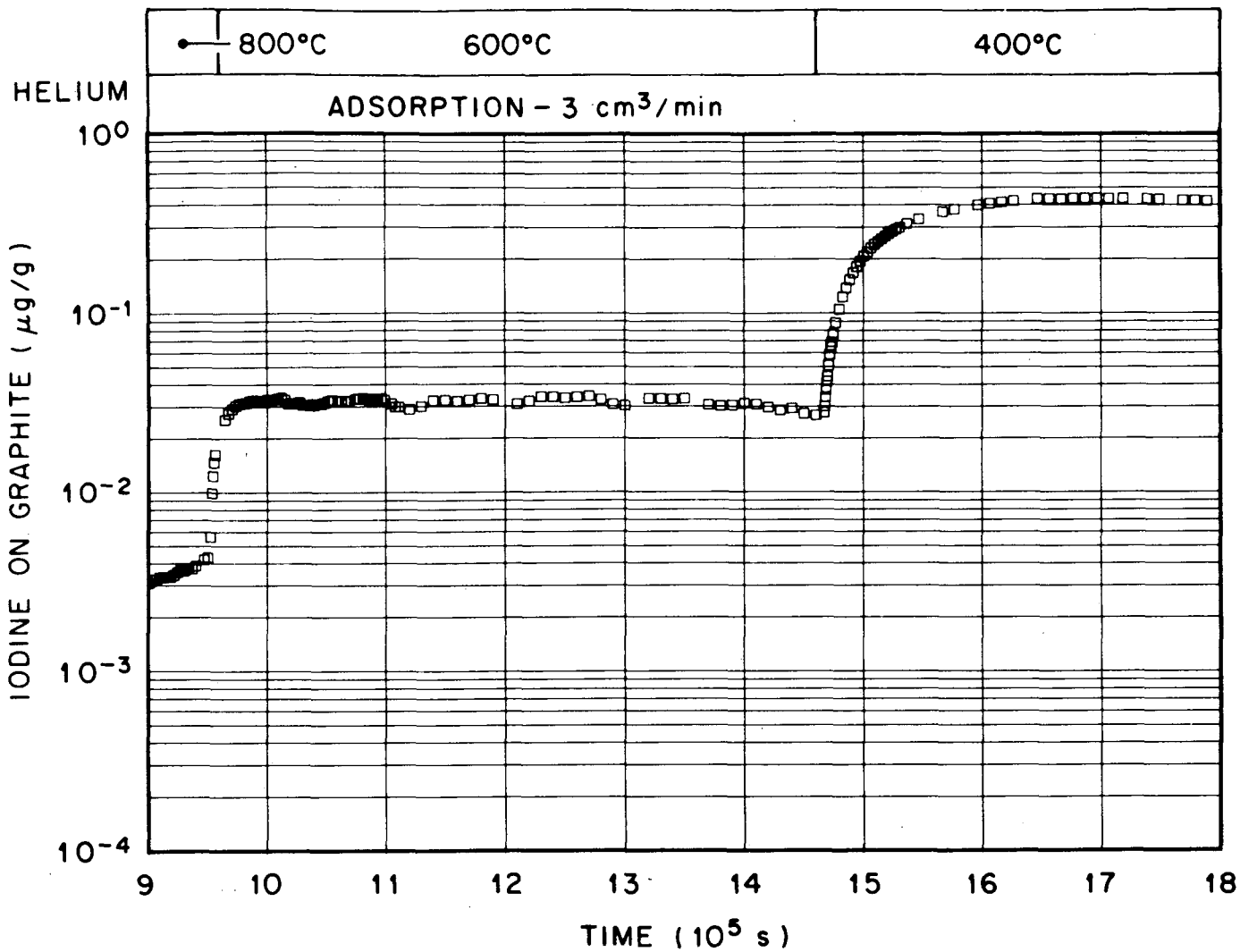

Fig. 9. Iodine loading on graphite in run 5 (9-18 × 10^5 s).

ORNL DWG 82-968

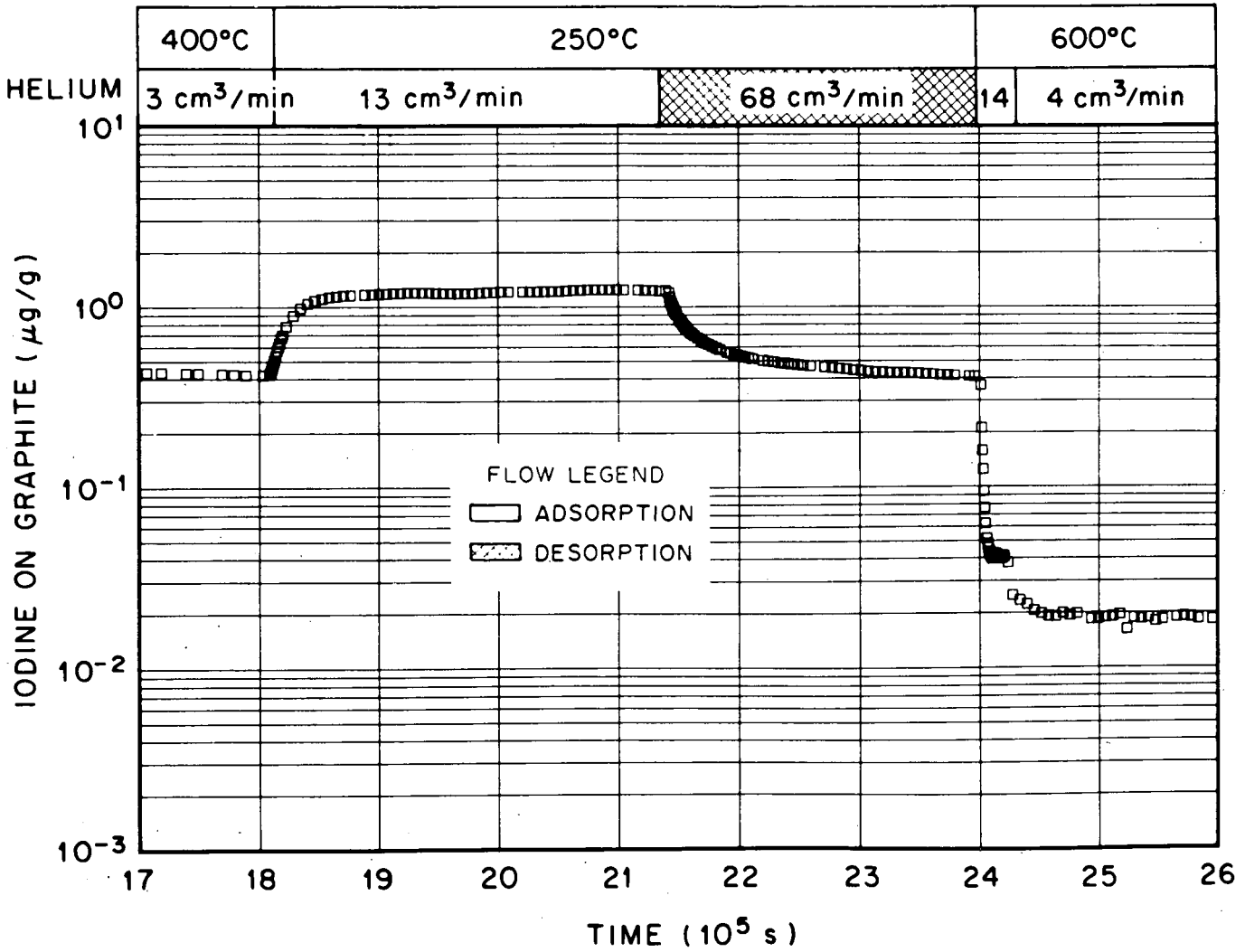

Fig. 10. Iodine loading on graphite in run 5 (17-26 × 10^5 s).

ORNL DWG 82-969R

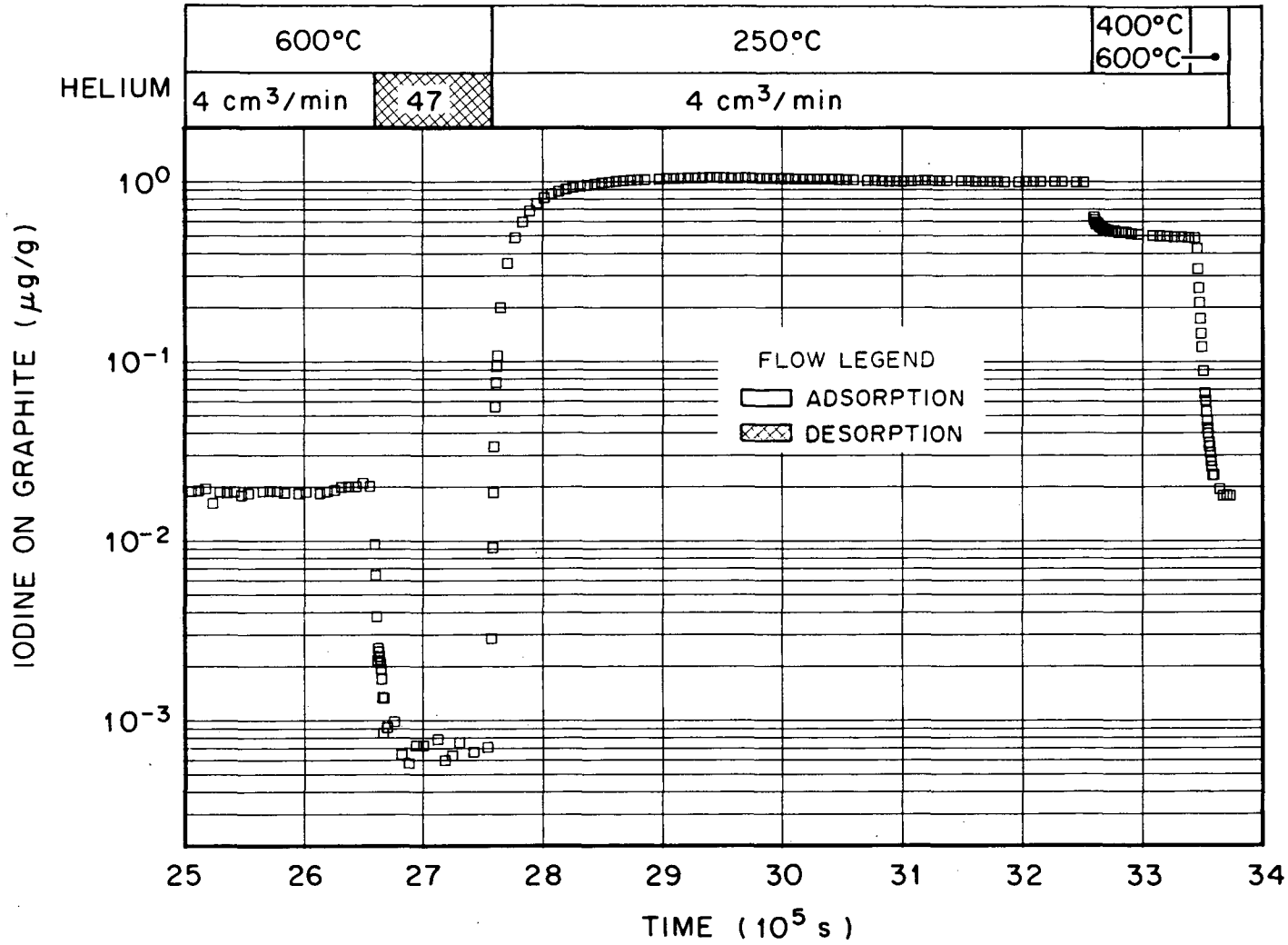

Fig. 11. Iodine loading on graphite in run 5 (25-34 × 10^5 s).

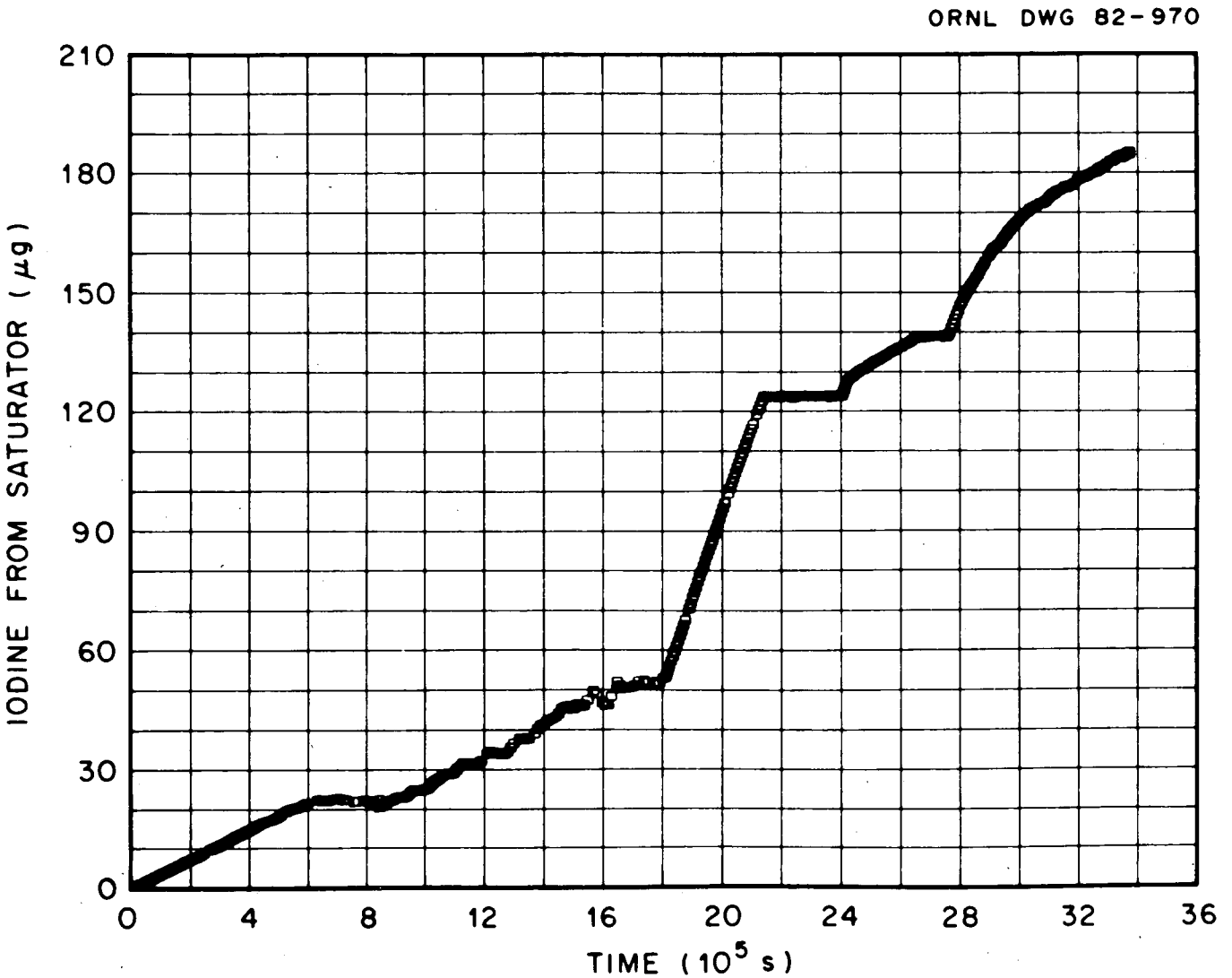

Fig. 12. Total iodine from saturator during run 5.

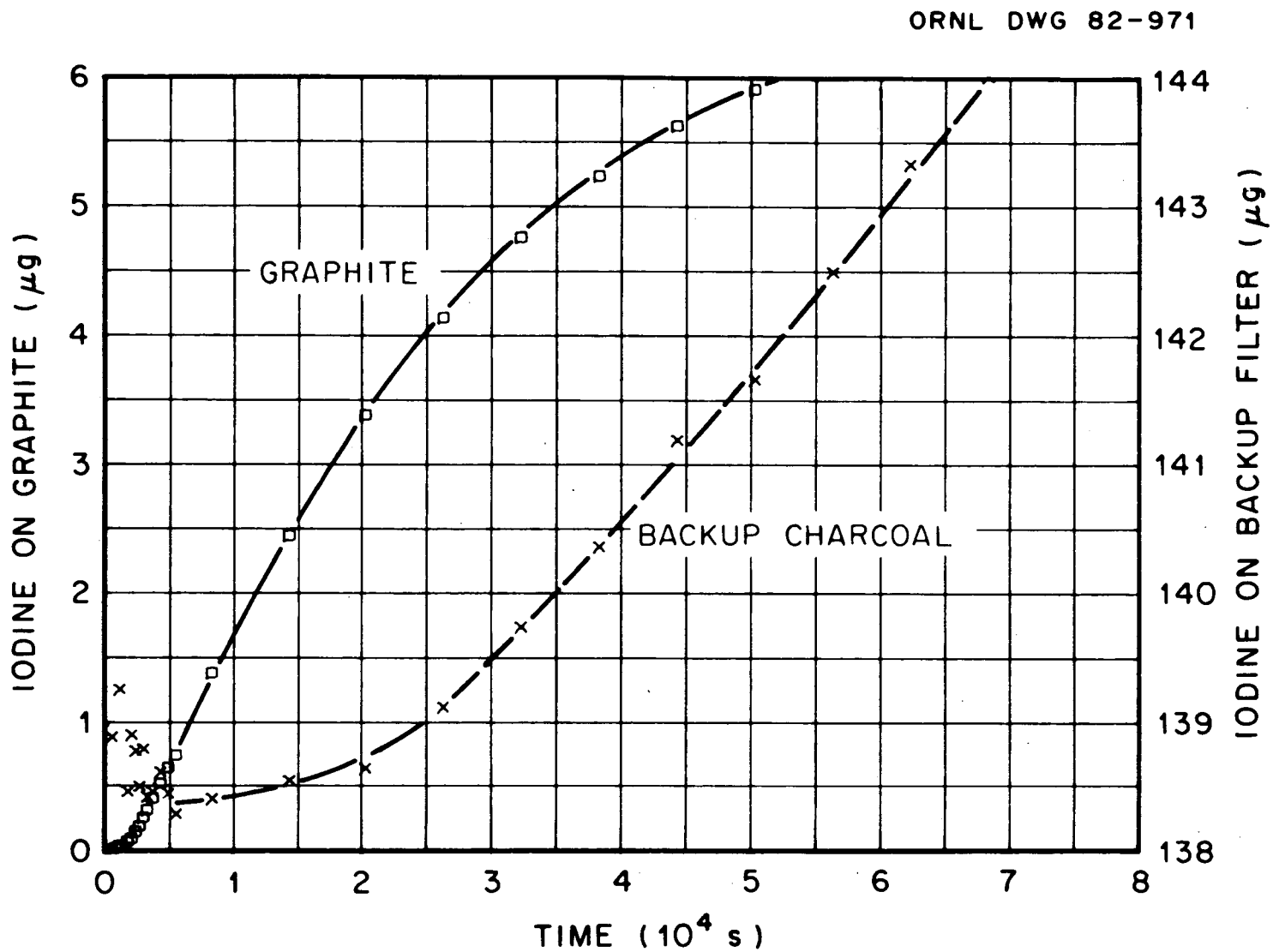

Fig. 13. Increased loading of iodine on graphite after a temperature decrease from 600 to 250°C during run 5.

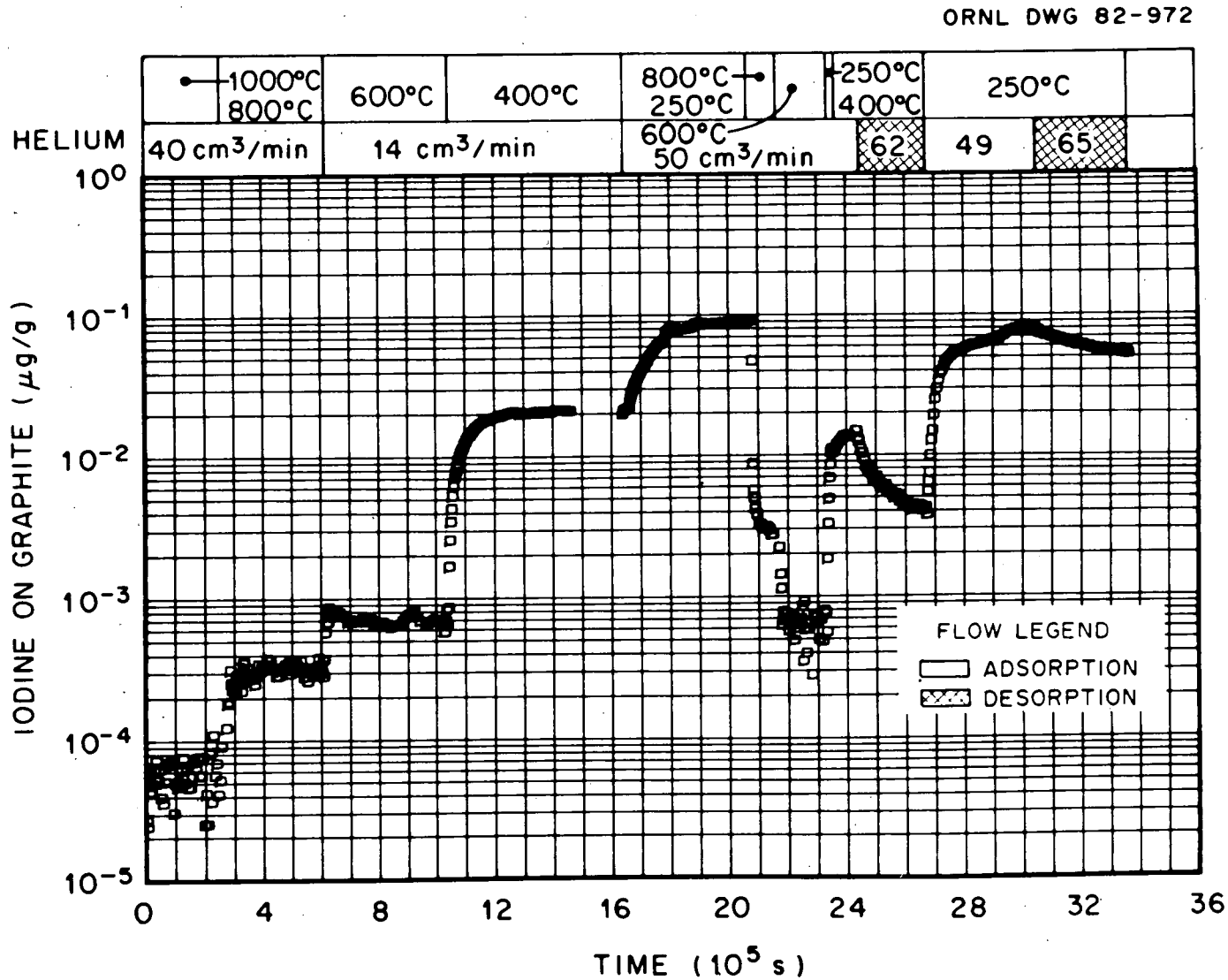

Fig. 14. Iodine loading on graphite, run 6.

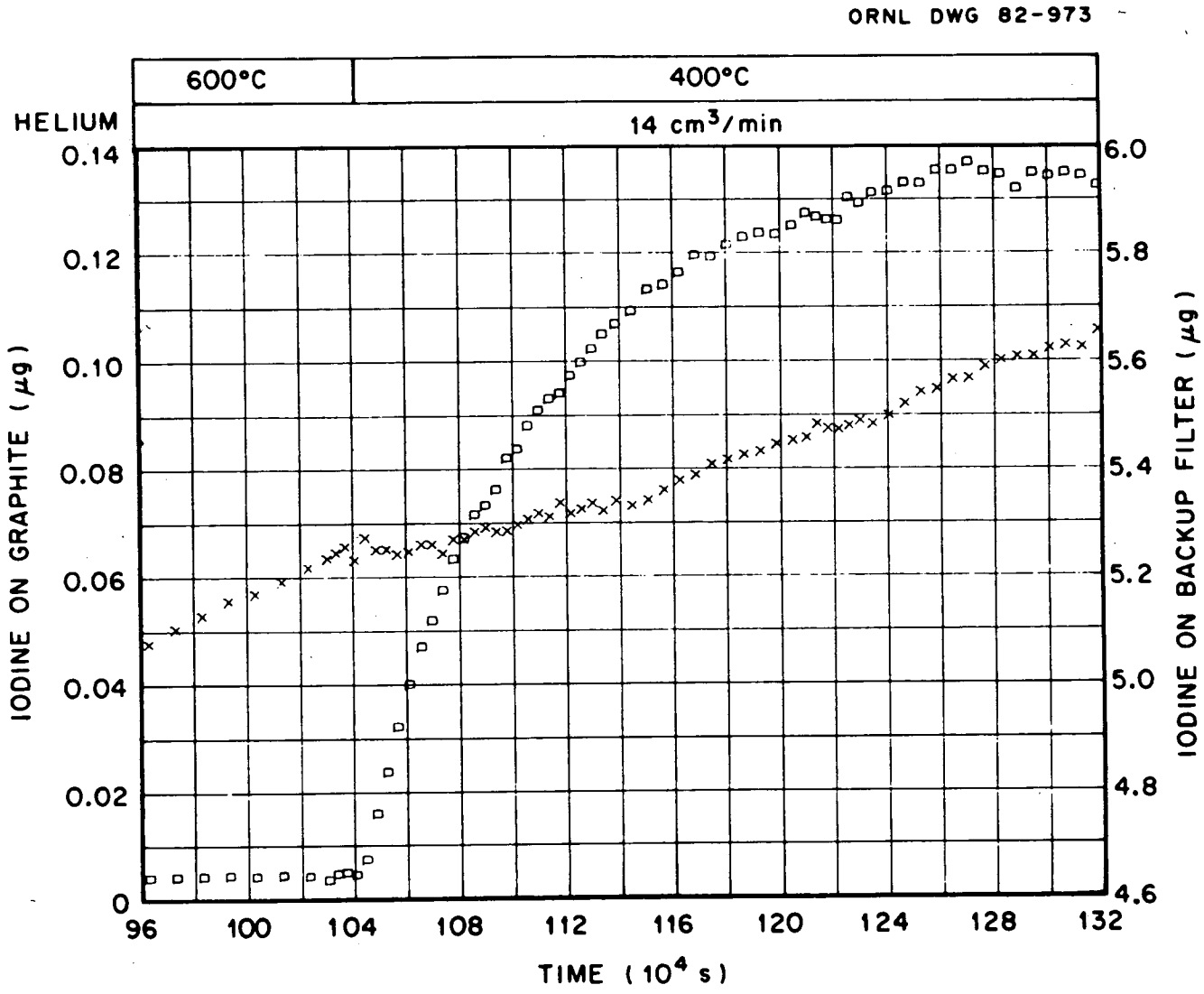

Fig. 15. Increased sorption of iodine with the decrease in graphite temperature from 600 to 400°C during run 6.

ORNL DWG 82-974

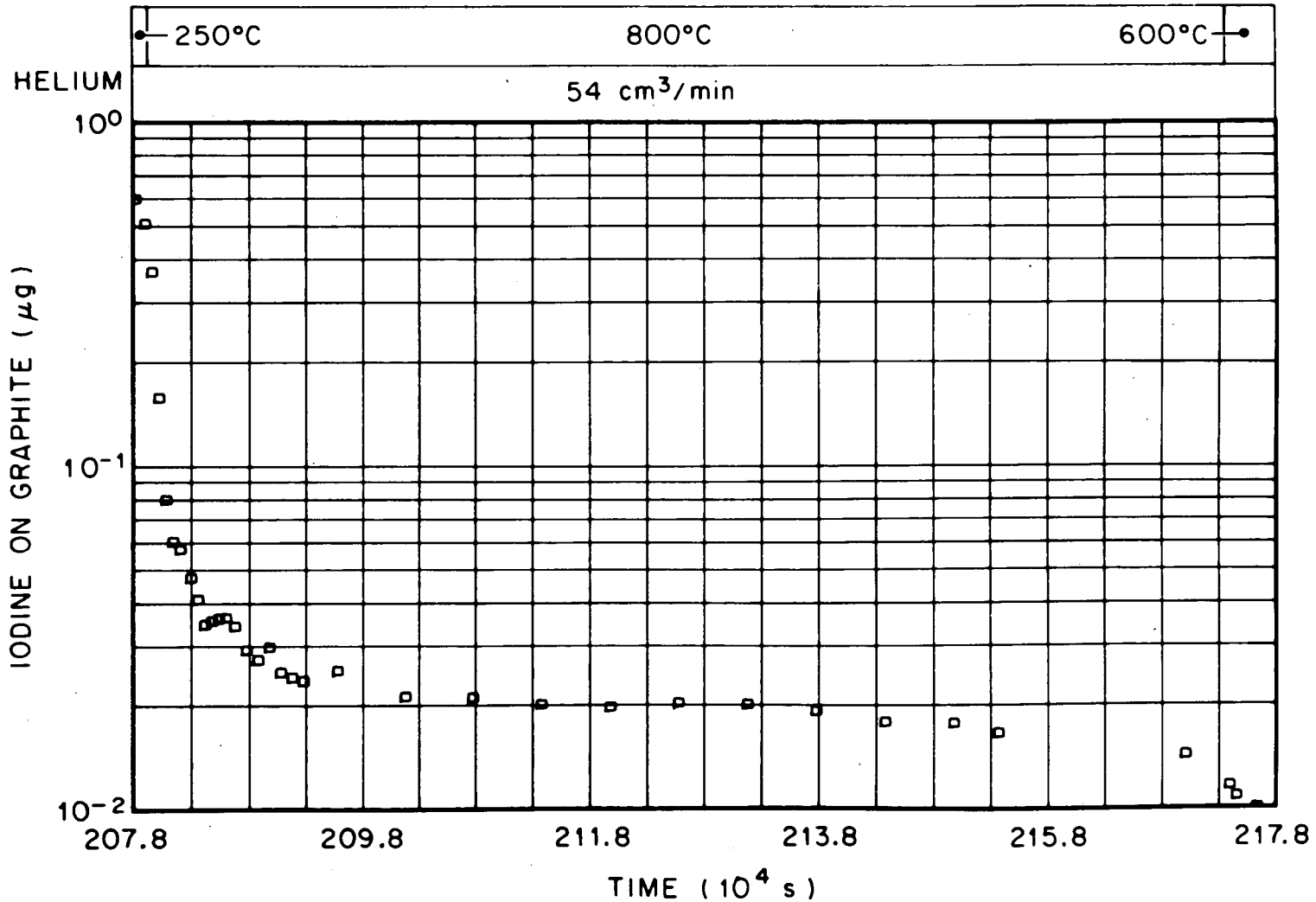

Fig. 16. Decrease in iodine loading with the increase in graphite temperature from 250 to 800°C during run 6.

ORNL DWG 82-975

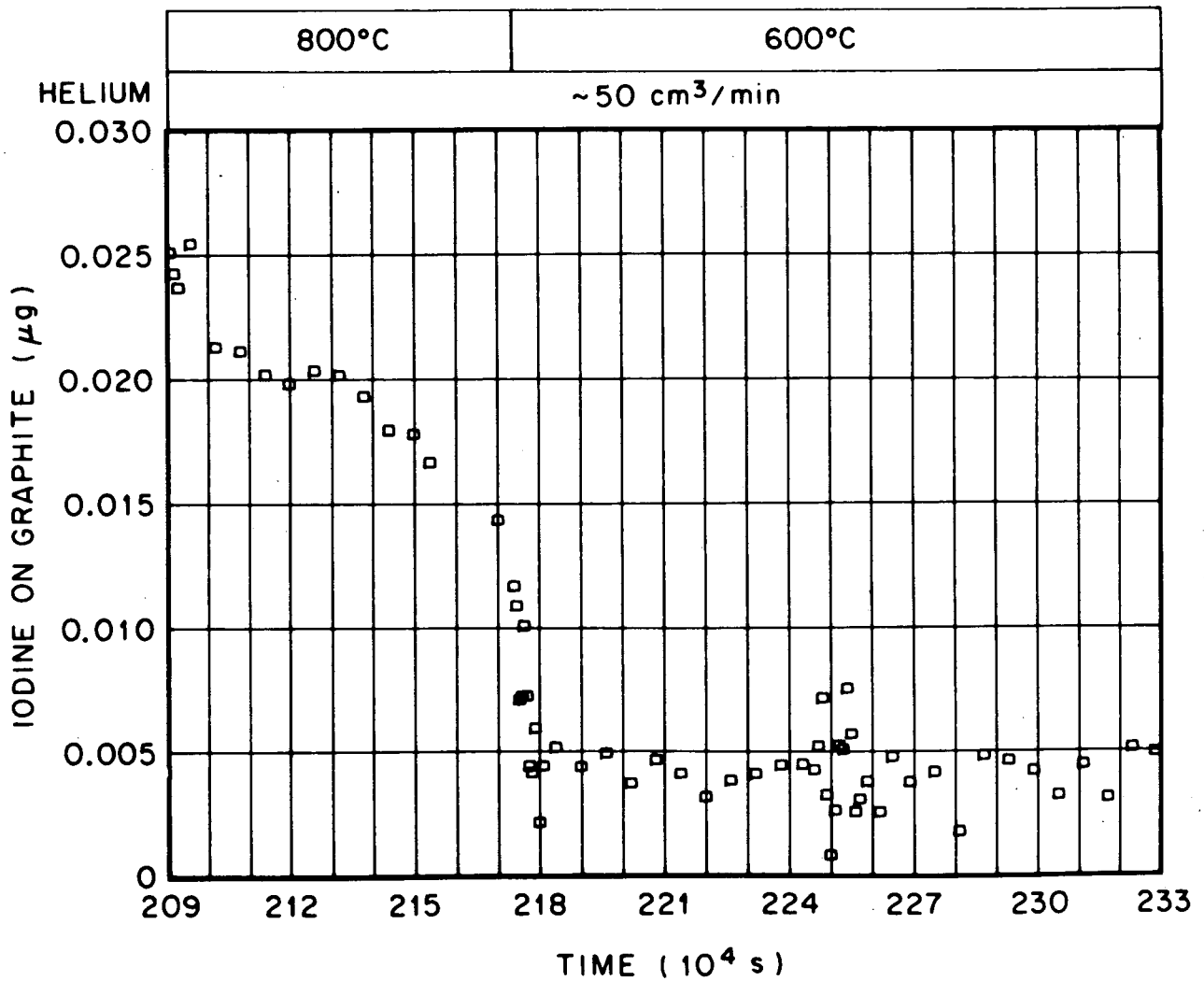

Fig. 17. Iodine desorption from graphite cooled from 800 to 600°C during run 6.

ORNL DWG 82-976

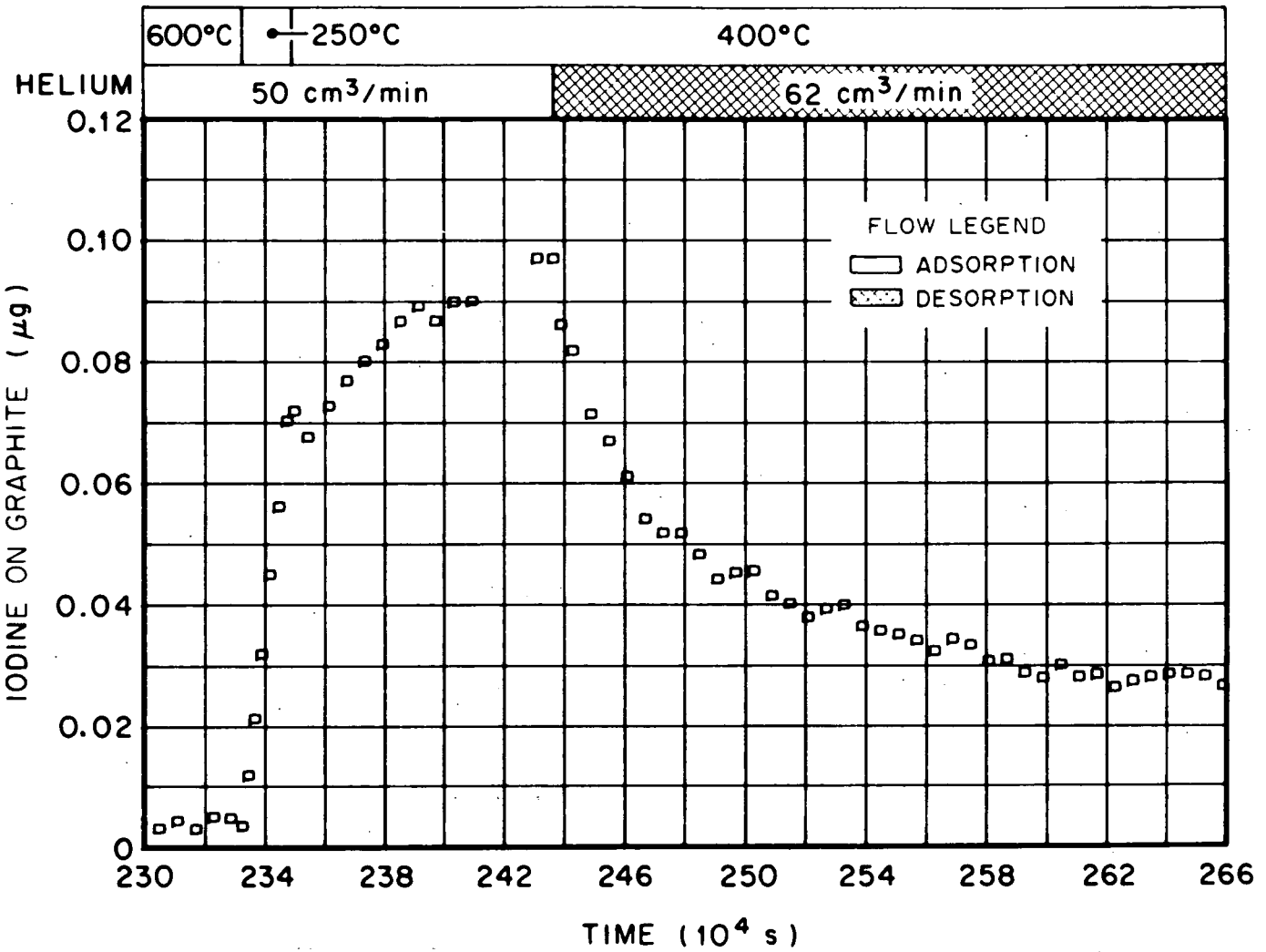

Fig. 18. Sorptive behavior of iodine on graphite heated sequentially at 600, 250, and 400°C during run 6.

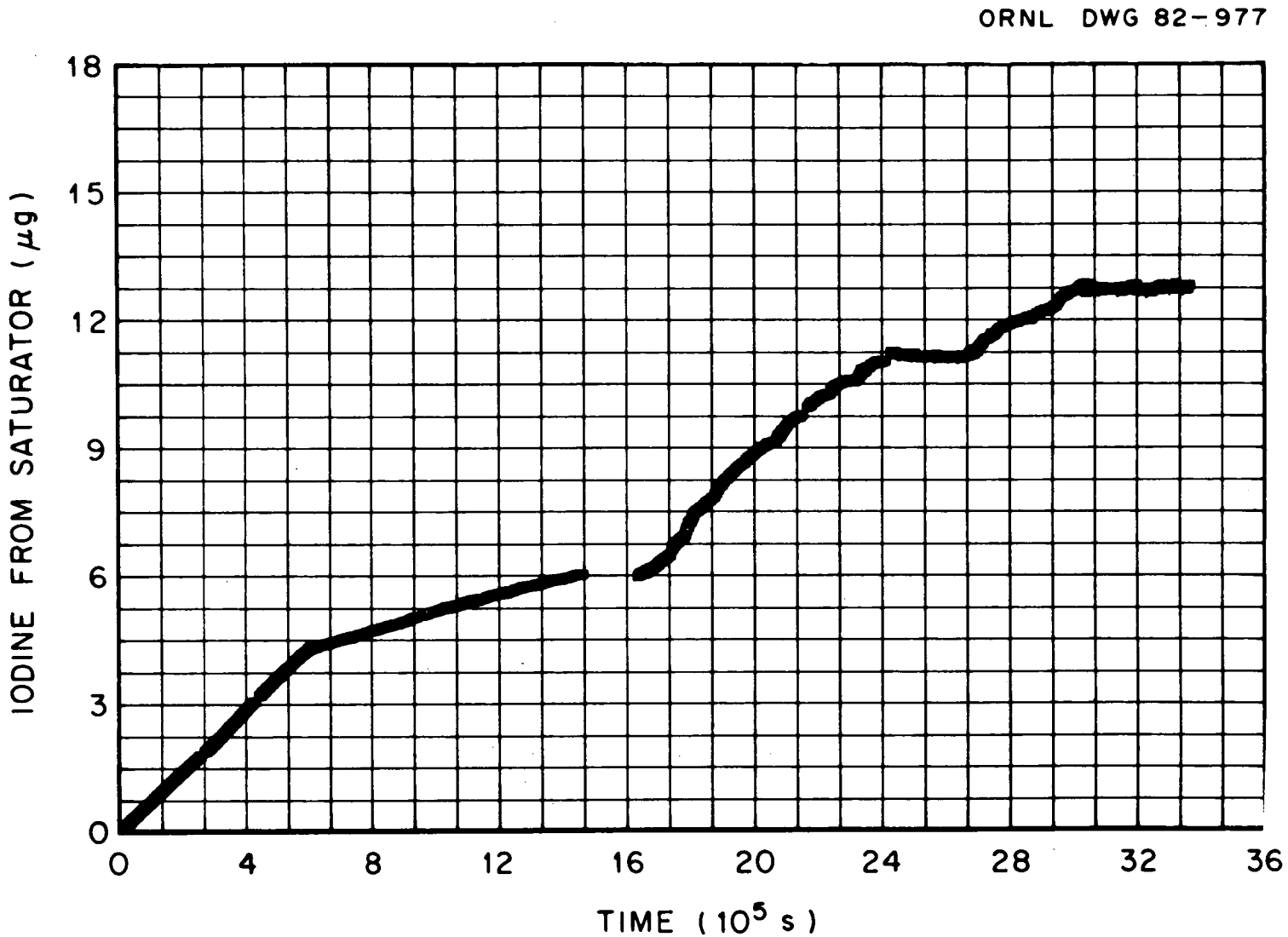

Fig. 19. Total iodine from saturator, run 6.

ORNL DWG 82-978

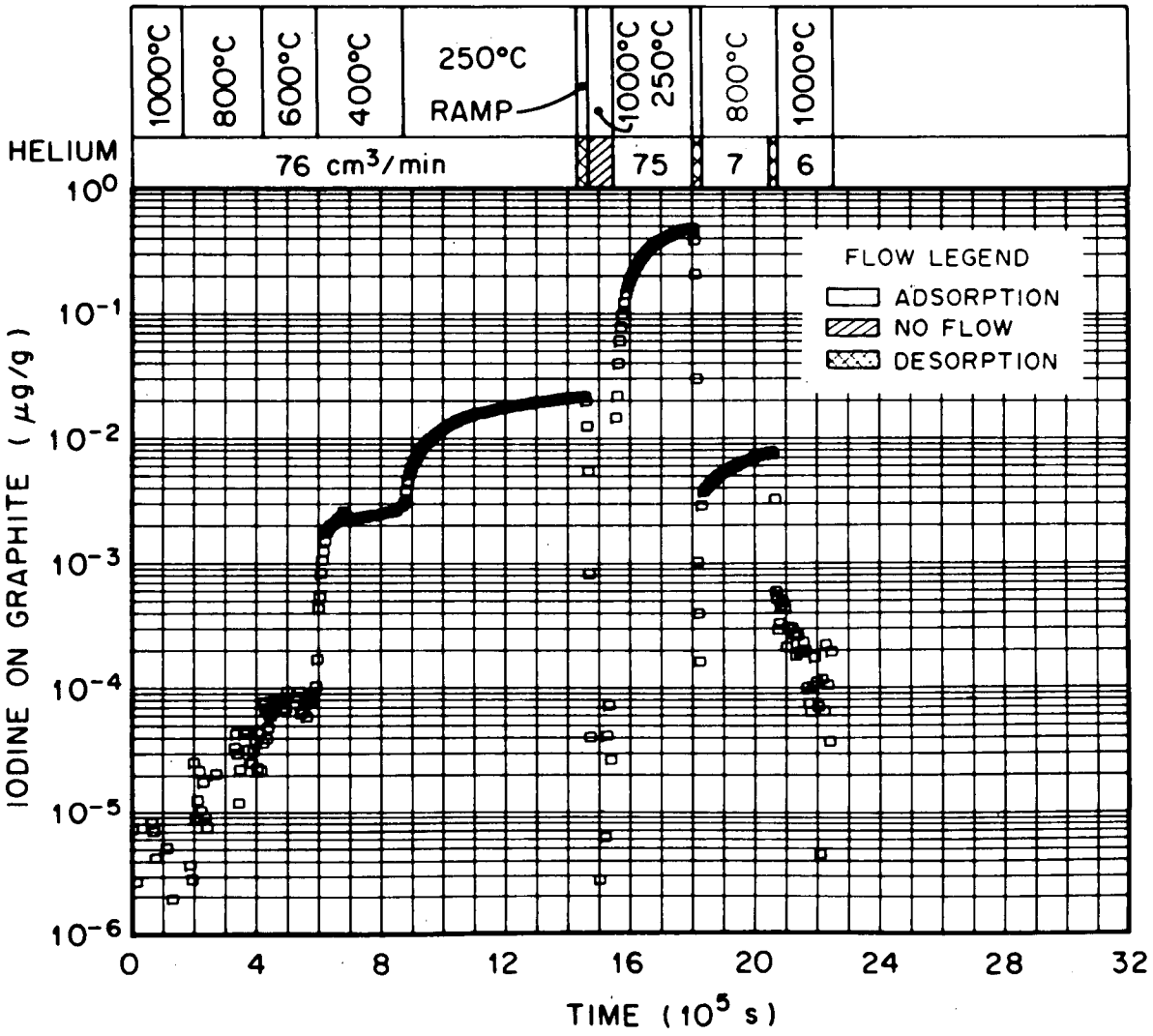

Fig. 20. Iodine loading on heated graphite during run 7.

ORNL DWG 82-979

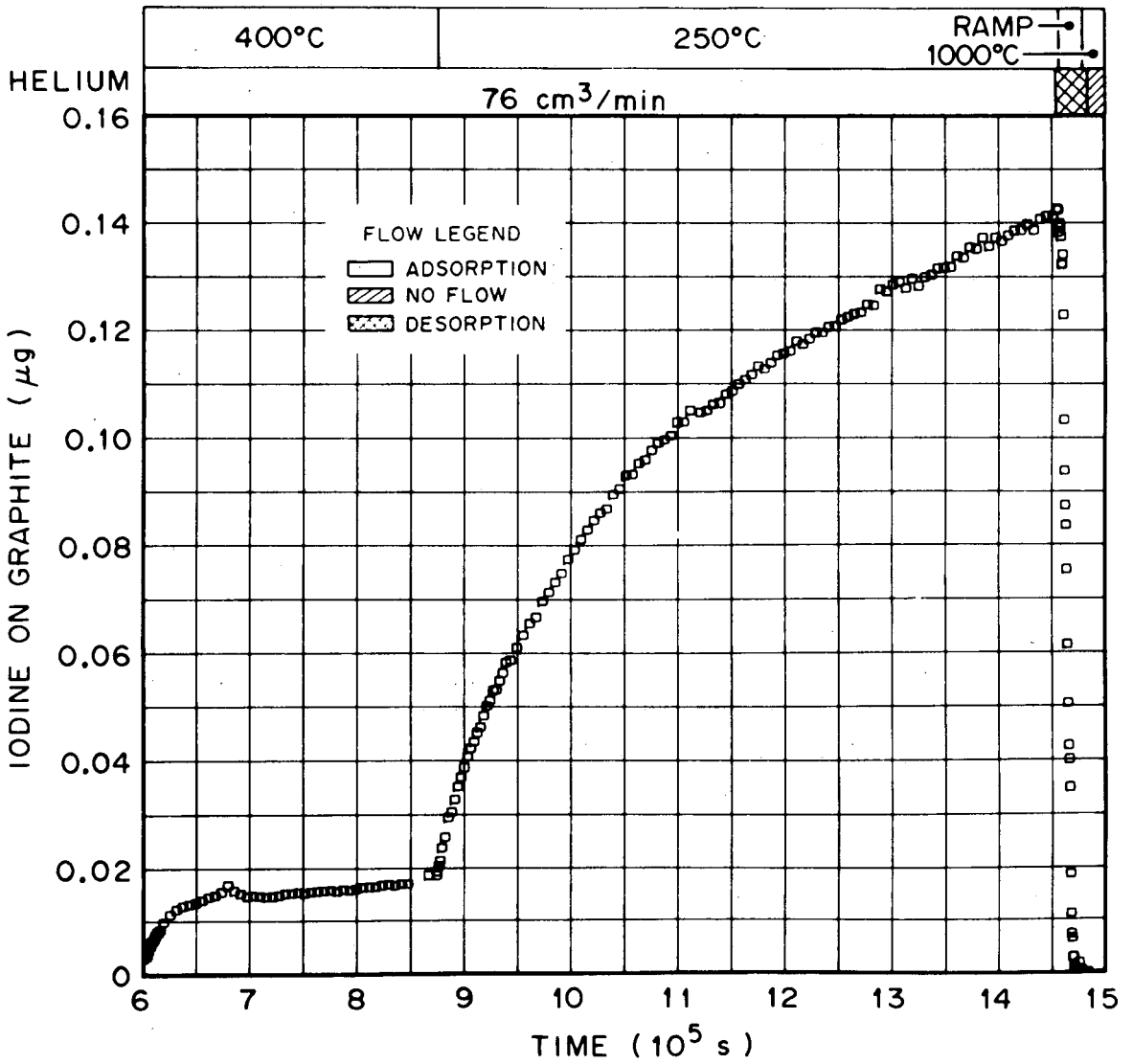

Fig. 21. Changes in iodine sorption on graphite heated sequentially at 400, 250, and 1000°C during run 7.

ORNL DWG 82-980

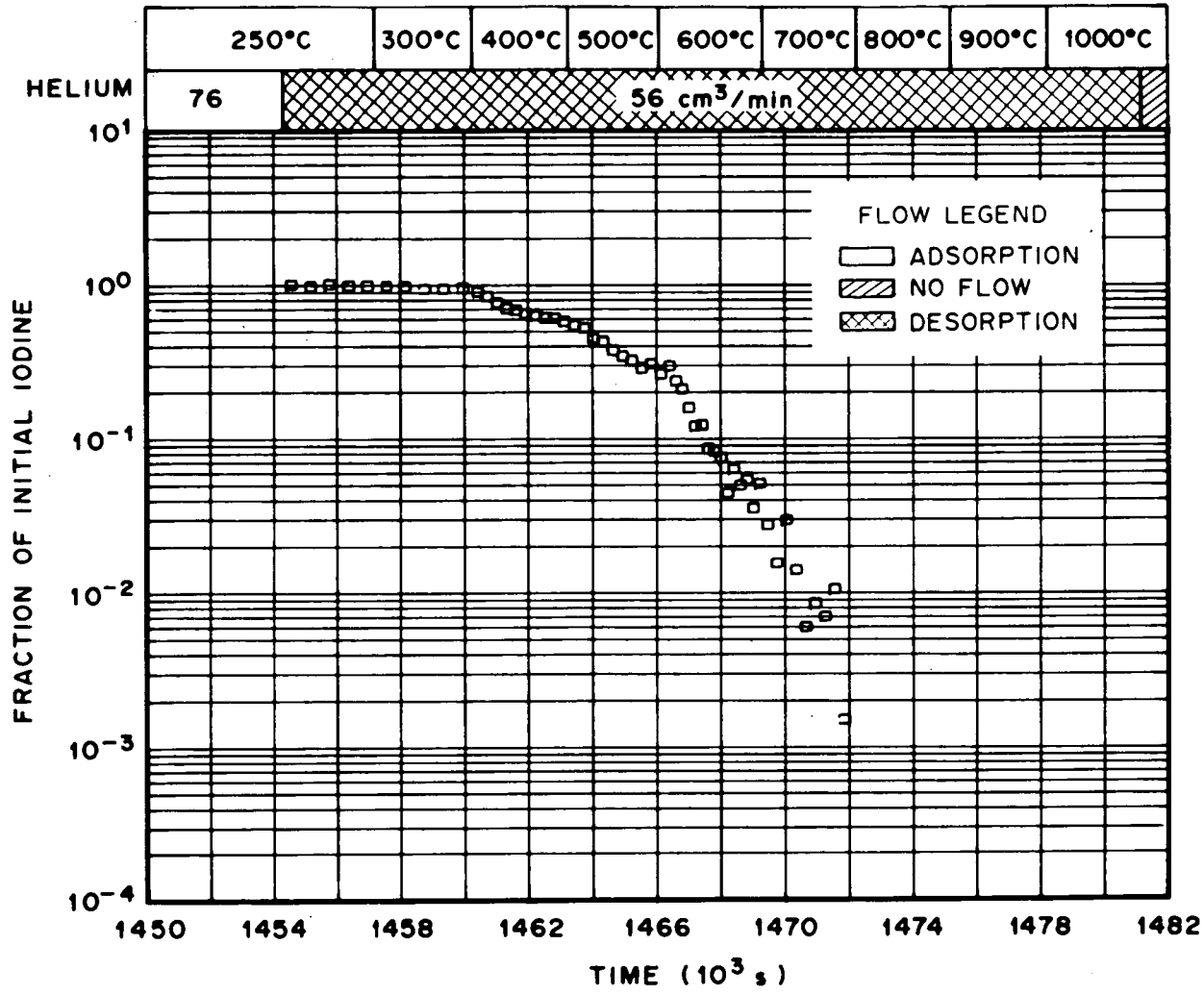

Fig. 22. Desorption of iodine from graphite heated in stepwise temperature ramps from 250 to 800°C during run 7, first experiment.

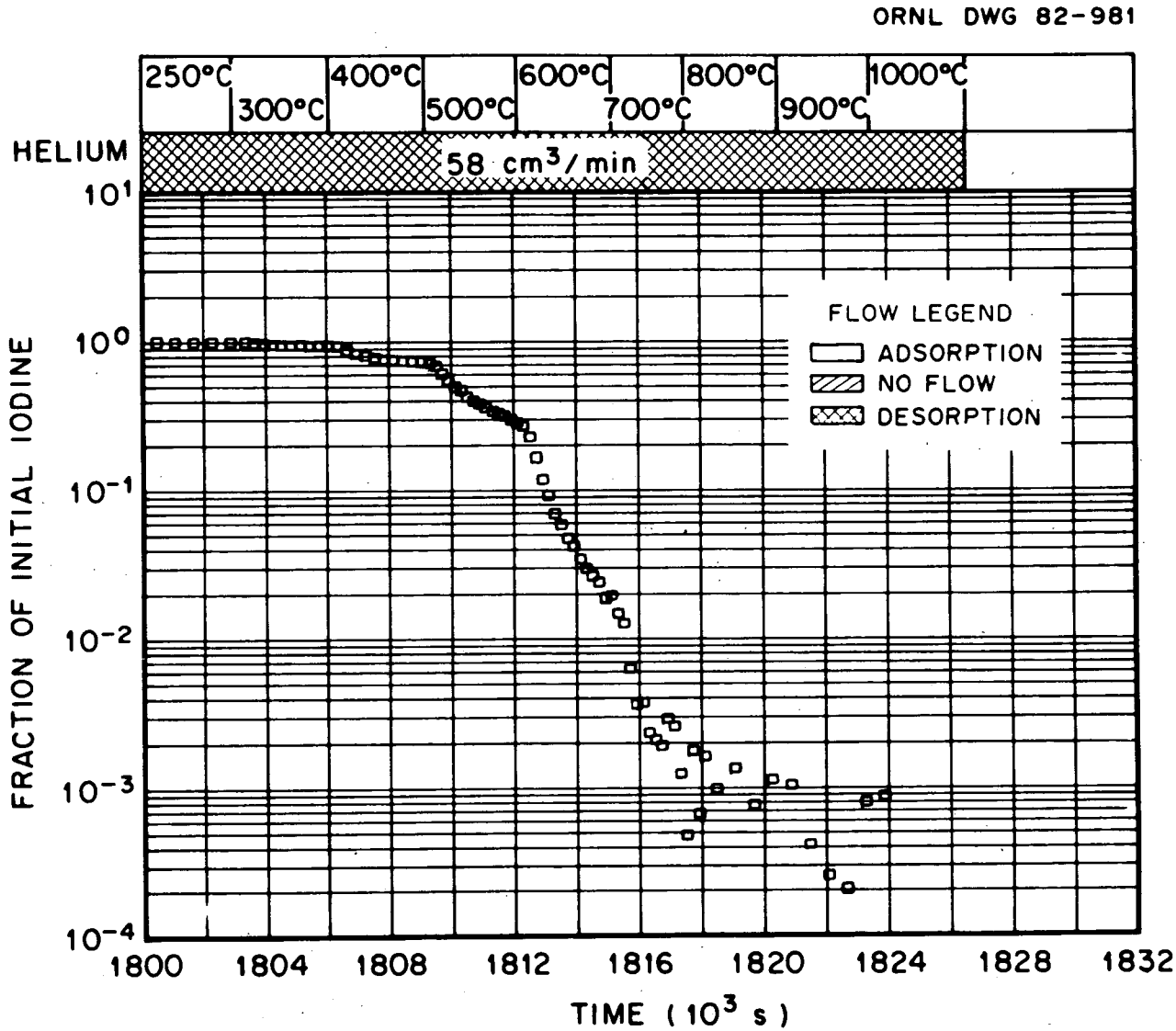

Fig. 23. Desorption of iodine from graphite heated in stepwise temperature ramps from 250 to 1000°C during run 7, second experiment.

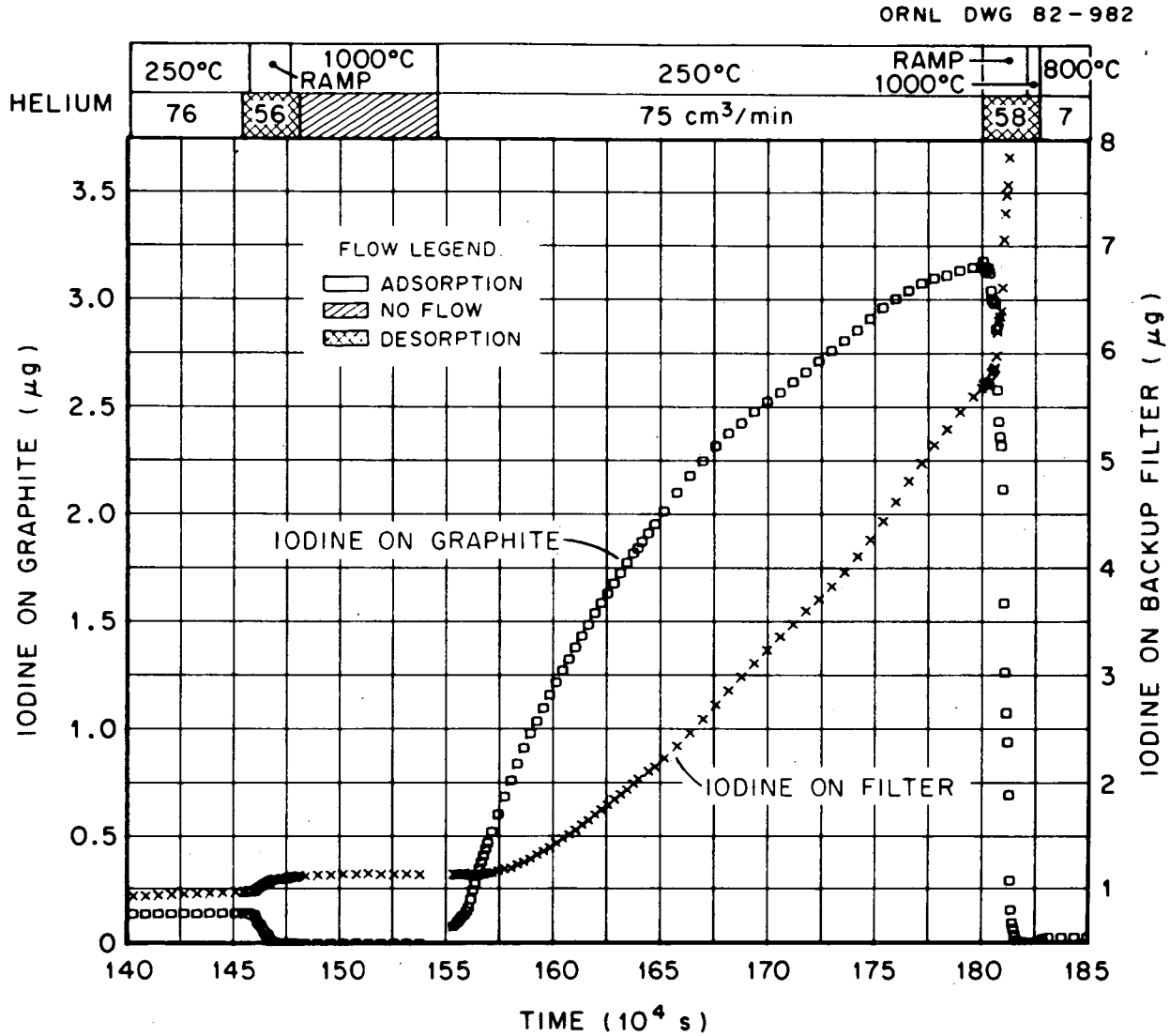

Fig. 24. Desorption of iodine loaded on graphite at 250°C by a temperature ramp to 1000°C, run 7.

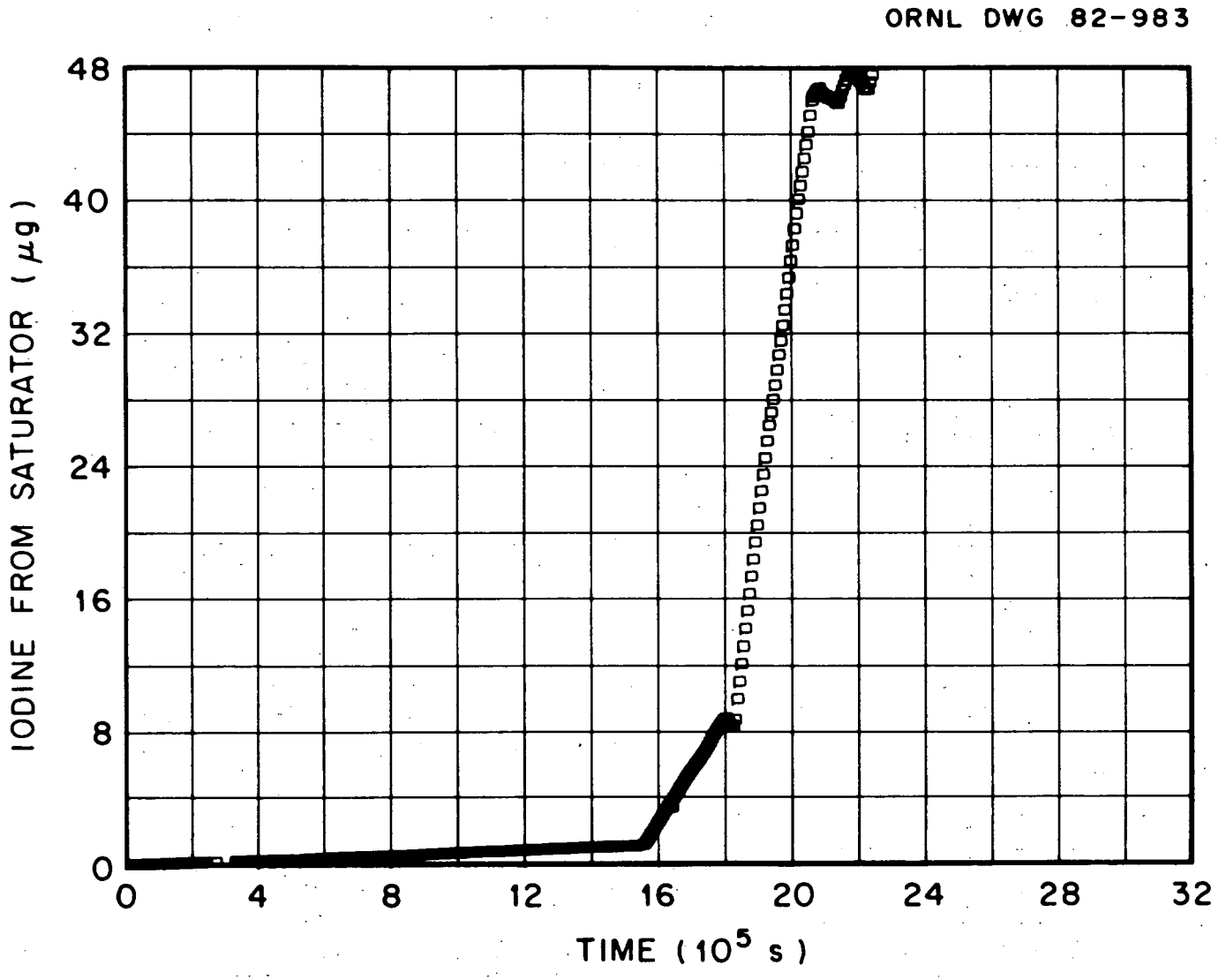

Fig. 25. Total iodine from saturator, run 7.

ORNL DWG 82-984

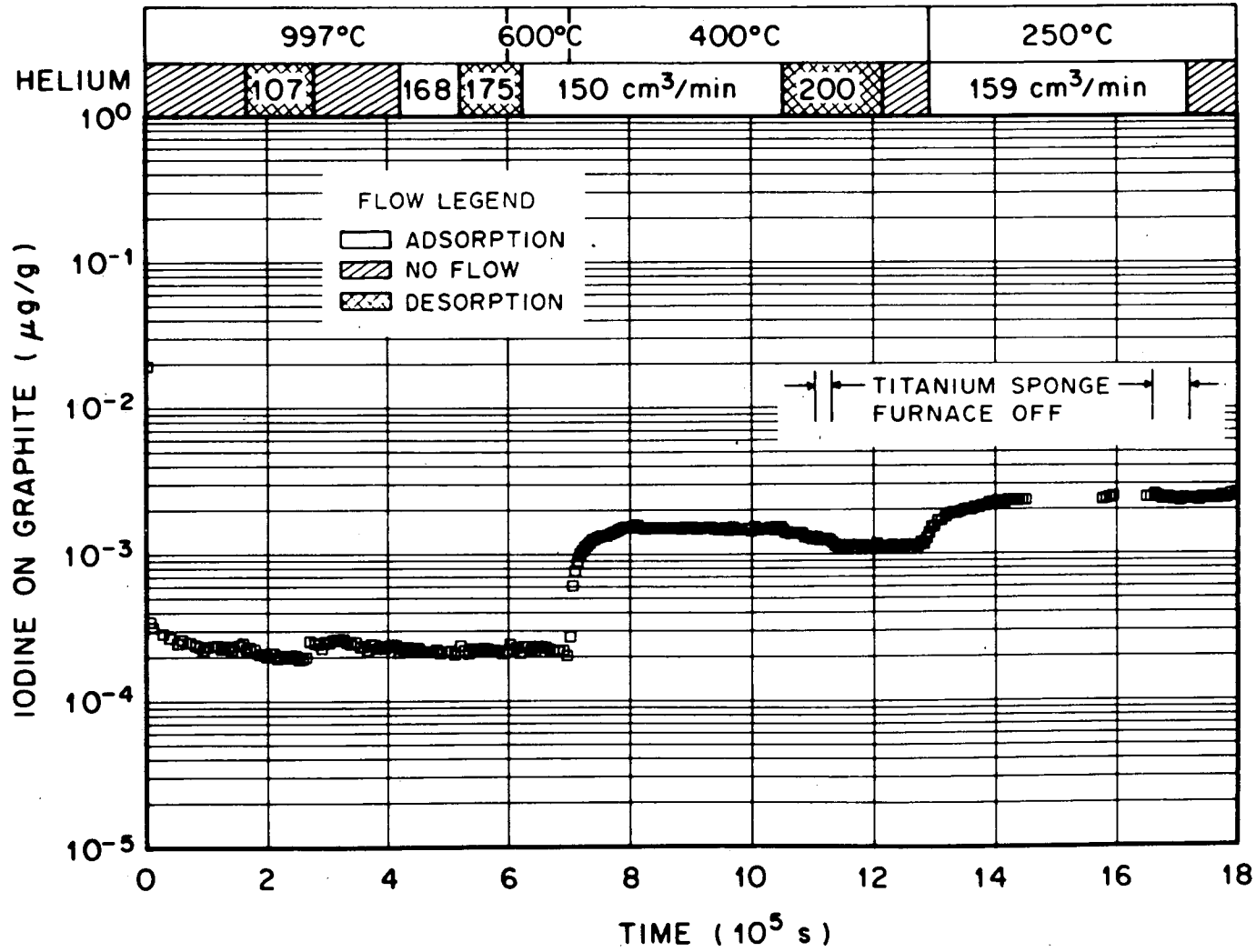

Fig. 26. Iodine loading on heated graphite in run 8 (0–18 × 10^5 s).

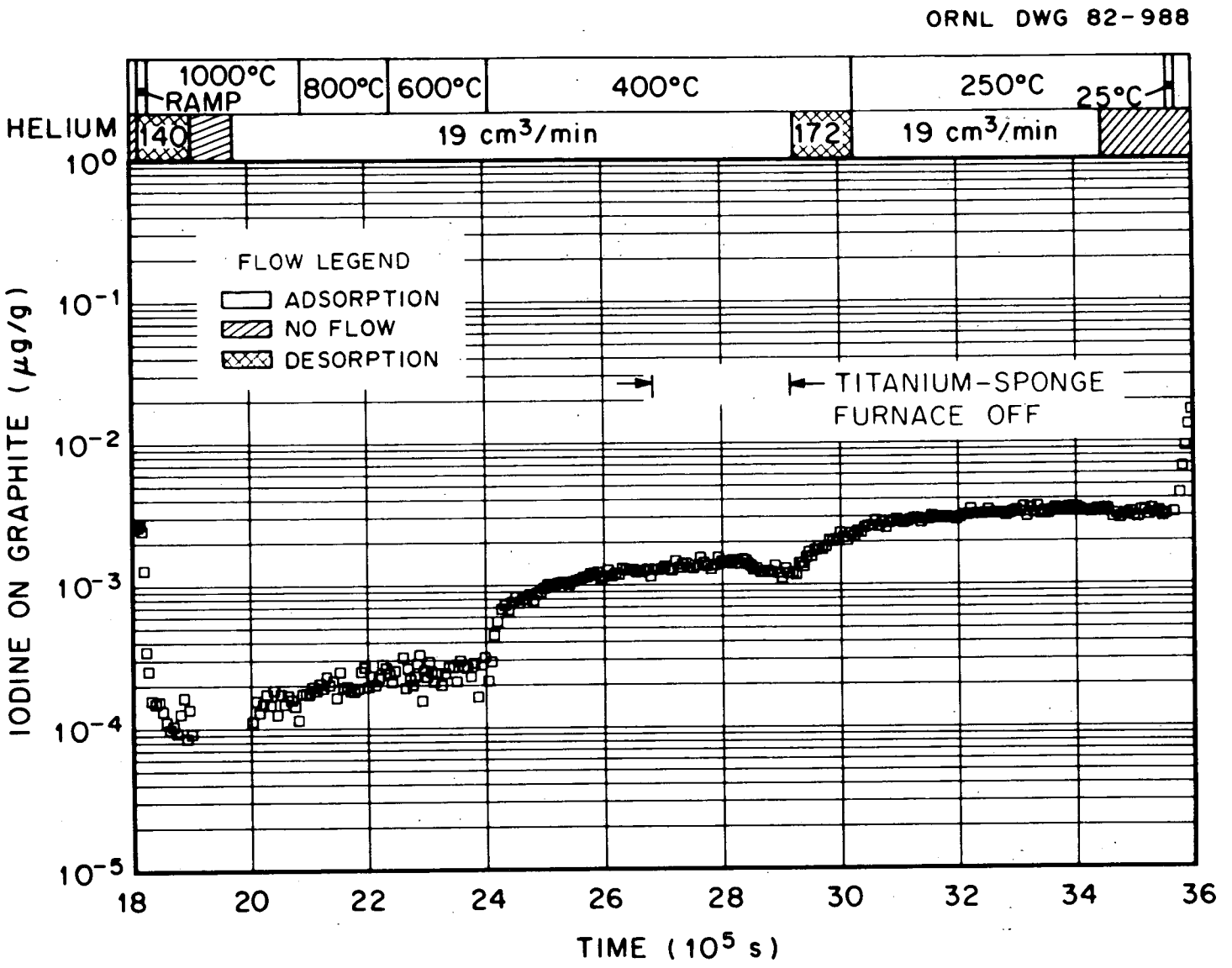

Fig. 27. Iodine loading on heated graphite in run 8 (18–36 × 10^5 s).

ORNL DWG 82-987

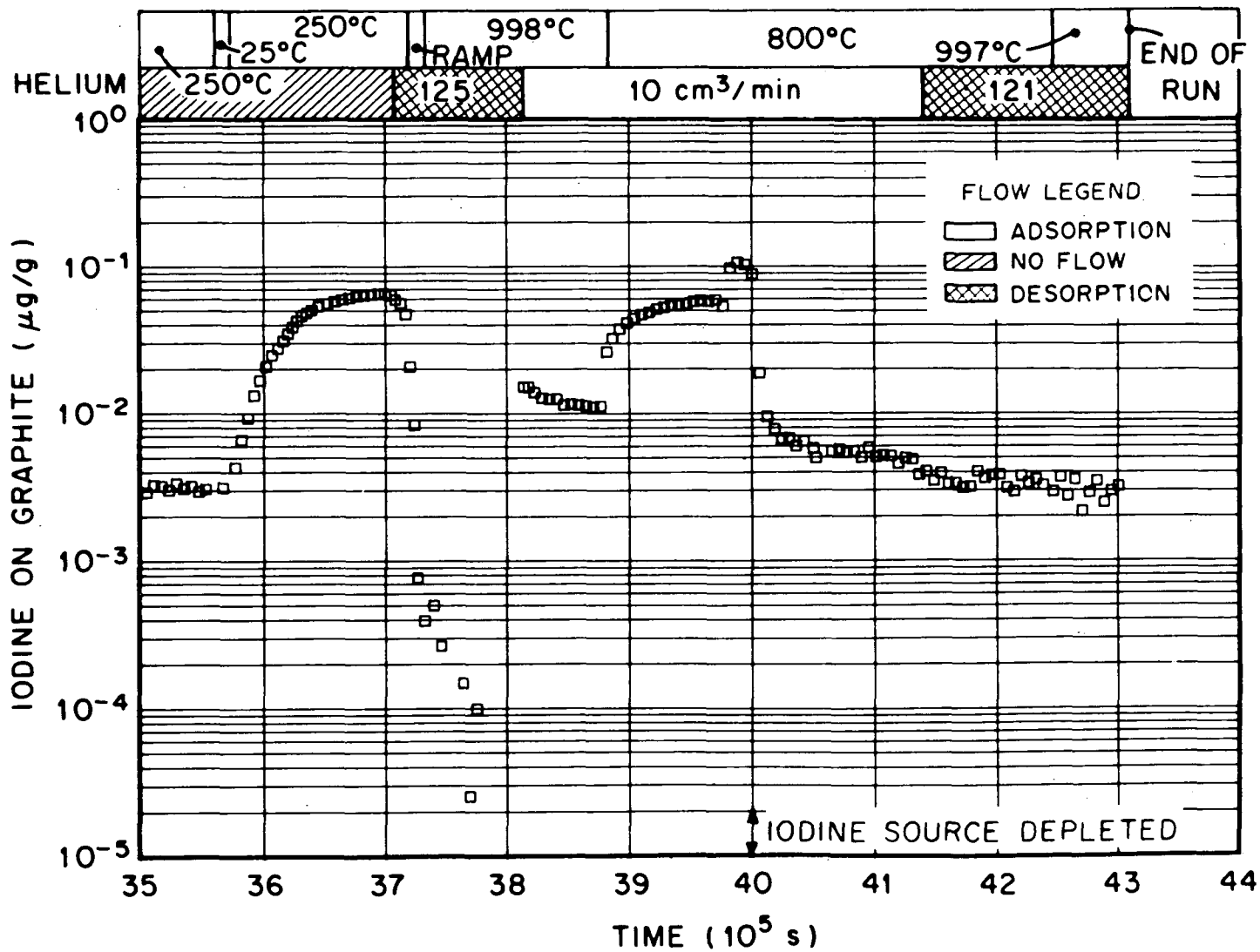

Fig. 28. Iodine loading on heated graphite in run 8 (35–44 × 10^5 s).

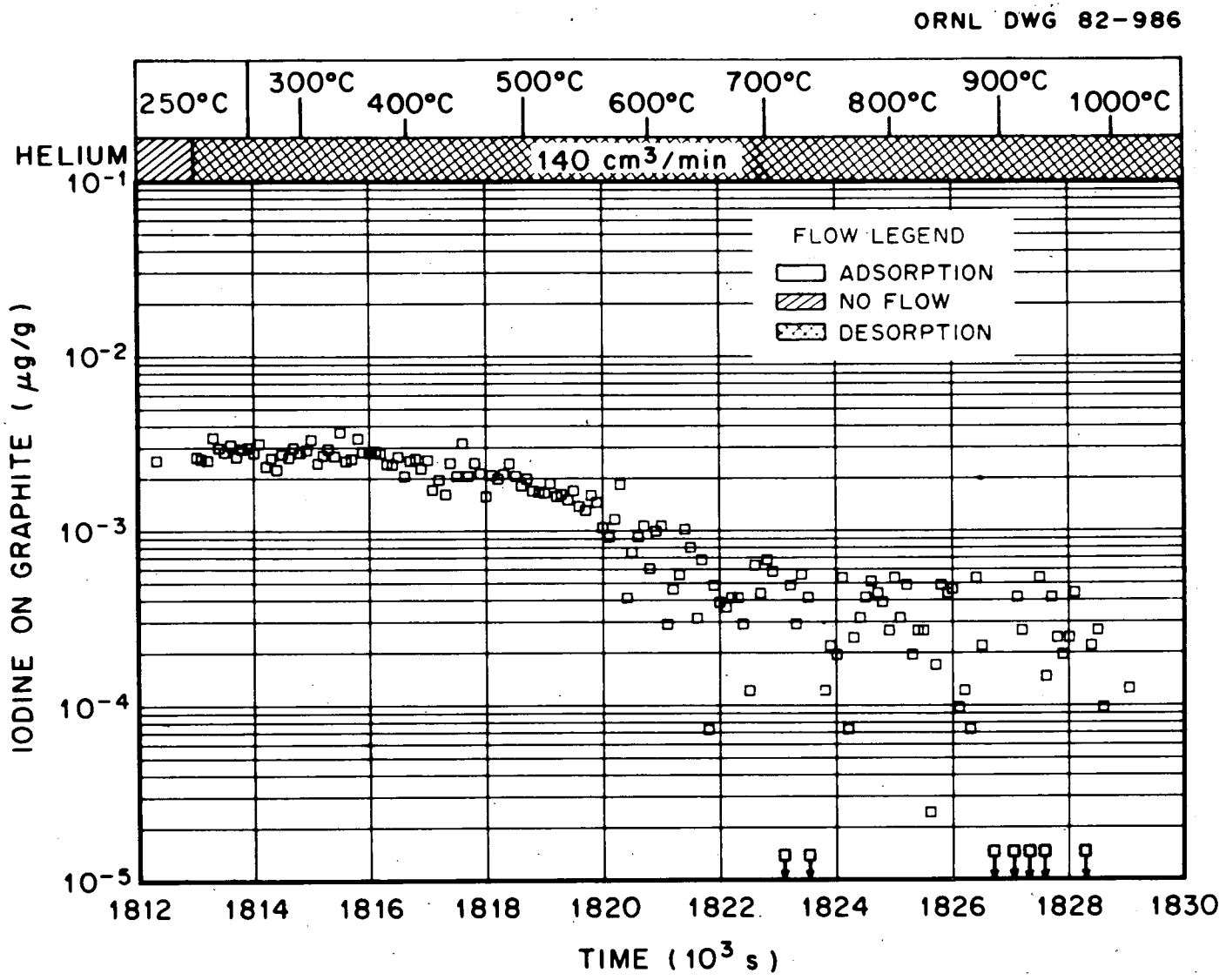

Fig. 29. First test of iodine desorption from graphite during a temperature ramp, run 8.

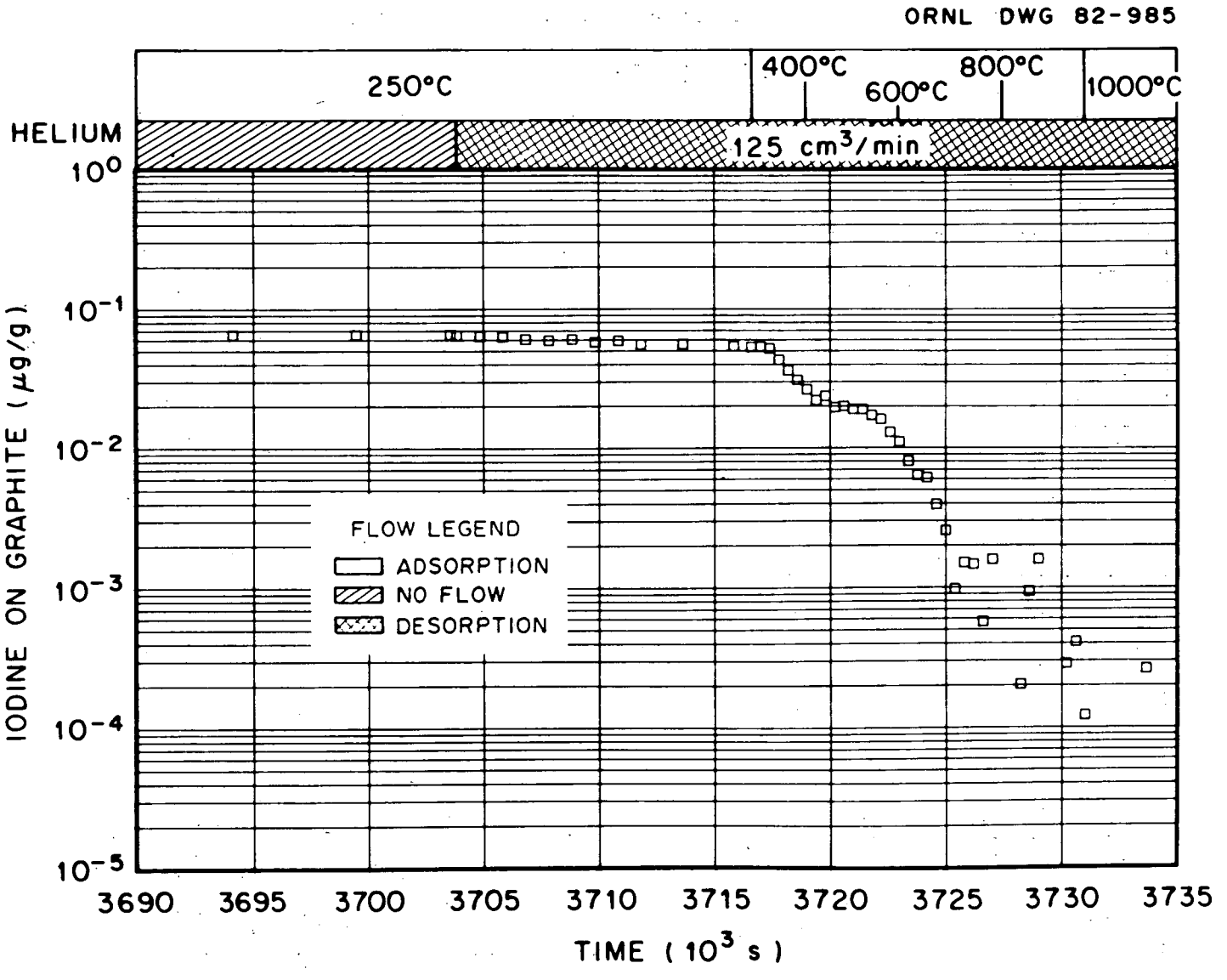

Fig. 30. Second test of iodine desorption from graphite during a temperature ramp, run 8.

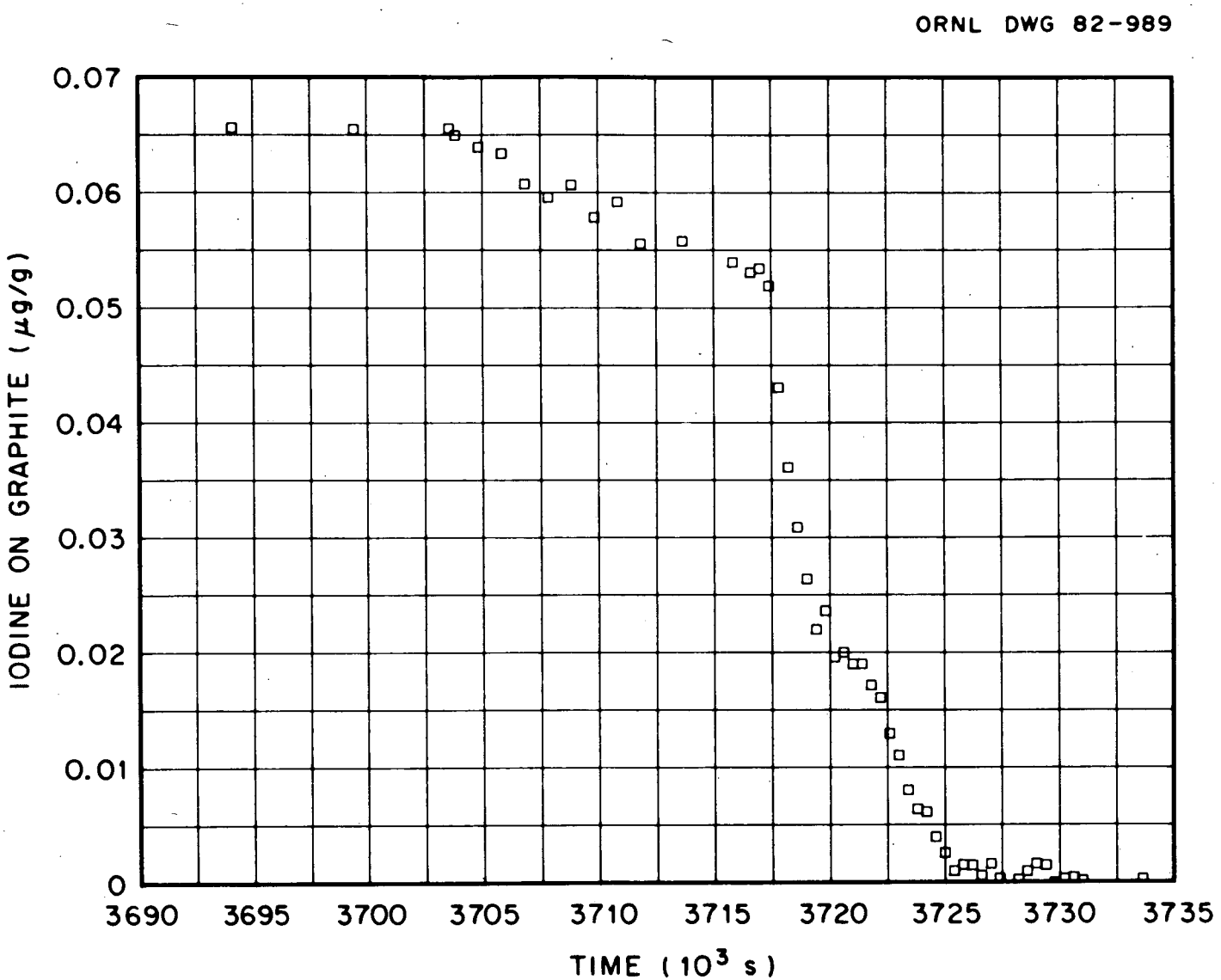

Fig. 31. Details of the second iodine desorption from graphite test (see Fig. 30) in run 8.

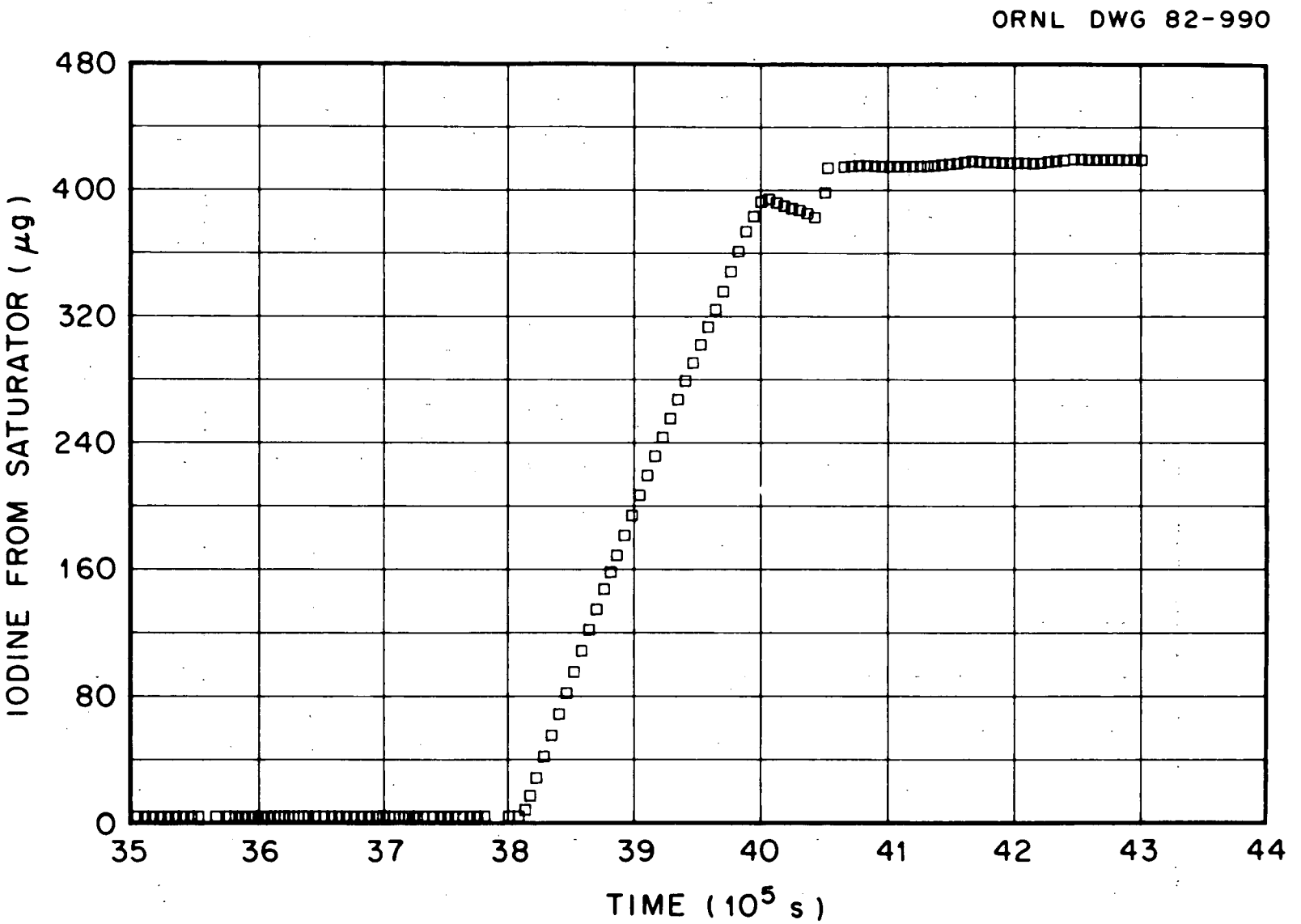

Fig. 32. Total iodine transferred from saturator, run 8.

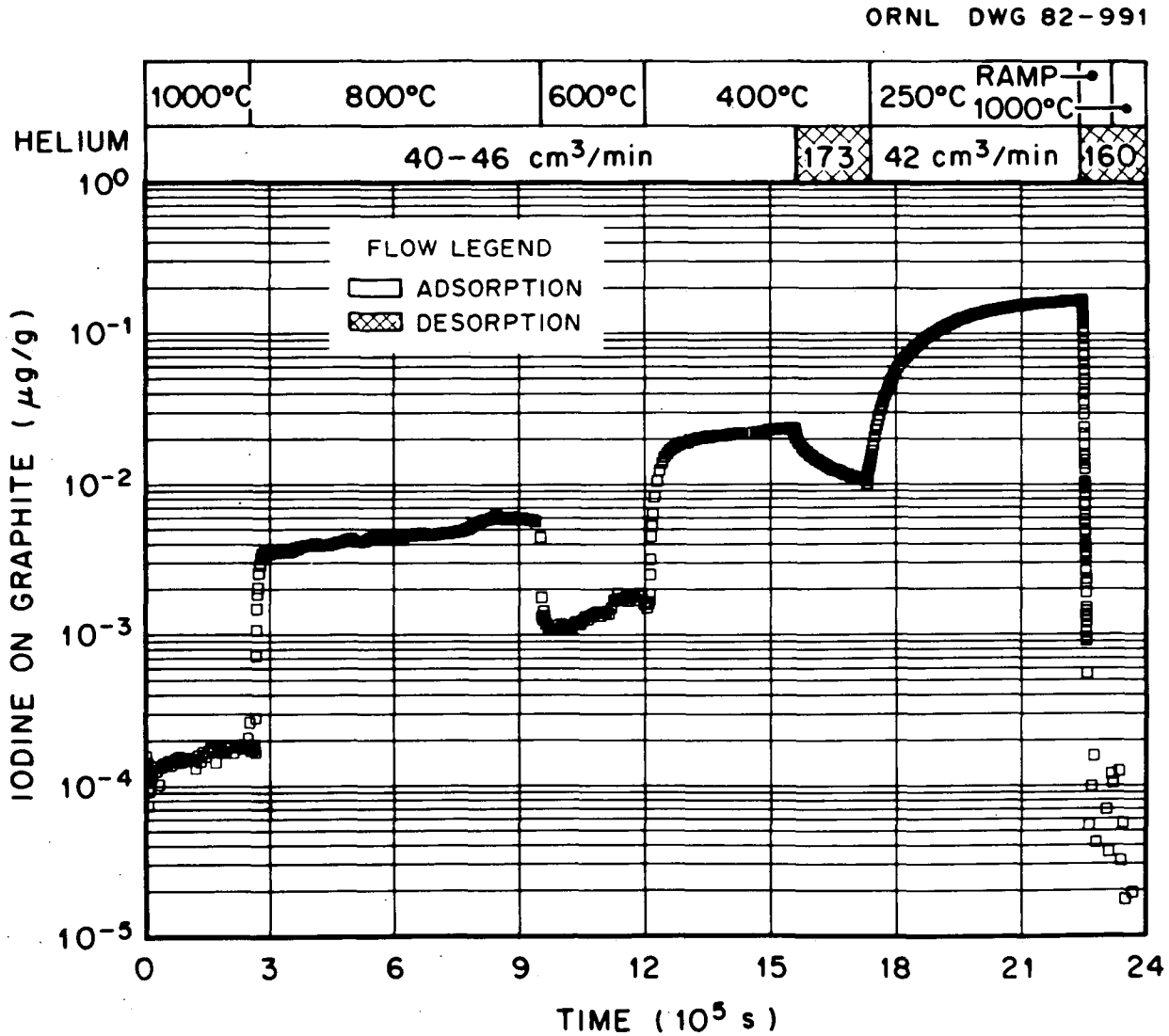

Fig. 33. Iodine loading on heated S-2020 graphite in run 9 ($0-24 \times 10^5$ s).

ORNL DWG 81-658R

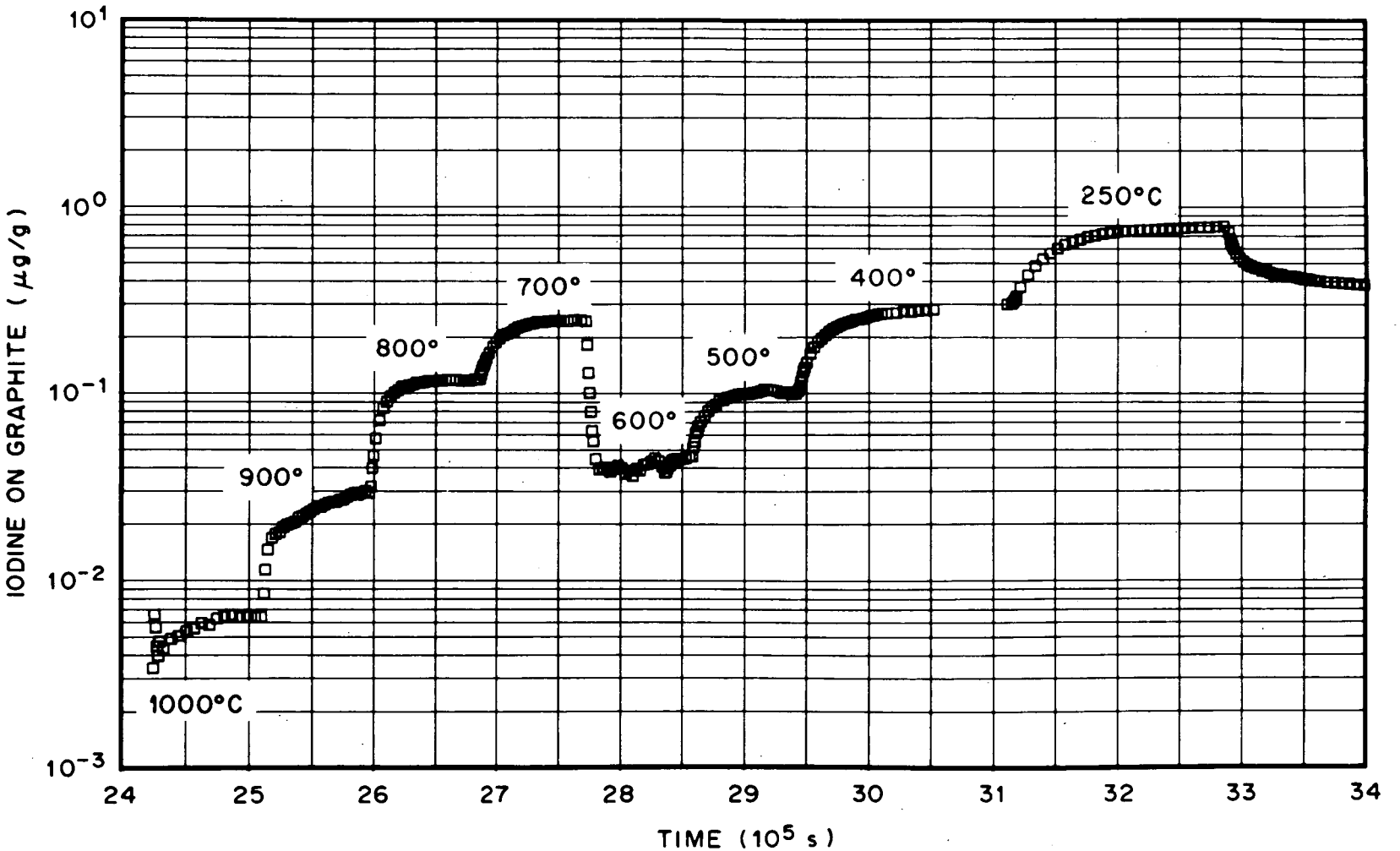

Fig. 34. Iodine loading on heated S-2020 graphite in run 9 ($24\text{-}34 \times 10^5$ s).

ORNL DWG 82-993

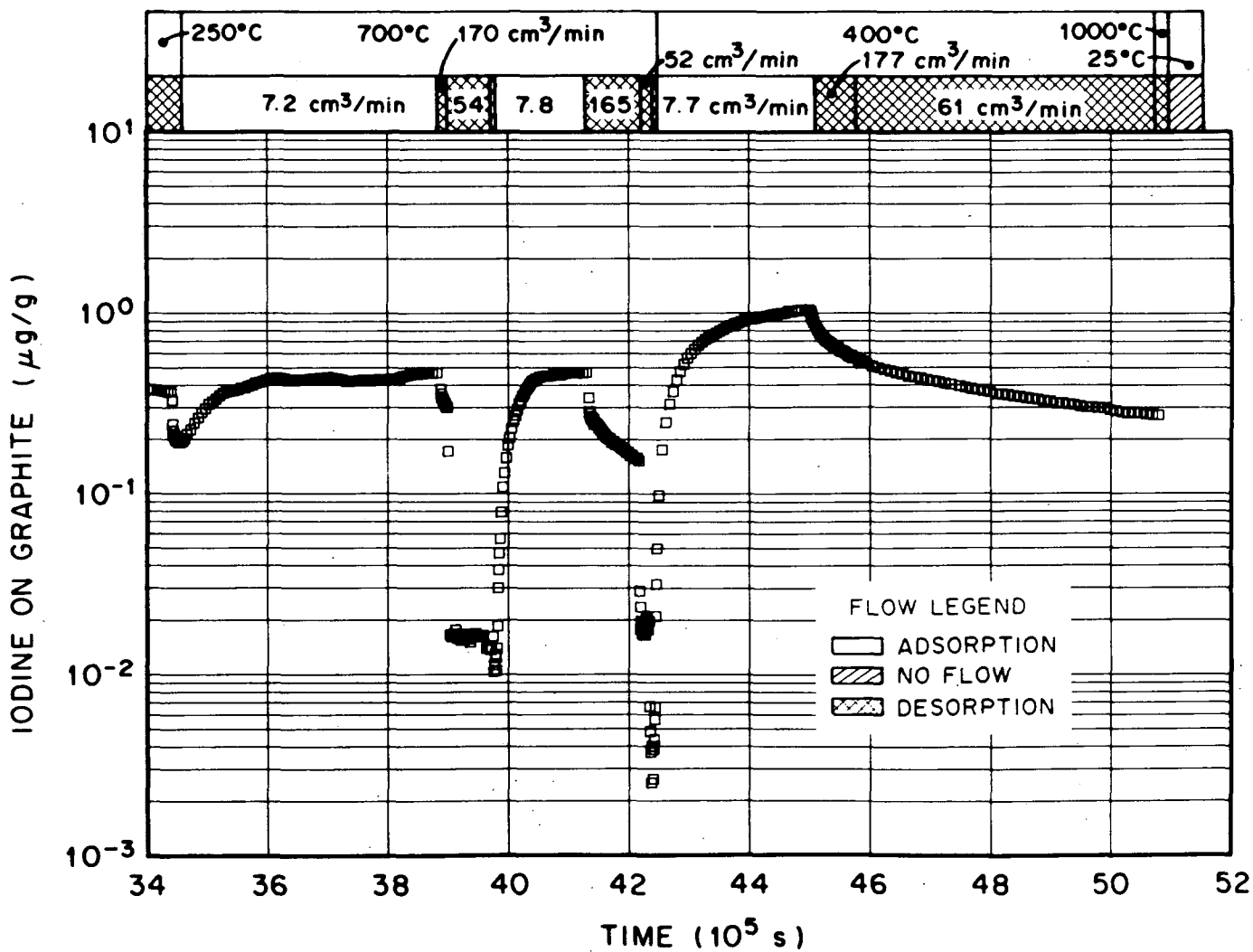

Fig. 35. Iodine loading on heated S-2020 graphite in run 9 ($34\text{-}52 \times 10^5$ s).

ORNL DWG 82-992

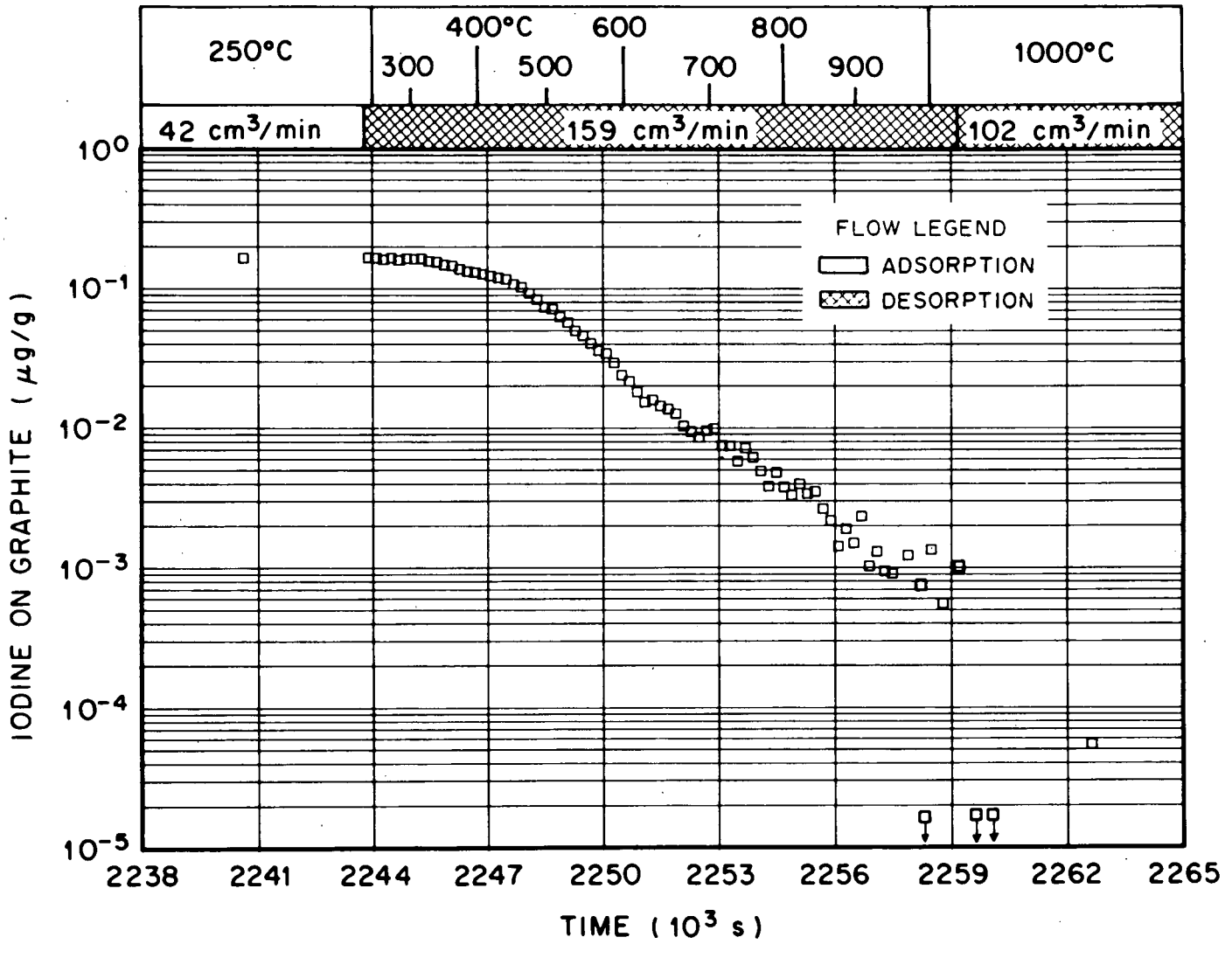

Fig. 36. Iodine desorption from S-2020 graphite during a temperature ramp in run 9.

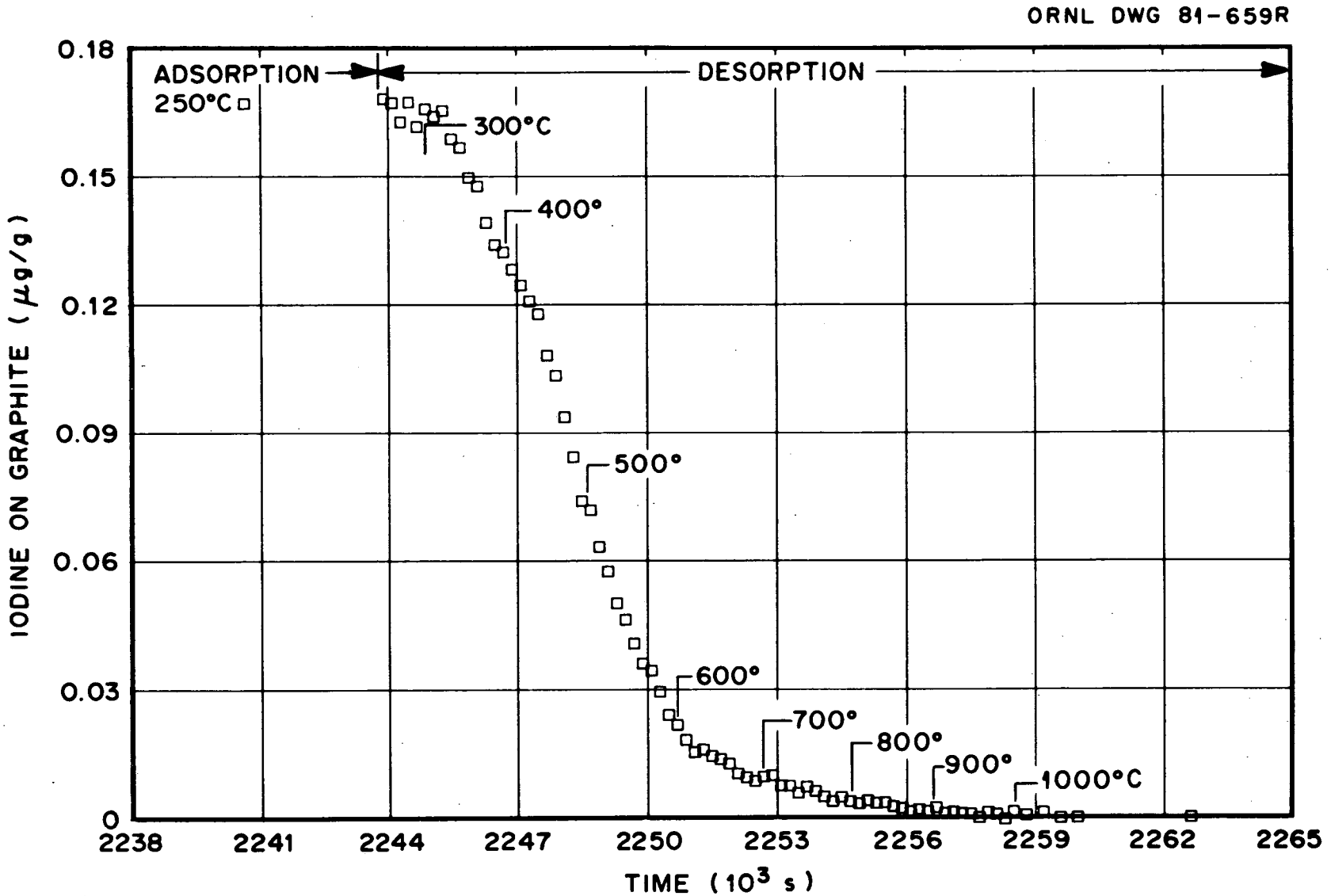

Fig. 37. Iodine desorption from S-2020 graphite during a temperature ramp of 3°C/min, run 9.

ORNL DWG 82-999

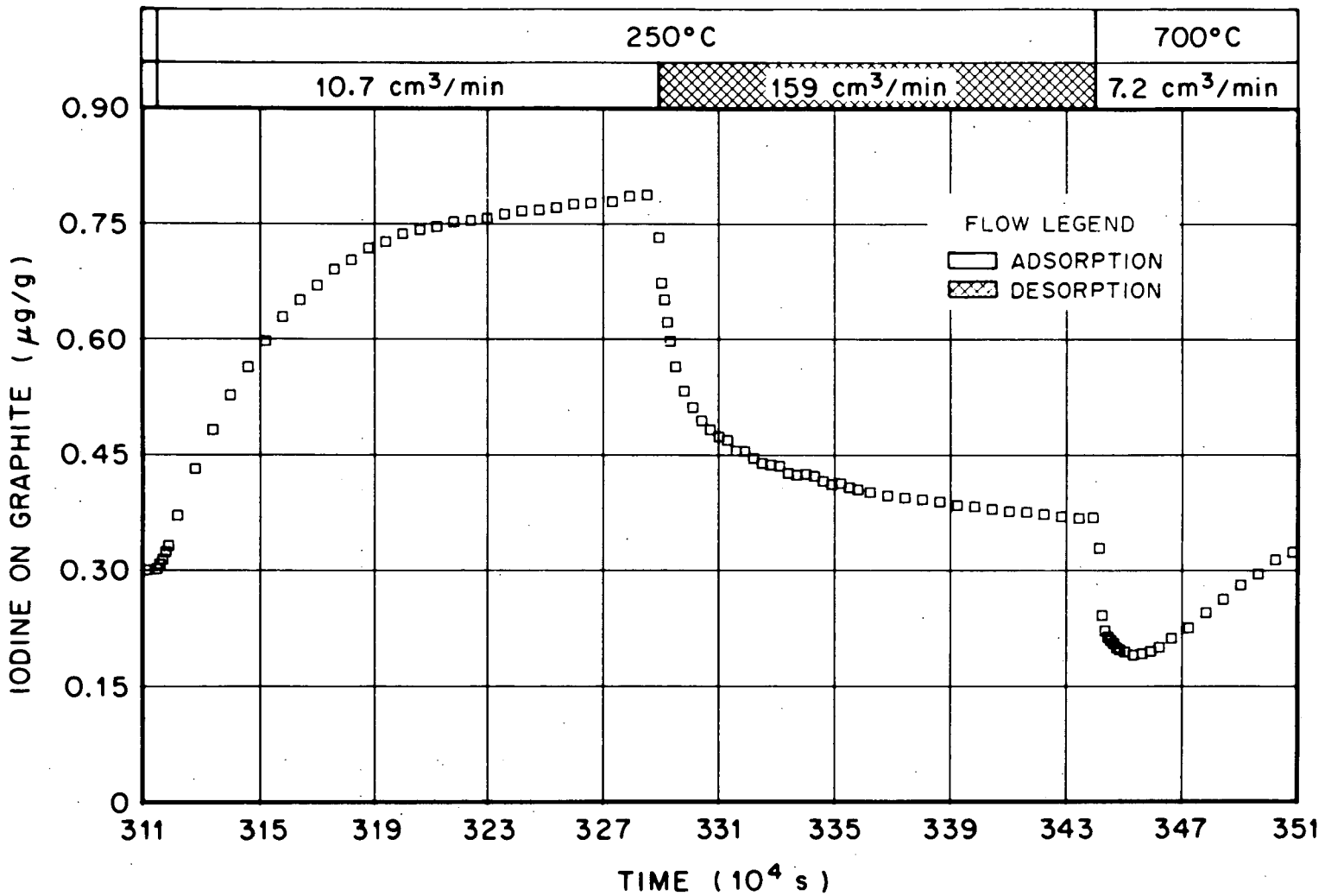

Fig. 38. The change in iodine loading on heated S-2020 graphite with temperature, run 9 (31.1-35.1 × 10^5 s).

ORNL DWG 82-998

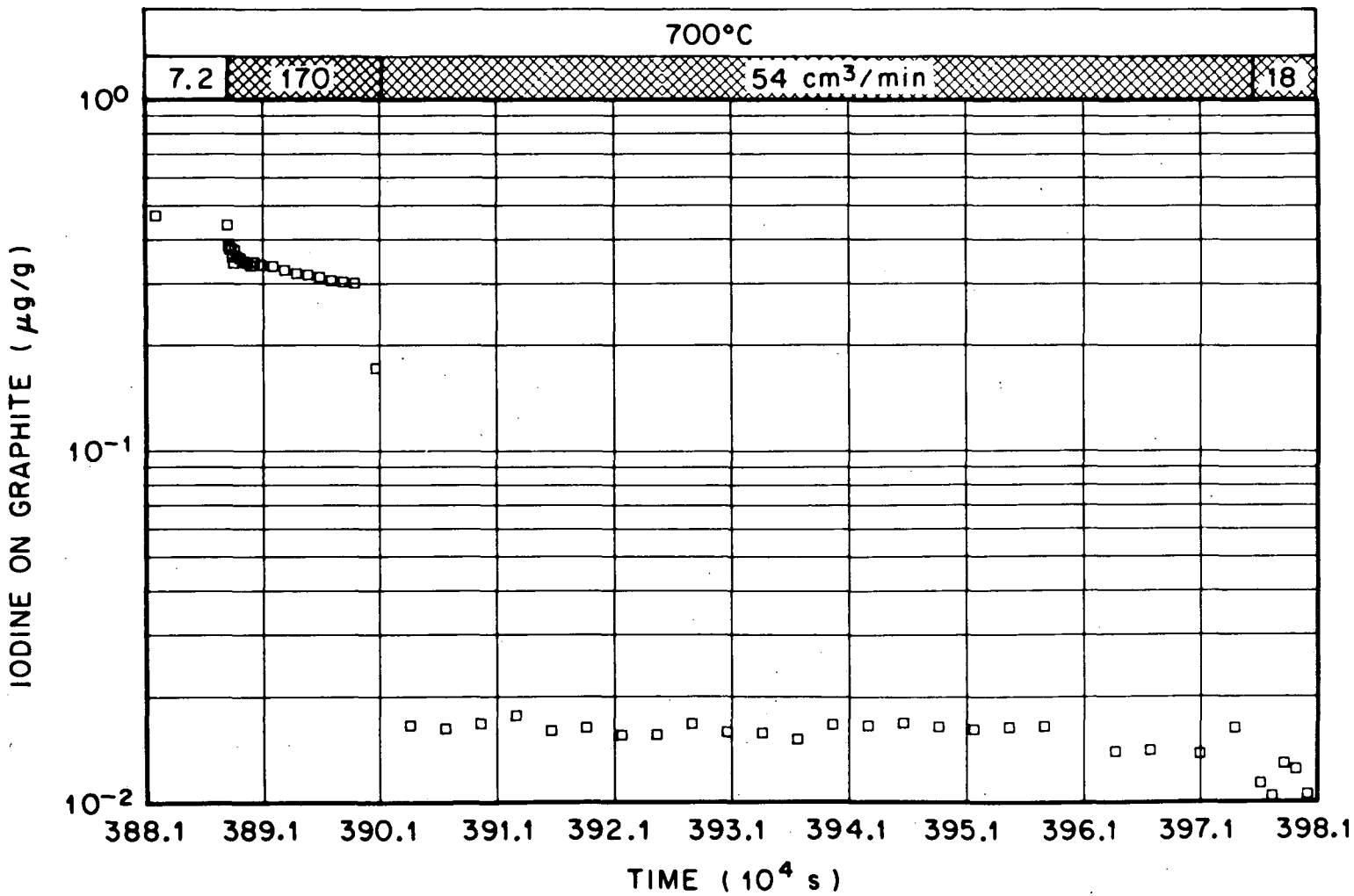

Fig. 39. The effect of helium flow rate on iodine desorption at 700°C from S-2020 graphite, run 9 (38.81-39.81 × 10^5 s).

ORNL DWG 82-997

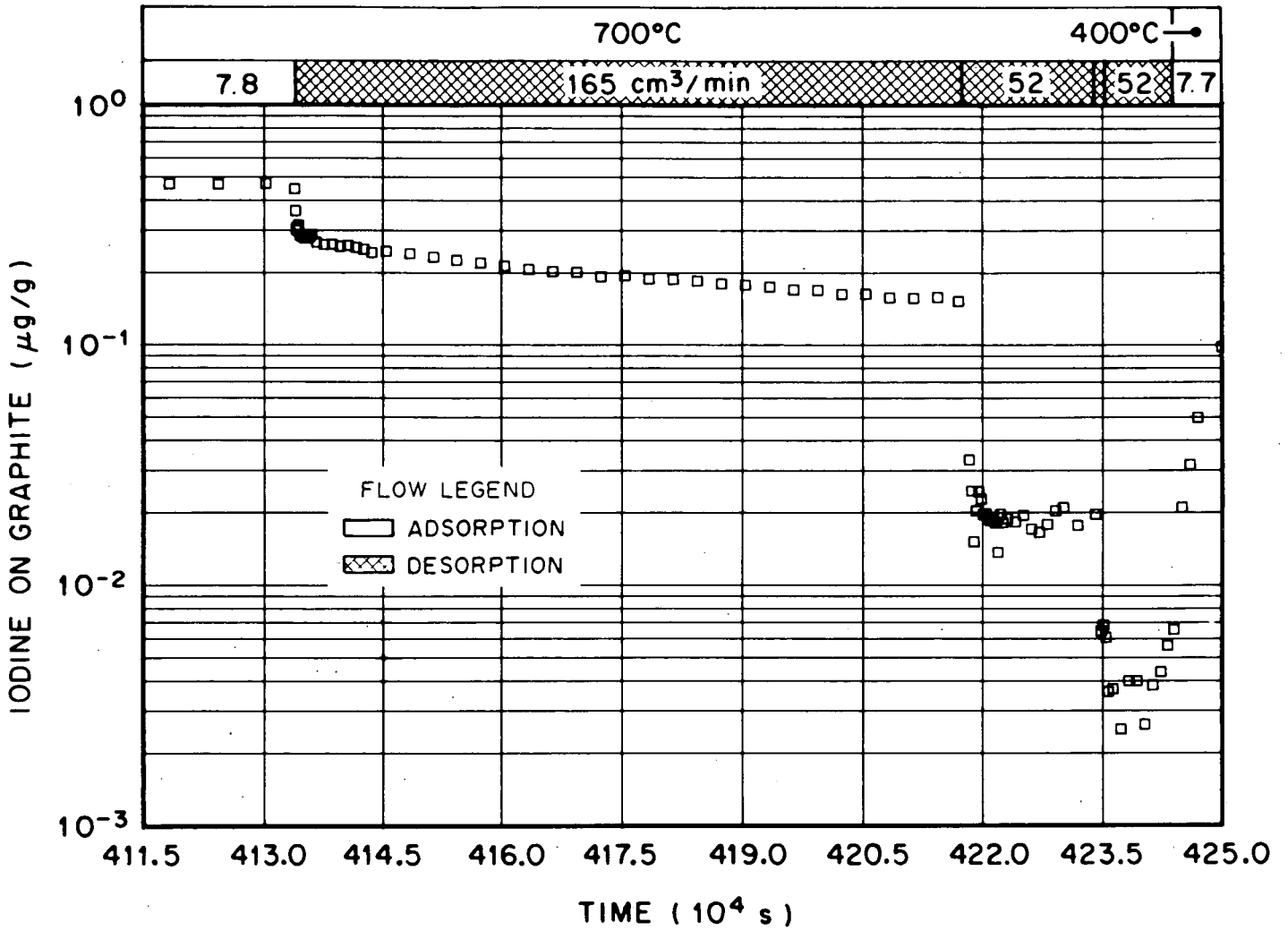

Fig. 40. Verification of the effect of helium flow rate on iodine desorption at 700°C from S-2020 graphite, run 9 (41.15-42.50 × 10^5 s).

ORNL DWG 82-996

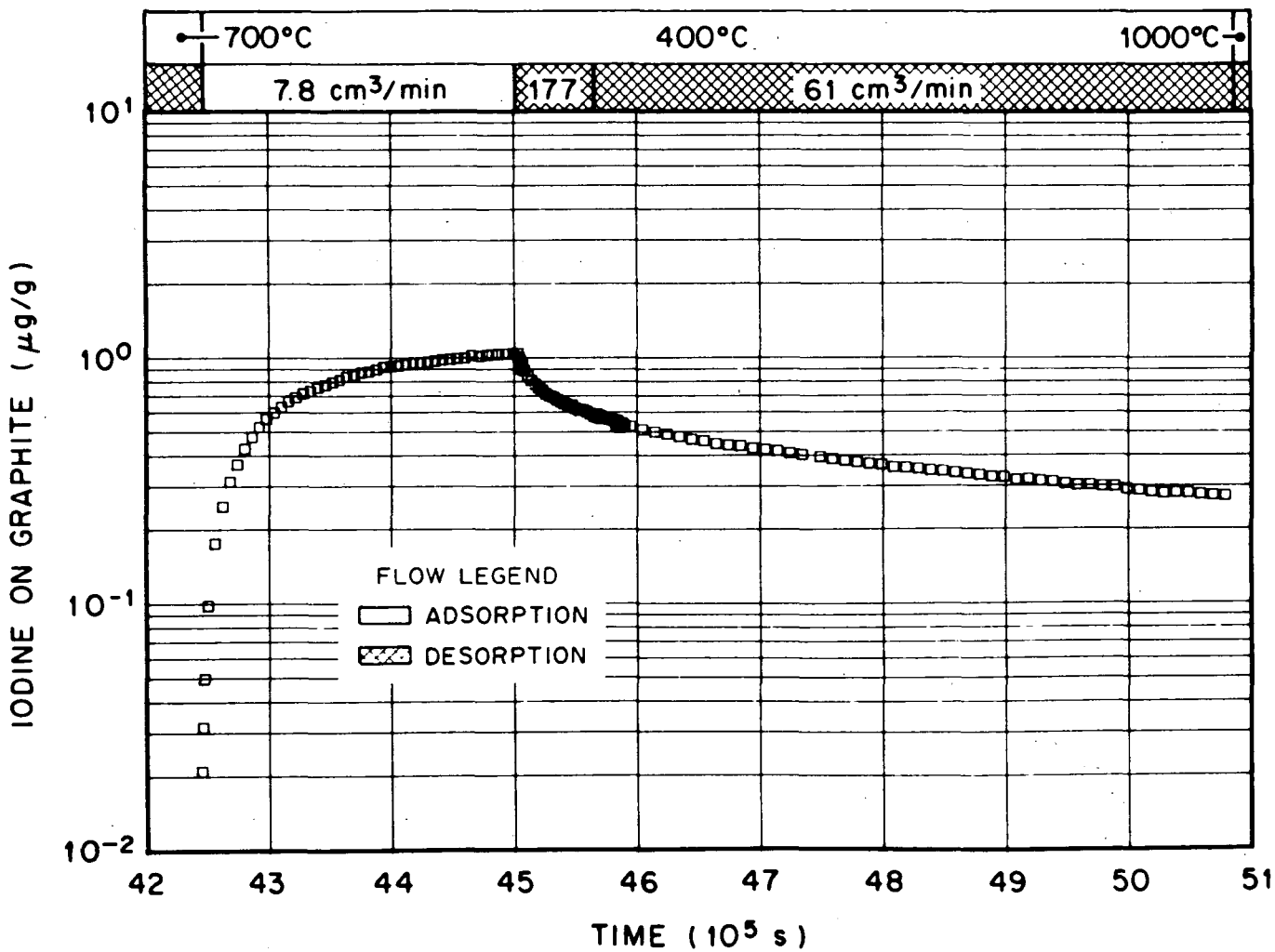

Fig. 41. The effect of helium flow rate on iodine desorption at 400°C from S-2020 graphite, run 9. Iodine loaded on graphite at 400°C.

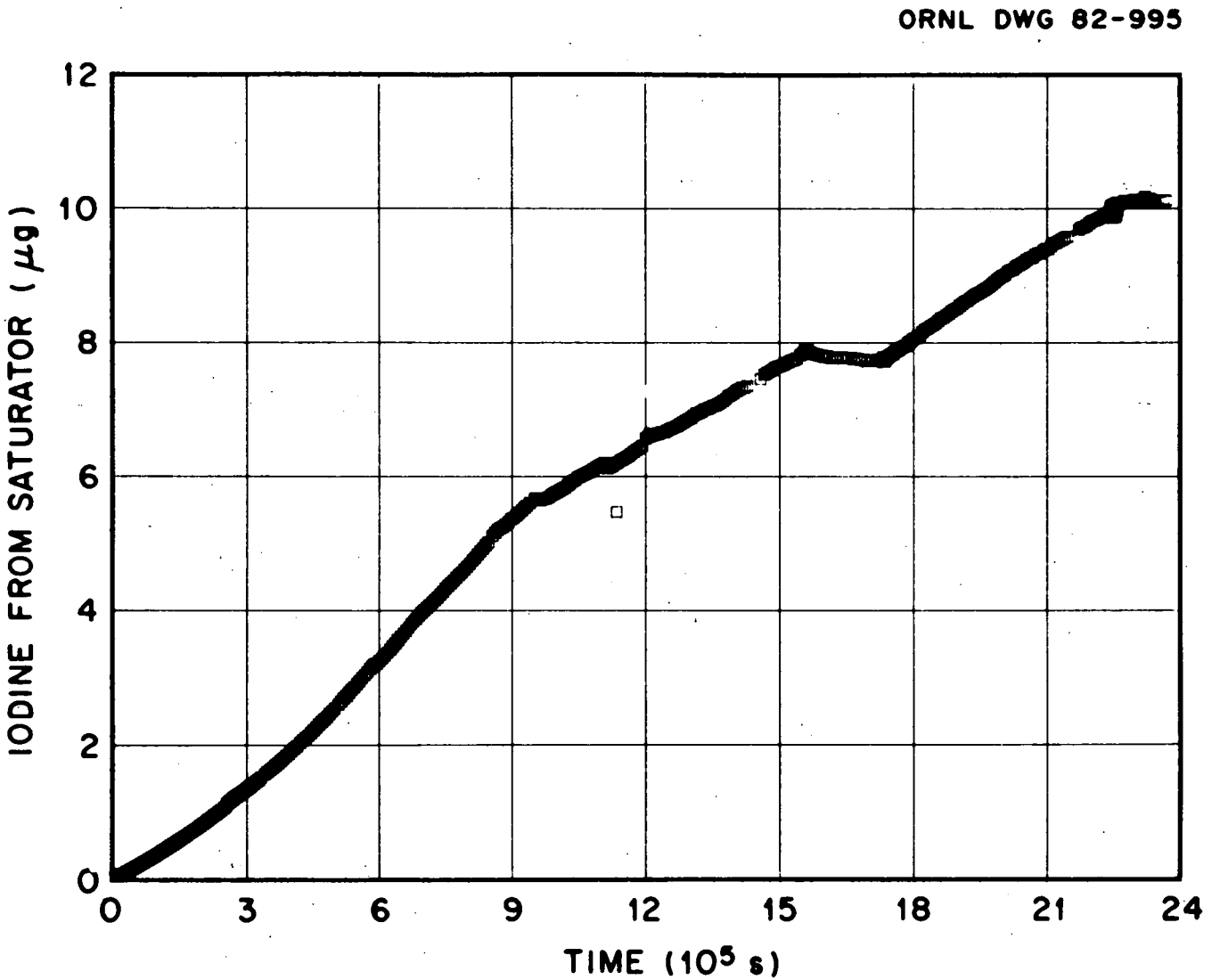

Fig. 42. Iodine transported from saturator, run 9 (0-24 × 10^5 s).

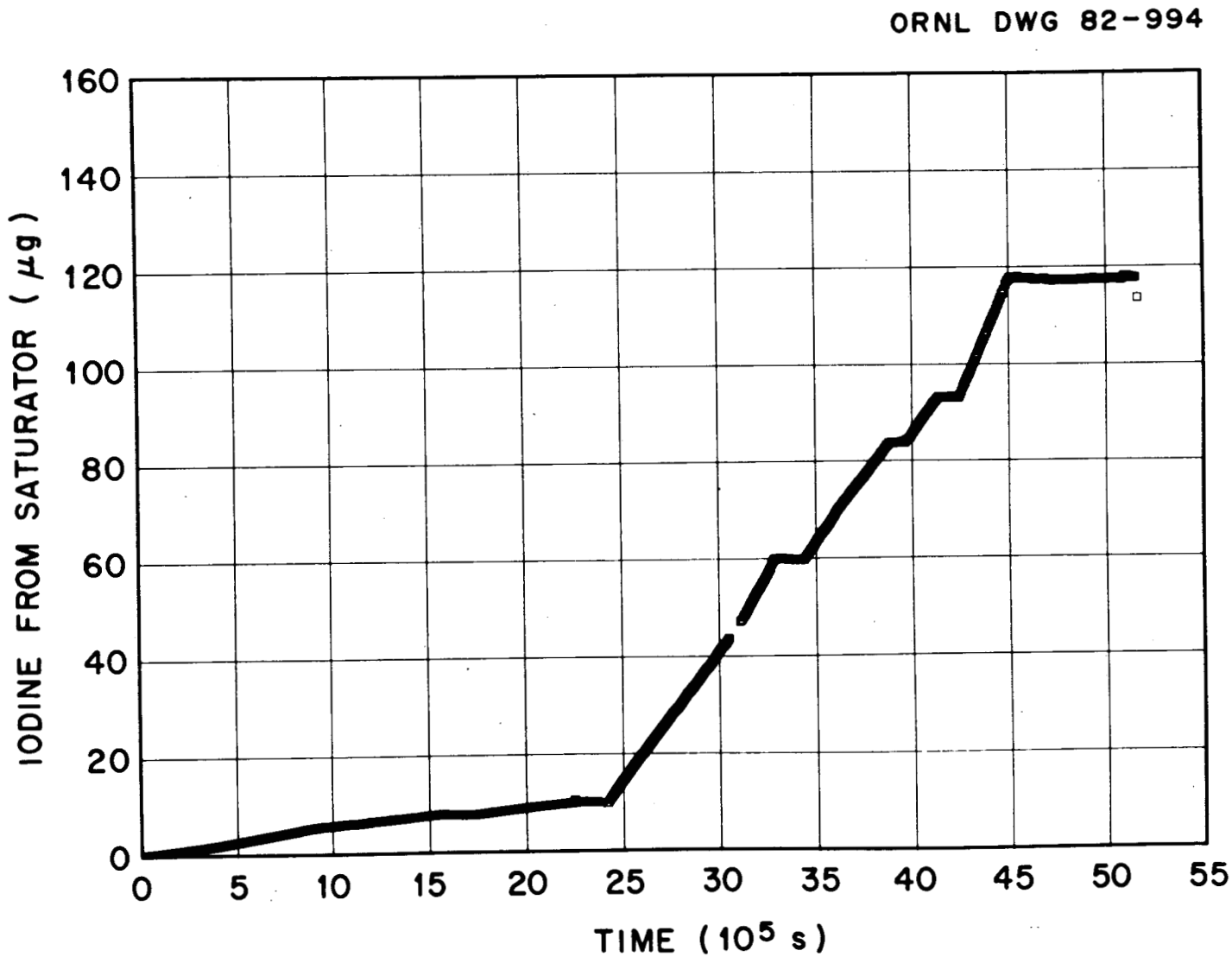

Fig. 43. Total iodine transported from saturator, run 9 ($0-55 \times 10^5$ s).

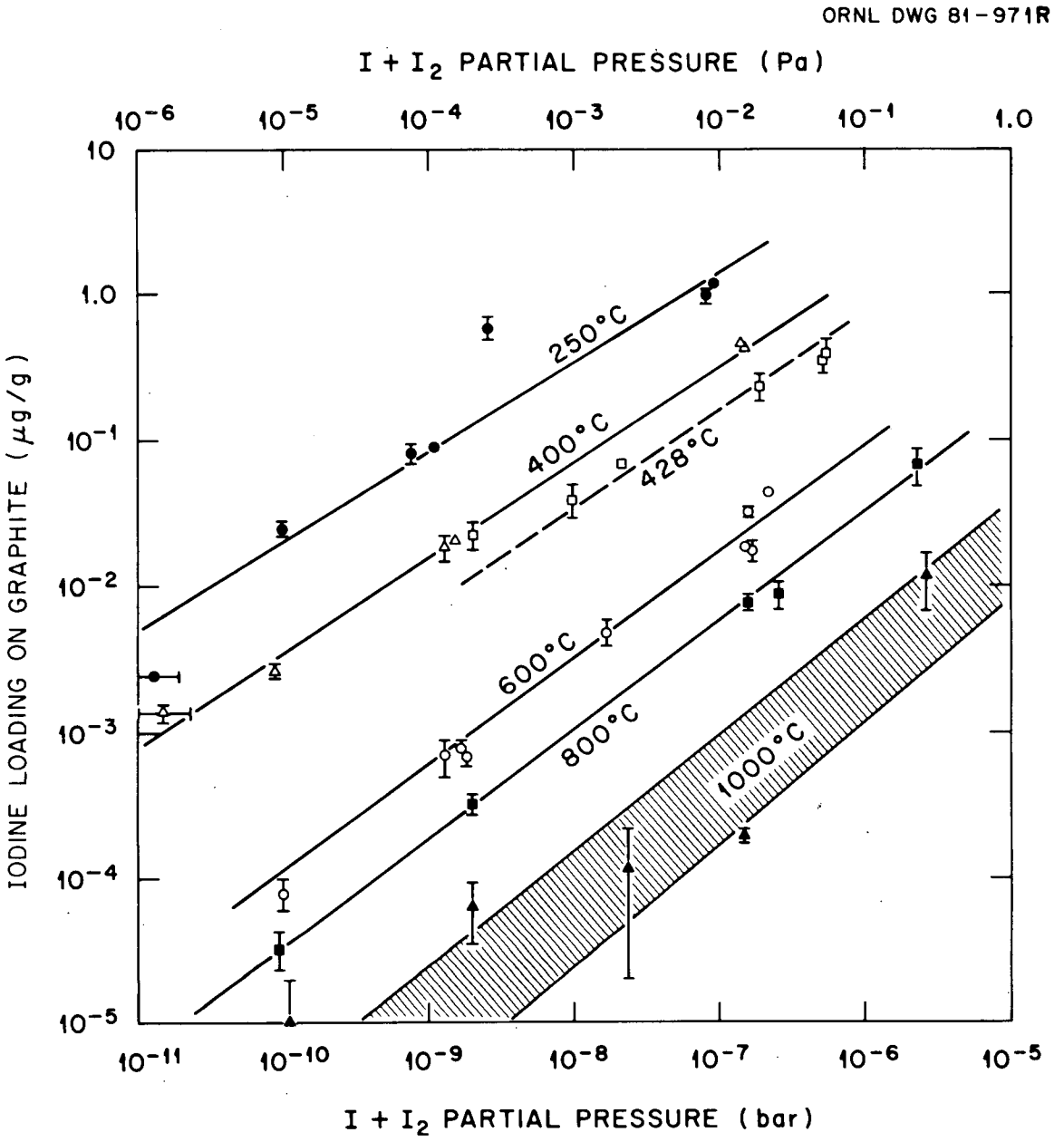

Fig. 44. Sorption isotherms for iodine on H-451 graphite.

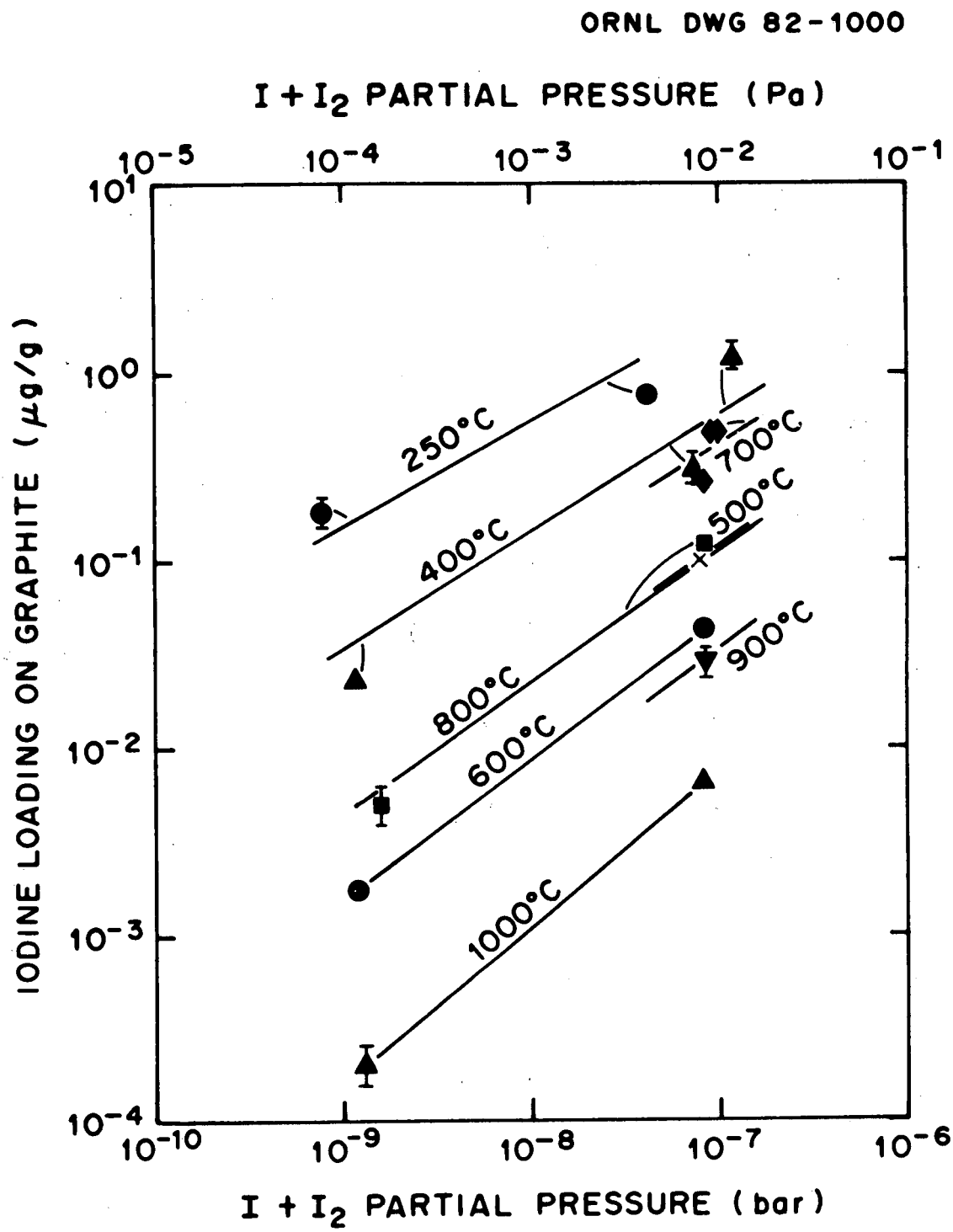

Fig. 45. Sorption isotherms for iodine on S-2020 graphite.

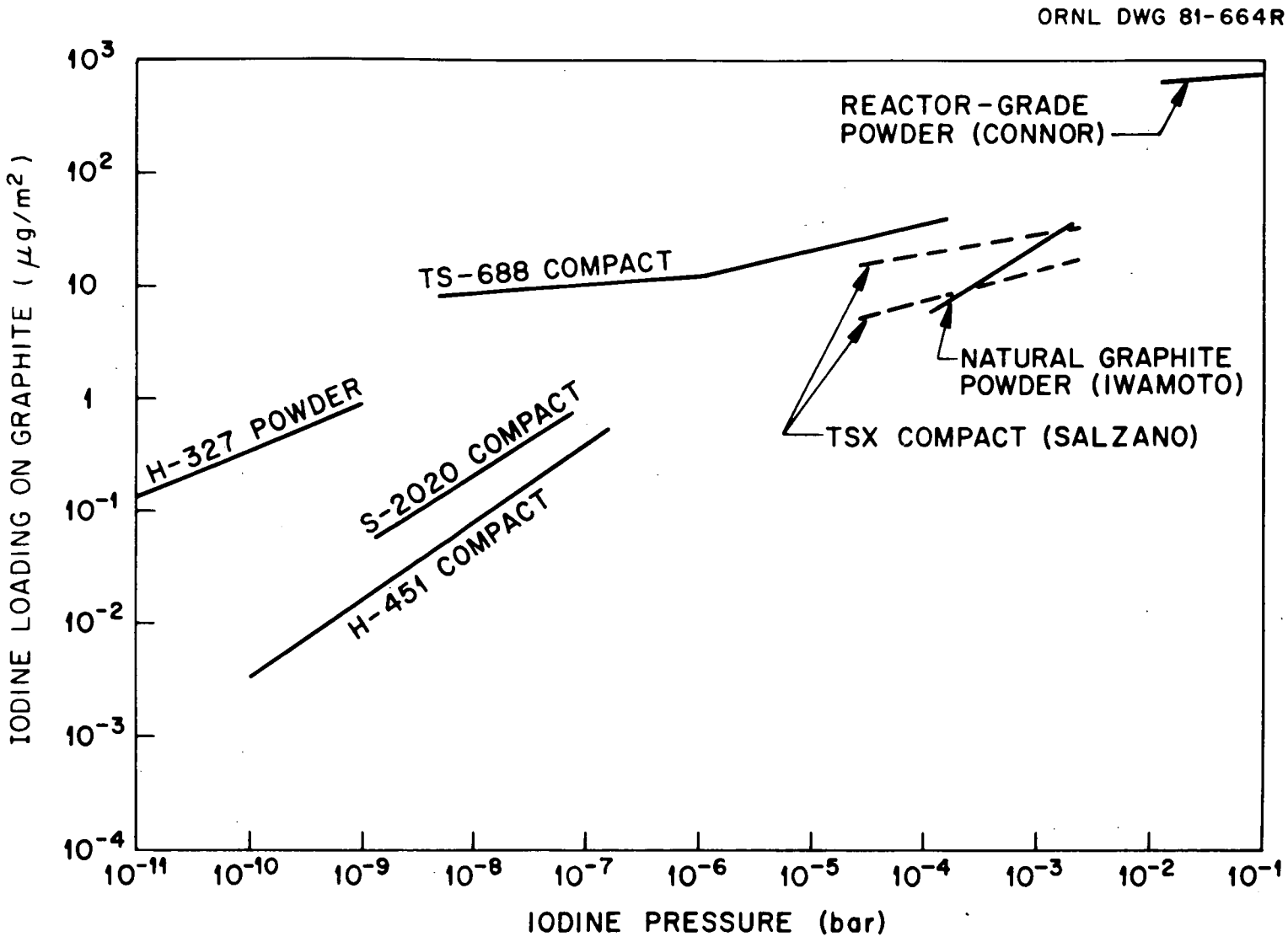

Fig. 46. Adsorption of iodine on various graphites at 400°C.

ORNL-DWG 81-654R

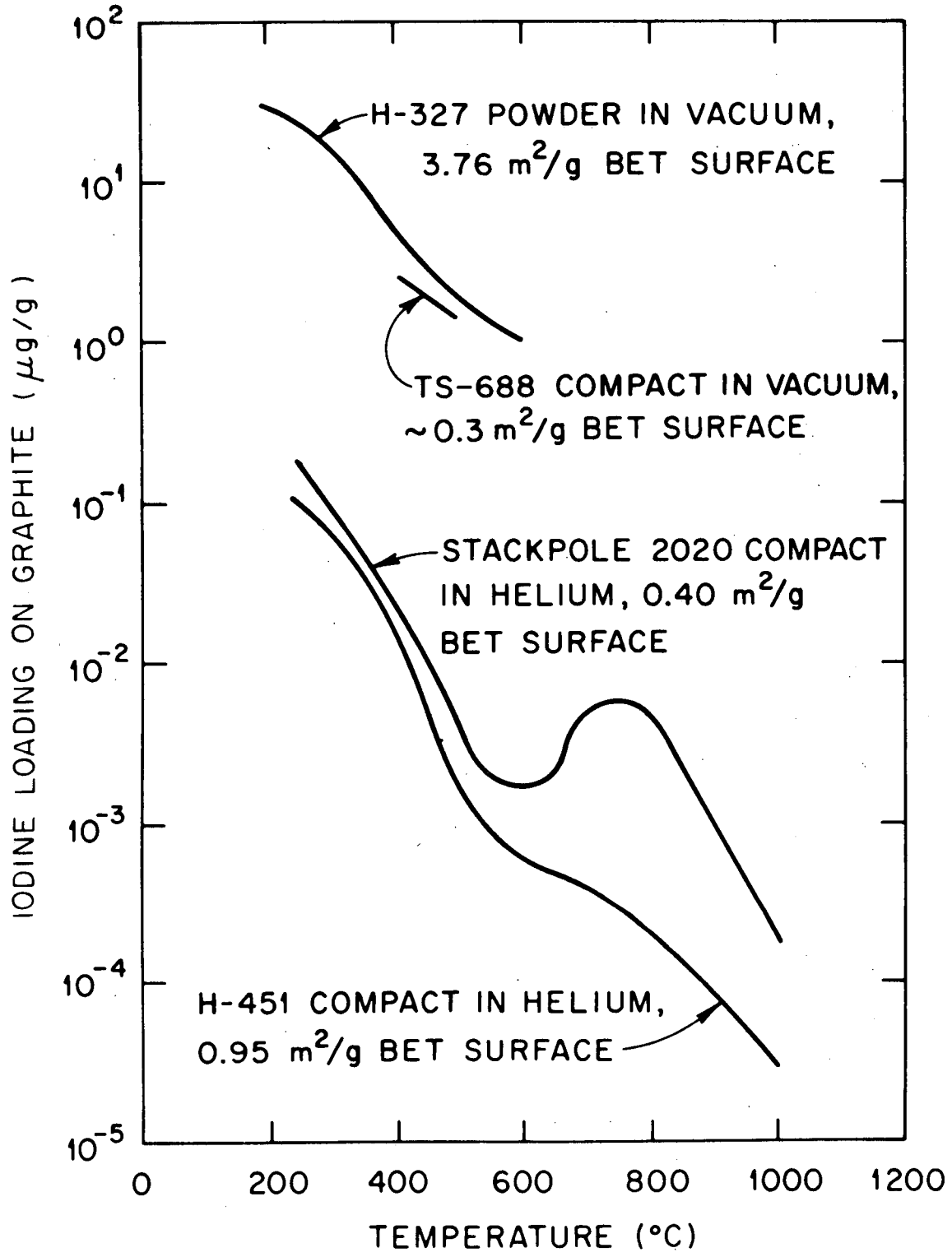

Fig. 47. Adsorption of iodine on graphites; iodine partial pressure 1.25×10^{-4} Pa (1.25×10^{-9} bar).

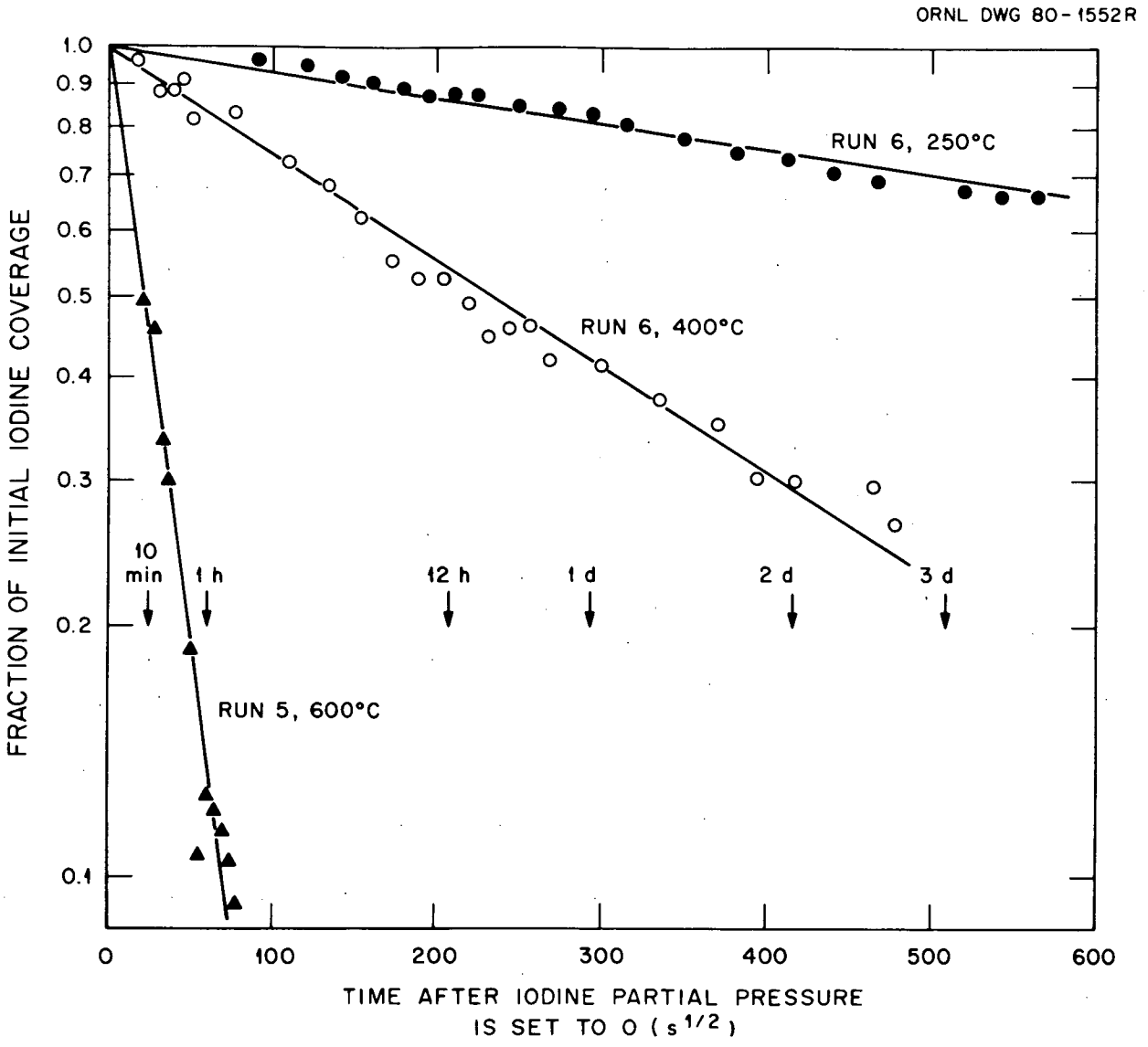

Fig. 48. Isothermal desorption of iodine from H-451 graphite.

ORNL/TM-8284
Dist. Category UC-77

INTERNAL DISTRIBUTION

1. J. T. Bell
2. J. A. Conlin
3-7. F. F. Dyer
8. F. J. Homan
9-18. P. R. Kasten
19. A. D. Kelmers
20. T. S. Kress
21. C. E. Lamb
22. T. B. Lindemer
23-27. R. A. Lorenz
28. A. L. Lotts
29. A. P. Malinauskas
30. F. H. Neill
31. M. F. Osborne
32. G. W. Parker
33. P. L. Rittenhouse
34. M. G. Stewart
35. O. K. Tallent
36-40. R. L. Towns
41. S. K. Whatley
42. R. P. Wichner
43-44. Central Research Library
45. ORNL—Y-12 Technical Library Reference Section
46-47. Laboratory Records
48. Laboratory Records, R.C.
49. ORNL Patent Section

EXTERNAL DISTRIBUTION

50. Office of Assistant Manager for Energy Research and Development, DOE/ORO, P. O. Box E, Oak Ridge, TN 37830
51. Director, Division of HTR Development, Office of Converter Reactor Deployment, U.S. Department of Energy NE-15/GTN, Washington, D.C. 20545
52. J. E. Fox, Division of HTR Development, Office of Converter Reactor Deployment, U.S. Department of Energy NE-15/GTN, Washington, D.C. 20545
53. Senior Program Coordinator, U.S. Department of Energy, San Francisco Operations Office — San Diego, 110 West A Street, Suite 460, San Diego, CA 92101
54. M. J. Steindler, Argonne National Laboratory, Chemical Engineering — Bldg. 205, Argonne, IL 60439
55. M. Blumeier, General Atomic Company, P. O. Box 81680, San Diego, CA 92138
56. O. P. Chawla, General Atomic Company, P. O. Box 81608, San Diego, CA 92138
57. Ben Myers, General Atomic Company, P. O. Box 81608, San Diego, CA 92138
58. R. D. Burnette, General Atomic Company, P. O. Box 81608, San Diego, CA 92138
59. A. W. Barsell, General Atomic Company, P. O. Box 81608, San Diego, CA 92138

60. L. R. Zumwalt, Nuclear Engineering Department, North Carolina State University, Raleigh, NC 27607
61. E. M. Page, Detroit Edison, 2000 Second Avenue, Detroit, MI 48226
62. M. Plys, Room NW12-311, 138 Albany Street, Cambridge, MA 02139
63. P. R. Rowland, UKAEA, AEE, Winfrith, Dorchester, Dorset, DT2, Great Britian
64. H. J. de Nordwall, Avenue Francois Peeters 31, 1150 Bruxelles, Belgium
65. E. Hoinkis, Hahn-Meitner-Institut, Glienicker Str. 100, 1000 Berlin 39, Germany
66. H. F. E. Feuerstein, Kernforschungszentrum Karlsruhe, Postfach 3640, 7500 Karlsruhe, West Germany
67. J. G. Wilhelm, Kernforschungszentrum Karlsruhe, Postfach 3640, 7500 Karlsruhe, West Germany
68. K. Munchow, KFA — Julich, Postfach 1913, D5170 Julich 1, West Germany
69. B. Thiele, KFA — Julich, Postfach 1913, D5170 Julich 1, West Germany
70. W. Nowak, BBC Aktiengessellschaft, Brown, Boveri, and Cie, CH-4501 Baden/Schweiz, Switzerland
71. H. Nagao, NAIG Nuclear Research Laboratory, Nippon Atomic Industry Group, Ltd., 4-1, Ukishimo-cho, Kawasaki, Japan
72. Cesar Sastre, Brookhaven National Laboratory, Upton, Long Island, NY 11973
73. Don Sweitzer, Brookhaven National Laboratory, Upton, Long Island, NY 11973
74. Ron Foulds, Nuclear Regulatory Commission, Washington, DC 20555
75. O. E. Basset, Nuclear Regulatory Commission, Washington, DC 20555
76. Charles Kelber, Nuclear Regulatory Commission, Washington, DC 20555

77-209. Given distribution as shown in TID-4500 under Gas-Cooled Reactor Technology category UC-77